Title
Probing Mechanical Flexibility and Discrete Stepping of an Ultra-Fast Ring ATPase

Author
Liu, Ninning

Publication Date
2013

Peer reviewed|Thesis/dissertation

Probing Mechanical Flexibility and Discrete Stepping of an Ultra-Fast Ring ATPase

By

Ninning Liu

A dissertation submitted in partial satisfaction of the

requirements for the degree of

Doctor of Philosophy

in

Molecular and Cellular Biology

in the

Graduate Division

of the

University of California, Berkeley

Committee in charge:

Professor Carlos J. Bustamante, Chair
Professor James Berger
Professor Andreas Martin
Professor Jan Liphardt

Fall 2013

Probing Mechanical Flexibility and Discrete Stepping of an Ultra-Fast Ring ATPase

by Ninning Liu

Abstract

Probing Mechanical Flexibility and Discrete Stepping of an Ultra-Fast Ring ATPase

by

Ninning Liu

Doctor of Philosophy in Molecular and Cellular Biology

University of California, Berkeley

Professor Carlos J. Bustamante, Chair

DNA translocation is a fundamental process in biology, required for essential cellular processes including recombination, replication, and chromosome segregation. The SpoIIIE motor is a homo-hexameric dsDNA translocase, part of the ASCE [Additional Strand Conserved E (glutamate)] superfamily of oligomeric ring NTPases. SpoIIIE is found in the bacterium *Bacillus subtilis*, its biological role is to actively translocate DNA to ensure the proper segregation of sister chromatids. SpoIIIE accomplishes this task by coupling the chemical energy provided by ATP to generate mechanical work, pumping the DNA across a cellular membrane at a rate of 4 kbp/s. While generating mechanical work is a common function of ring NTPases, the timing and order of individual power strokes applies this work in a nuanced manner to better suit particular biological tasks. Understanding the mechanical aspects of fast DNA translocation provides a unique insight into the diverse mechanical strategies employed by these large class of ring NTPases.

Using single-molecule optical trapping techniques, I present real-time measurements of SpoIIIE DNA translocation. By challenging the motor with different lengths of modified DNA substrates, I have determined that SpoIIIE makes critical phosphate contacts with the DNA backbone during translocation and characterized the periodicity of motor-DNA interactions, suggesting a fundamental step size of 2 bp. Furthermore, velocity dependence on an applied external load and various concentrations of ATP, ADP and P_i have demonstrated that translocation is coupled to phosphate release. Finally, ATP analogue experiments are presenting an emerging model of a unique, partially coordinated mechanism of hydrolysis between the individual subunits of SpoIIIE.

Table of Contents

List of Figures

Chapter 1

Chapter 2

Chapter 3

Chapter 4

Chapter 5

Chapter 6

List of Tables

List of Abbreviations

µm	Micrometer
µM	Micromolar
ADP	Adenosine Diphosphate
ATP	Adenosine Triphosphate
bp	Basepair
CI	Confidence Interval
DNA	Deoxyribonucleic Acid
kbp	Kilobasepair
KOPS	FtsK Orienting Polar Sequence
MeP	Methyl Phosphonate
mM	Millimolar
msec	Millisecond
nm	Nanometer
nM	Nanomolar
P_i	Inorganic phosphate
pN	Piconewton
s.e.m	Standard error of the mean
SRS	SpoIIIE Recognition Sequence

Acknowledgements

The work presented in this thesis is a culmination of the efforts of many talented individuals, people who took time out of their busy schedules and nurtured a project that was not their own. I would like to thank Jerod Ptacin, Carolina Caffaro, and Marcelo Nollmann for their initial guidance over the SpoIIIE project, for training me in molecular biology and passing on such a promising and fruitful avenue of scientific research. To Steven Smith, I express my gratitude over the time and effort he devoted to training me in the use of the optical tweezers. I would also like to thank Maurizio Righini, Yuanbo Cui, and Lisa Alexander for their contributions on the project in the later stages. To Bibiana Onoa, I express my sincerest gratitude for scientific guidance and advice that will no doubt prove invaluable in my scientific career.

Throughout the course of my graduate career, I have had the privilege of working with many highly motivated and talented people. I would like to acknowledge Dr. Alyssa Rosenbloom for her unconditional support through the best and worst times, without which I undoubtedly would have stumbled along the way. To my many friends in the Bustamante lab both past and present, Pim Dangkulwanich, Varsha Desai, Daniel Goldman, Shannon Yan and Troy Lionberger; I have greatly enjoyed our conversations about science, life, and a myriad of other topics that make each day a privilege to come to work. I would also like to express my gratitude to the motor subgroup, Sara Tafoya, Shixin Liu, and Maya Sen, for giving me a deeper appreciation of motor proteins, for challenging ideas, and for their unfailing willingness to discuss the latest results. To the Spo-PALM group, Jae Yen Shin, Sanghyuk Lee, and Antony Lee, I would like to thank them for insightful conversations on sporulation and to always consider the biological relevance of an *in vitro* result. And lastly I must thank Gheorghe Chistol, for being a great scientist and friend, for making monumental contributions to the project at every stage, and for his invaluable help in interpretation and data analysis.

To my thesis committee members, James Berger, Andreas Martin and Jan Liphardt, I am deeply grateful for the many years of guidance and advice over my scientific career. Finally, I owe an incredible debt to my scientific advisor, Dr. Carlos Bustamante. For his trust in me to devote time and resources to this project, for sharing his deep insights into science, for guiding me through many years of hard work, for his gentle reminders of never resting on your laurels, and for offering me this great privilege of undertaking scientific research at the highest levels.

Chapter 1 Introduction

DNA translocation is a fundamental process in biology, required for recombination, replication, and proper segregation of sister chromatids (*1*). Considering the large size of even relatively short genomes, it is clear that such an enormous macromolecular complex cannot be moved through a cellular environment through thermal forces alone; instead it must be physically moved.

This inherently mechanical process is accomplished by a class of enzymes known as molecular motors. Varied as they are numerous, their functions range from nucleic acid helicases (*2*), polymerases (*3*), translocases (*4*), and peptide translocation and degradation (*5, 6*). As functionally diverse as these mechanical processes are, ultimately they require a source of energy. Typically this energy is provided in the form of nucleotide triphosphates (NTP's) or a proton gradient, which is converted into mechanical work. Termed mechanochemistry, coupling of chemical energy to mechanical work is a basic property of all molecular motors (*7*).

The work presented in this thesis will focus on one such molecular motor, a double-stranded DNA (dsDNA) translocase, SpoIIIE. I will describe the mechanical aspects of this remarkable DNA translocase using optical trapping techniques that allow us to directly probe the motor's mechanical properties in real time. Furthermore, I will demonstrate novel experimental set-ups measuring discrete units of work, ie. the step size, of the motor without the need for an ultra-high resolution instrument. Portions of this thesis will be submitted in the future for publication.

1.1 The DNA motor SpoIIIE

SpoIIIE is a homohexameric dsDNA motor protein found in the common soil bacterium *Bacillus subtilis* and is involved in chromosome segregation during the bacterium's sporulation lifecycle. The motor accomplishes a remarkable physical task of translocating several megabases of the *B. subtilis* genome across a division septum while stripping off a myriad of DNA bound proteins (*8–11*). Given the large size of the bacterial genome, DNA translocation must proceed at a high velocity in order to complete chromosome segregation in a timely manner (*1*). A distinguishing feature of the SpoIIIE motor is its high velocity of DNA translocation and ability to work against high forces, reaching up to 4 kbp/s (*12*) and 50 pN of force. During sporulation in *B. subtilis* an asymmetric cellular division septum will form and completely enclose around one of the sister chromatids before the chromosomes are properly segregated (Figure 1.1). The SpoIIIE motor is then required to export the remaining DNA across the division septum and into the developing spore (*13*). Before chromosome segregation occurs, SpoIIIE localizes to the leading edge of the division septum and is believed to form an active complex around DNA when the septum encircles the chromosome (*13–15*). SpoIIIE then couples the hydrolysis cycle of adenosine triphosphate (ATP) to the mechanical motions required to move the remaining ~3 megabases of DNA trapped outside of the developing forespore. Under optimal conditions, the entire process can be completed in 20 minutes (*13*). Interestingly, SpoIIIE is not involved in chromosome segregation during vegetative growth. Instead it occupies a more specialized role clearing DNA that occasionally gets trapped around a fully formed division septum (*16*), similar to its role in sporulation.

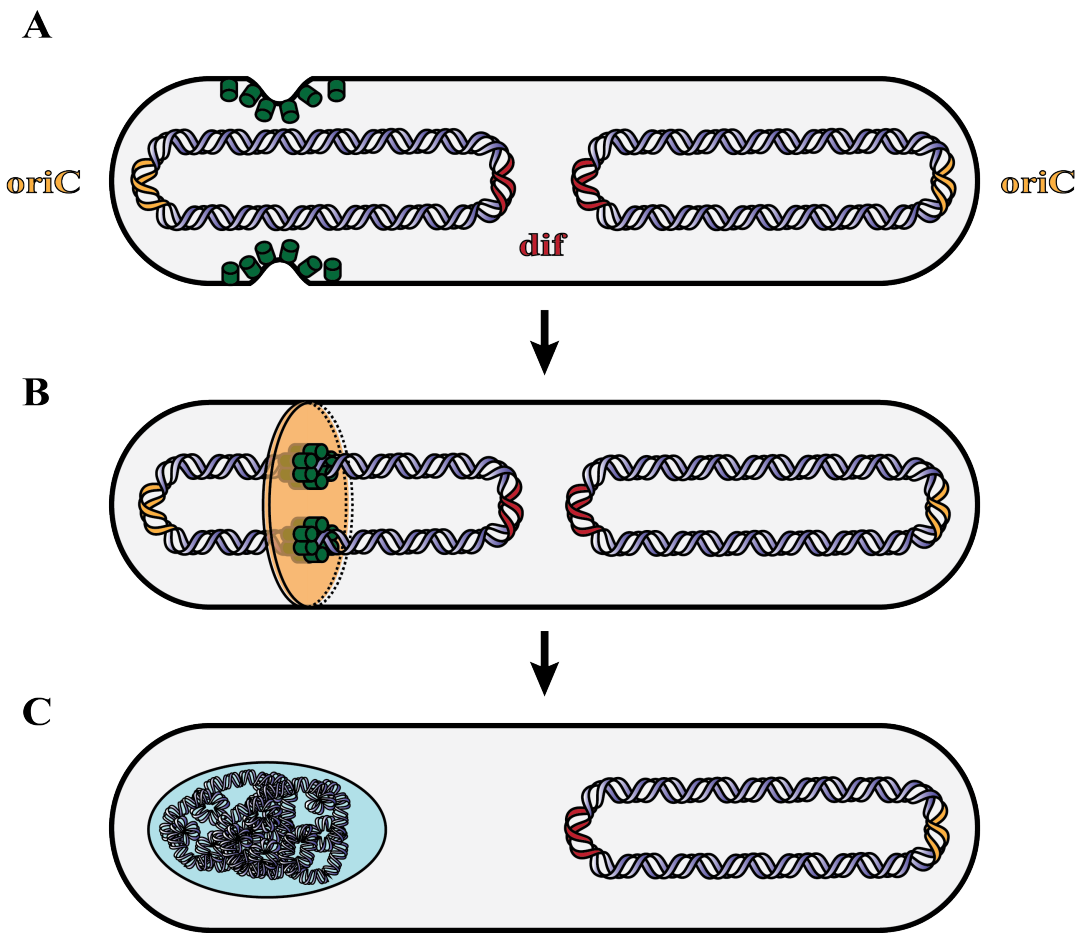

Figure 1.1 Model of SpoIIIE Organization Around DNA at the Division Septum

(A) After chromosome replication, the oriC region (yellow) of the chromosome is oriented towards the cellular poles with the dif region (red) 180 degrees away. SpoIIIE (green rods) localizes to the leading edge of an invaginating septum.
(B) A division septum (orange disc) encircles the chromosome and SpoIIIE oligomerizes around the DNA. It is thought that at least two active complexes are required to accommodate each arm of the circular chromosome.
(C) Translocation is complete and the endospore (cyan oval) has completely formed.

SpoIIIE belongs to the FtsK/HerA family of ATPases (*17*). Its structure is composed of an N-terminal, four pass transmembrane domain followed by a putatively unstructured linker (Figure 1.2 A). The unstructured linker domain is believed to give individual membrane-bound subunits of SpoIIIE the flexibility it needs to self-assemble into an active hexamer, however it has also been shown to play a role in septal localization and membrane fission after translocation (*18*, *19*). The C-terminal motor domain, containing both the ATPase and translocase properties of SpoIIIE, is highly conserved among this family of DNA translocases (*16*, *20*). The motor domain itself is subdivided into three subdomains (α, β, and γ) (Figure 1.2 A). Crystal structures of FtsK, the *E. coli* homologue of SpoIIIE, show that the α domain adopts a fold that is unique to this family of DNA translocases, whereas the β domain adopts a canonical RecA-like fold containing the conserved Walker motifs for ATP binding and hydrolysis (*21*). The γ domain has also recently

been co-crystallized with its DNA substrate and is shown to adopt a winged-helix DNA binding motif (*22*). In addition, single-molecule experiments have shown that the γ domain plays a role in imparting directionality to DNA translocation (*12*, *23–25*).

The active state of the FtsK/HerA family of proteins generally adopt a homohexameric ring conformation, with the NTP binding pocket sandwiched between the interface of two adjacent subunits (*17*). The FtsK protein has been shown to form a homohexameric ring in both crystal structures and electron microscopy (EM) studies (*21*). Rings are topologically closed structures and thus provide a mechanism to ensure processivity of translocation. Currently, a co-crystal structure of a dsDNA translocase ring and its DNA substrate is not available. However, EM studies of FtsK have shown that the DNA substrate is threaded through the central pore of the ring (*21*). The active, oligomeric state of SpoIIIE has also been determined to adopt a homohexameric ring using fluorescent correlation spectroscopy, atomic force microscopy and EM (*10*, *26*). In lieu of a crystal structure of SpoIIIE, a structural prediction was done by Gheorghe Chistol using the Phyre2 server (*27*). Not surprisingly, the predicted structure of SpoIIIE is very similar to FtsK, given their high sequence similarity (>70%) (*20*).

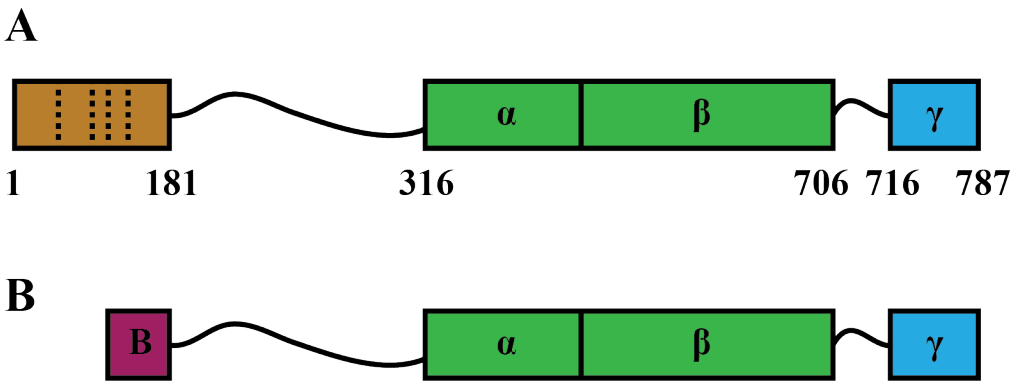

Figure 1.2 Cartoon of SpoIIIE protein domains

(A) Wild-type SpoIIIE consists of an N-terminal four pass transmembrane domain (tan box w/ dotted lines), a putatively unstructured linker (wavy black line), the motor domain (green box) and a sequence recognition domain (blue box). The amino acid position of each domain is listed below. Previous *in vitro* experiments with SpoIIIE purified from pJB103 plasmid has the transmembrane domain removed (*8*).

(B) The SpoIIIE protein used in single-molecule experiments has the transmembrane domain replaced with a protein fragment that is biotinylated (purple box).

Note that structural modeling predicts the central pore of the SpoIIIE hexamer is only wide enough for a single piece of B-form dsDNA to be threaded through (Figure 1.3). Given the circular nature of bacterial genomes, this has led to the prevailing model that DNA translocation must be accomplished by at least two SpoIIIE complexes, one for each arm of the chromosome (Figure 1.1 B). It has been a matter of some debate as to whether SpoIIIE forms a co-axially stacked ring of two or four hexamers to form a channel for DNA (Figure 1.1 B). The existence of a DNA channel structure would predict double the amount of SpoIIIE molecules present at the division septum (24 molecules, assuming two rings per channel) than a model without a channel (12 molecules assuming one ring per chromosome arm). Furthermore, there has been some evidence that the

active state of FtsK and SpoIIIE is not a single hexamer, but a dodecameric complex where two rings form a head-to-head dimer (*21*). The head-to-head dimer configuration has been proposed as a model to explain the bidirectional translocation behavior seen in FtsK (*28*). Extrapolating the dodecameric model to the motor architecture *in vivo,* a DNA channel comprised of two dodecameric rings would predict at least 48 molecules of SpoIIIE at the division septum (one channel for each chromosome arm). A single dodecameric ring for a DNA channel is essentially equivalent to the two co-axially stacked ring model.

There have been several publications that attempt to quantify the number of SpoIIIE molecules at the division septum, with numbers ranging from 24-72 (*13*, *15*, *29*). Currently, super-resolution microscopy experiments observing the localization of SpoIIIE at the division septum suggest that a DNA channel is comprised of either a single hexameric ring (*15*) or paired rings (*29*) (unpublished work), thus the model of paired dodecameric rings forming a channel has fallen out of favor.

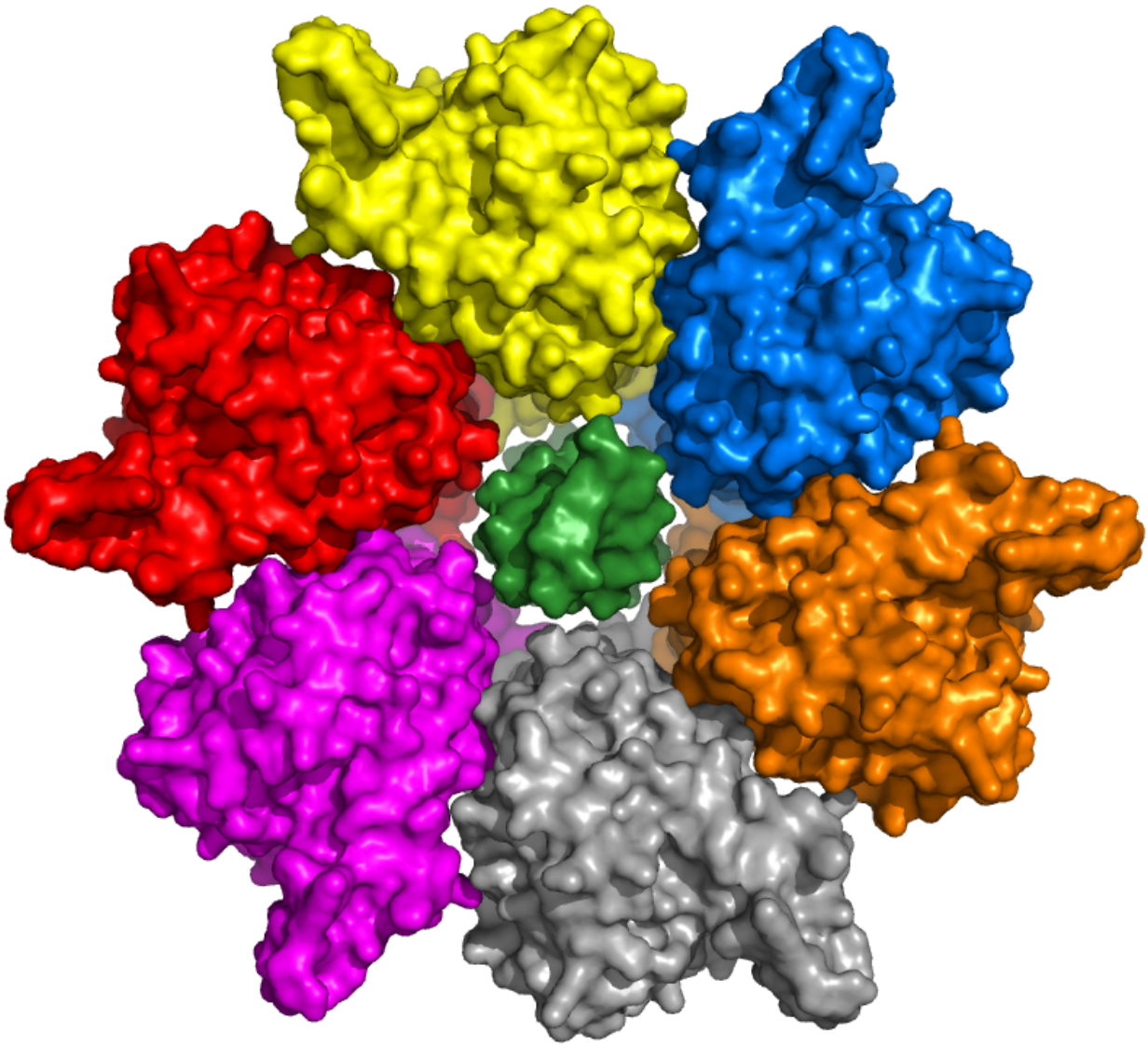

Figure 1.3 SpoIIIE Structural Prediction

A SpoIIIE homohexamer structure with each individual subunit labeled in a different color (red, yellow, blue, orange, gray, purple) was modeled by Gheorghe Chistol using the Phyre2 server http://www.sbg.bio.ic.ac.uk/phyre2/html/page.cgi?id=index (*27*). A B-form piece of dsDNA (green) is also modeled threading through the central channel.

1.2 The ASCE SuperFamily

The FtsK/SpoIIIE motors are part of the larger ASCE [Additional Strand Catalytic E (glutamate)] superfamily of oligomeric, ring-shaped NTPases that encompass a wide array of

enzymes involved in diverse cellular functions, including nucleic acid unwinding, replication initiation, cargo transport, and chromosome segregation (*30*, *31*). The ASCE superfamily shares a basic structural core for NTP binding and hydrolysis, comprised of several α-helices that sandwich five parallel β-sheets (Figure 1.4). The components of the structural core contains the highly conserved Walker A (WA) and Walker B (WB) motifs involved in binding to the phosphate groups of NTP and coordinating the Mg^{2+} metal ion cofactor. The catalytic glutamate (CE) is involved in coordinating the γ-phosphate of NTP with a water molecule for nucleophilic attack and hydrolysis. The location of the catalytic glutamate varies between the RecA and AAA+ branches. For the most part the CE either resides within the Walker B motif or some other proximate position within the active site. Finally, the NTP binding pocket for ASCE ring NTPases lies at the interface of two adjacent subunits, with the arginine finger (RF) from an adjacent subunit interacting with the γ-phosphate of NTP. The arginine finger is generally proposed as the structural mechanism by which two adjacent subunits can coordinate their activities, conformational changes in one subunit can be transmitted to an adjacent subunit (*31*, *32*).

From a mechanical point of view, the ASCE core acts essentially as a modular domain that is responsible for harnessing the chemical energy from NTP. Attaching other structural elements to the ASCE module can then couple this chemical energy to mechanical work, fine tuning the motor towards specific cellular functions (*30*, *32*). There is an enormous body of literature focused on characterizing the mechanisms of these motor proteins, undoubtedly some proteins will be overlooked in this thesis. Figure 1.4 gives an indication on the level of diversity encompassed by the ASCE family. Generally speaking, there are two central questions surrounding these class of motor proteins. Firstly, which portion of the catalytic cycle is coupled to the mechanical transition? Secondly, do the individual subunits of a multimeric ring coordinate their activities? Single-molecule experiments on ring NTPases have demonstrated that motor mechanochemistry and intersubunit coordination is specifically tuned towards its biological task, such as DNA packaging (*33*, *34*), or protein translocation/unfolding (*6*). Understanding the operating principles behind these class of motor proteins carries great interest in deciphering the mechanical strategies employed by nature to accomplish biological tasks.

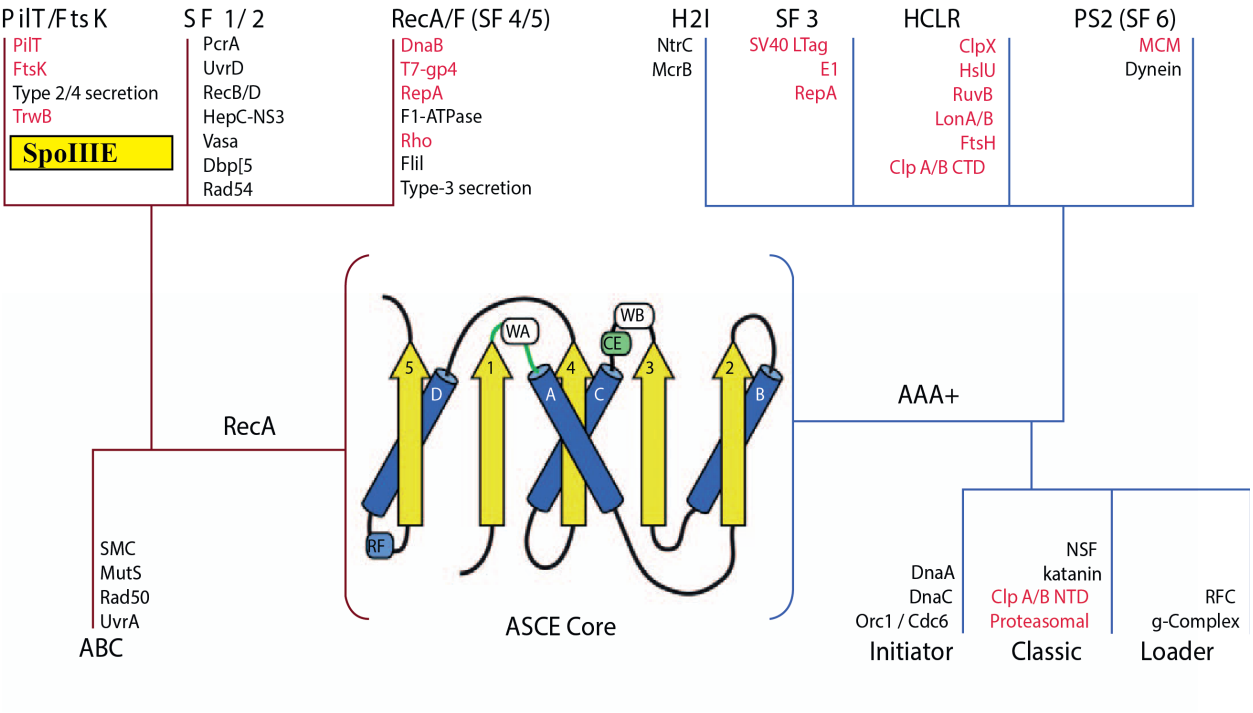

Figure 1.4 The ASCE superfamily

A large portion of the ASCE NTPases oligomerize into homomeric rings (highlighted in red). The ASCE superfamily is subdivided into RecA-like (left branch) or AAA+ (right branch). The SpoIIIE motor (added in to figure, yellow box) belongs to the PilT/FtsK clade of the RecA-like branch. Adapted from Lyubimov et al., 2011 (*31*), with permission from Elsevier © 2011.

1.3 Single-Molecule Optical Tweezer Geometry

1.3.1 Why single-molecule?

The questions mentioned earlier are uniquely suited for experimentation on single-molecule optical tweezers. Optical tweezers come with the distinctive capability of measuring the force generation and displacement of a molecular motor. The optical tweezers moniker is intricately linked with the concept of single-molecule experimentation, where the activity of enzymatic systems can be measured one molecule at a time. What is the advantage of studying molecular motors one at a time? Traditional biochemical experiments involve large ensembles of enzymes. These so-called 'bulk' experiments provide large amounts of data, but only reflect the ensemble average of the system. Thus, transient kinetic/mechanical events, fluctuations in activity, all of which provide detailed information on motor mechanics tend to be averaged out with bulk experiments. Molecular motors by definition operate within cyclical kinetic events. These events are discrete and generally occur at the piconewton (pN) and nanometer (nm) scale, both of which the optical tweezers is capable of measuring.

1.3.2 Optical tweezer layout

The instrument used in this thesis, nicknamed 'minitweezers', was custom built in the lab by Steven Smith (*35*). The optical layout of the instrument is shown Figure 1.5. There are two unique technical aspects of the minitweezers that should be mentioned. First, the instrument is designed to collect nearly all of the exiting laser light by using high numerical aperture (NA) objectives and a counter-propagating trap. The high NA objectives are used twice, first to focus one laser and again to collect the diverging rays of the second laser. By collecting nearly all of the laser light, the force exerted on a particle trapped by the laser beam can be estimated from first-principles by the change in angular momentum of the laser beam. The counter-propagating trap serves the purpose of preventing scattering forces from pushing the bead out of the trap. Second, the light that forms the trapping spot is circularly polarized by a series of polarizing beam-splitters and quarter-wave plates. The two lasers carry opposite degrees of circular polarization to prevent interference (*35*).

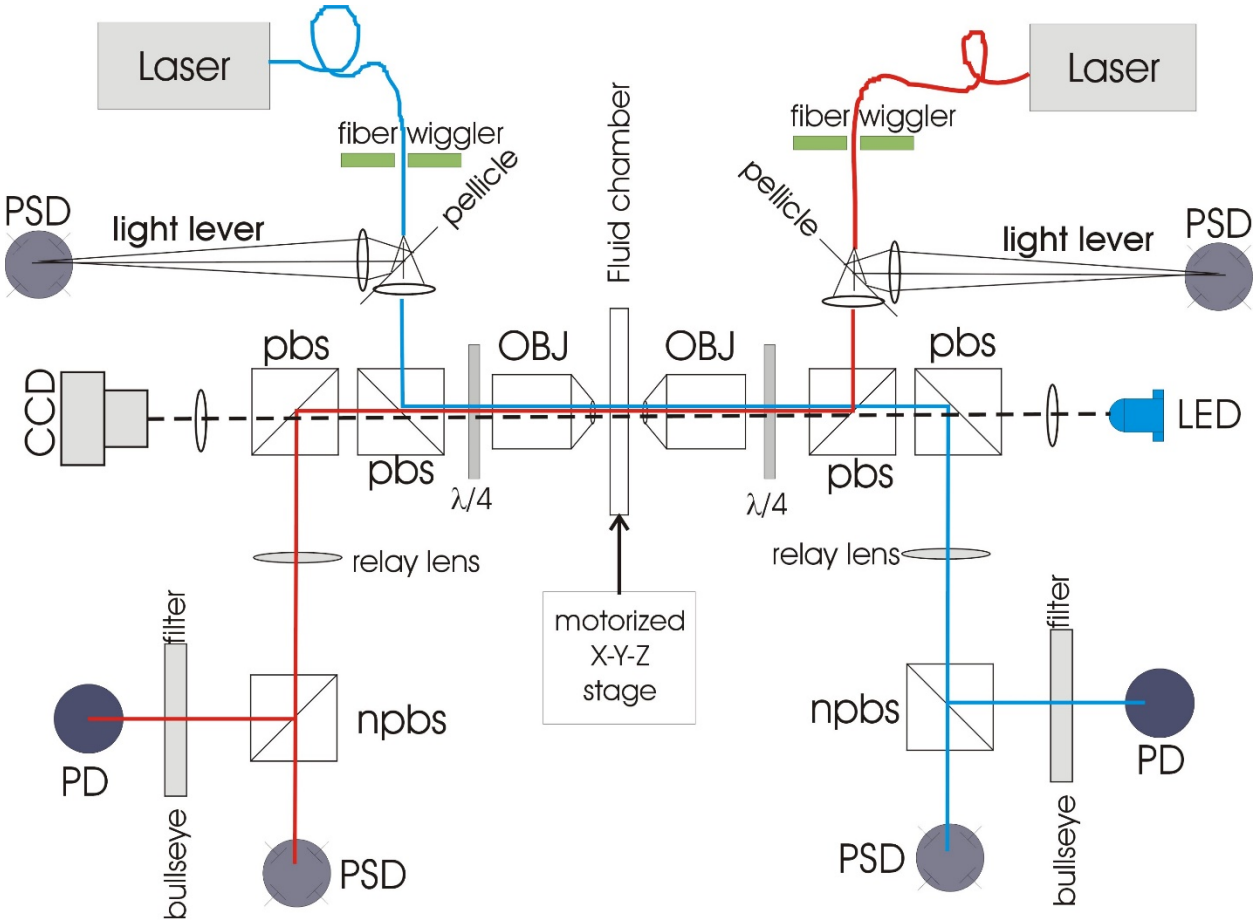

Figure 1.5 Minitweezer Optical Layout

The minitweezers uses two, counter-propagating, 845 nm lasers. Each laser has a set of position sensitive detectors (PSD) that measure the XY displacement, movement of the fiber wiggler and Z displacement for a total of six detectors in the instrument. Non-polarizing beam splitters (npbs) are used to split the laser light into separate detectors. Figure courtesy of Steven Smith.

Another unique aspect of the minitweezers is its small size (giving its namesake), fitting on a table quite nicely. This has allowed relatively easy relocation of the instrument without the accompanying alignment headaches.

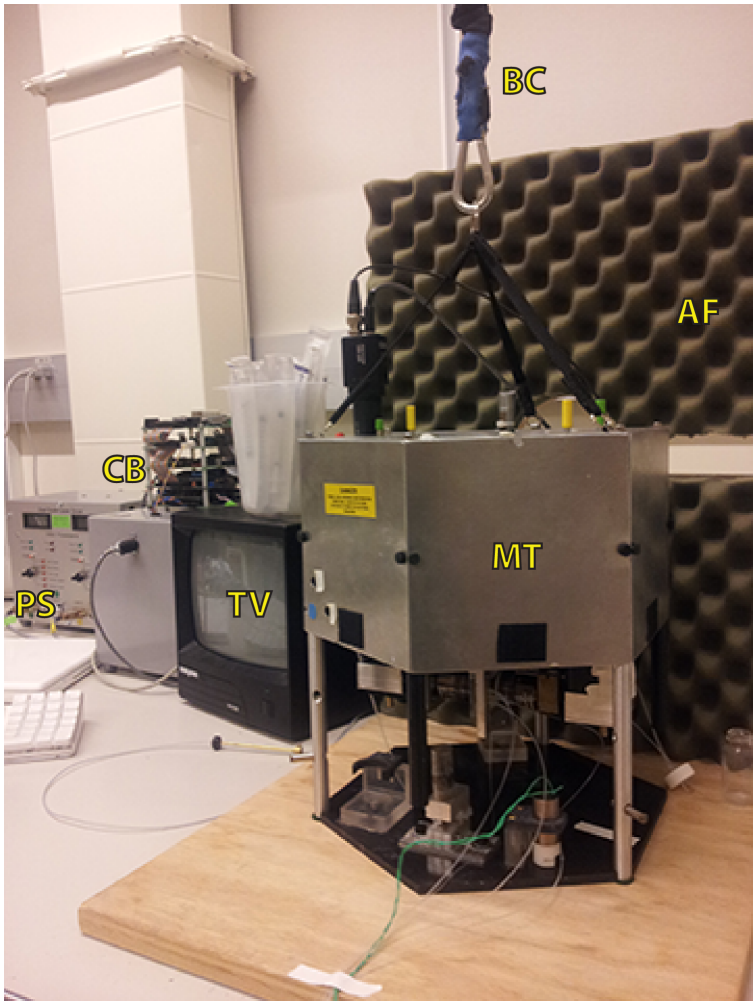

Figure 1.6 The Minitweezers

The minitweezers (MT) is isolated from environmental noise with acoustic foam (AF) and a bungee cord (BC). A television display (TV) is connected to the CCD camera. The controller board (CB) is the main hardware that controls the motorized stage and fiber wiggler movements. The power supply (PS) box for the lasers is shown at the edge of the figure. The complete enclosure is not shown in the figure.

The physics of an optical trap work on a simple principle, light carries momentum. When a micron sized bead with a dielectric constant is placed in the light path, the light is refracted with a corresponding change in momentum that is applied to the bead. If the bead is pulled out of the center of the trap, then the light is refracted further to apply a restoring force to the bead (*36*). The potential well of the laser trap is harmonic, within a certain range there is a linear relationship between force applied to the bead and distance the bead is pulled from the trap center. Thus the most straightforward way to model an optical trap within its linear regime is as a Hookean spring with a spring constant k. Then the force will be described as $F=k\Delta x$, where Δx is the displacement

of the bead from the center of the trap. By measuring how far the bead is displaced from the trap, one can find the force that is exerted on the bead. Determining the stiffness *k*, or trap stiffness, and precise calibration of force measurement is discussed in greater detail in Chapter 5.

Modeling the optical trap as a spring, we can exploit this property to determine the force velocity dependence of a motor. The tweezer geometry used is shown in (Figure 1.7 A). Briefly, a SpoIIIE protein is biotinylated on its N-terminus (Figure 1.2 B) and incubated onto a micron sized streptavidin bead. Separately, a DNA tether is also biotinylated on one end and attached to a streptavidin bead. The DNA substrate used is a shortened segment of commercially available DNA from bacteriophage lambda. These two reagents are incubated separately and the beads containing their respective reagent are spatially separated from the experimental chamber. The protein bound bead is typically held in a micropipette, this is done to prevent laser heating of the sample. The two beads are first brought into close proximity, allowing SpoIIIE to engage the DNA substrate. The beads were then moved apart until the presence of a DNA tether was confirmed by monitoring the force acting on the trapped bead (Figure 1.7 C). Due to the restoring force the bead feels when pulled out of the center of the trap, the force that the motor experiences will be an opposing force. Furthermore, the rate at which the bead is pulled can be converted into velocity.

Note that the experimental set-up involves loading SpoIIIE onto the DNA and forming active translocation complexes in the tweezers. This is generally not possible for other ring NTPases as ring loading is a highly complex process that occasionally involves multiple protein cofactors (*37–39*). In many ways, the single molecule set up mirrors the *in vivo* process of SpoIIIE assembly onto DNA. SpoIIIE is a constitutively expressed protein that is localized to the membrane (*14*, *40*). During septal fusion, SpoIIIE follows the leading edge of the invaginating septum and assembles around the DNA (*15*). SpoIIIE does not have the opportunity to load onto DNA during normal vegetative growth and must be physically brought to close proximity to the DNA by the invaginating septum. An analogy can then be drawn towards immobilizing SpoIIIE onto a bead and physically bringing the protein to close proximity of DNA.

Experiments were performed in either passive mode (Figure 1.8 B), in which the trap position is fixed, or in constant-force mode, in which the trap position was continuously adjusted to maintain a constant tension in the DNA tether (Figure 1.8 A). Both modes carry distinct advantages that should be taken into account when conducting single-molecule experiments. Passive mode allows the user to measure the velocity over a wide range of forces within one experimental pulling trace. The disadvantage such a strategy is the relatively small amount of data points within a single pulling trace, although this can be mitigated if the motor of interest is capable of re-engaging the DNA substrate and generate multiple pulls (Figure 1.8 B). In contrast, constant force mode provides a large amount of velocity data at a fixed force. However, building a force-velocity curve with constant force gets fairly tedious. A major disadvantage of constant force is its use of an active feedback mechanism. Depending on the response time of the feedback, this can introduce artifacts in the apparent motion of the bead (*41*). For the work presented in this thesis, the force-velocity curves were calculated using passive mode. Other aspects of SpoIIIE translocation that warranted a more in-depth analysis at a certain force (e.g. pausing or slipping) was conducted under constant force mode and will be specifically mentioned as such.

The measured displacement of the bead from the trap in nanometers/sec is not meaningful in terms of the motor's biological substrate, DNA. Instead, a more meaningful unit is basepairs/sec (bp/s). The equation for converting extension to base pairs was solved numerically in 1994 when a force-extension relationship was produced for DNA, modeled on the following extensible worm-like chain (WLC) equation (*42*, *43*)

$$\frac{x}{L_0} = 1 - \frac{1}{2}\left(\frac{k_B T}{FP}\right)^{1/2} + \frac{F}{S} \tag{1.1}$$

where x is the end-to-end extension, L_0 is the contour length of DNA, k_B is Boltzmann's constant, T is temperature, F is applied force, P is persistence length of B-form DNA and S is the stretch modulus. The first two terms corresponds to the entropic elasticity of DNA. As x approaches L_0, the DNA can also be stretched past its canonical B-form length; the third term reflects this enthalpic stretching regime (*43*). Typically the persistence length of DNA has been measured to be ~53 nm (*42*, *44*) and stretch modulus is ~1200 pN·nm (*43*, *45*). The persistence length of DNA was also found to be highly dependent on divalent cations (*43*), likely due to ionic bridges forming between the phosphate backbone. In 1x Reaction Buffer (Table 5-1) which contains 10 mM $MgCl^{2+}$, I have measured the persistence length to be closer to 30 nm. There is also an overstretch transition that occurs past 65 pN (*46*) that is not described by Eq. (1.1). This conversion demonstrates the relationship between force and velocity, shown as a force-velocity curve. Force-velocity relationships derived from both passive mode and constant force mode experiments have given similar quantitative results (Figure 1.9).

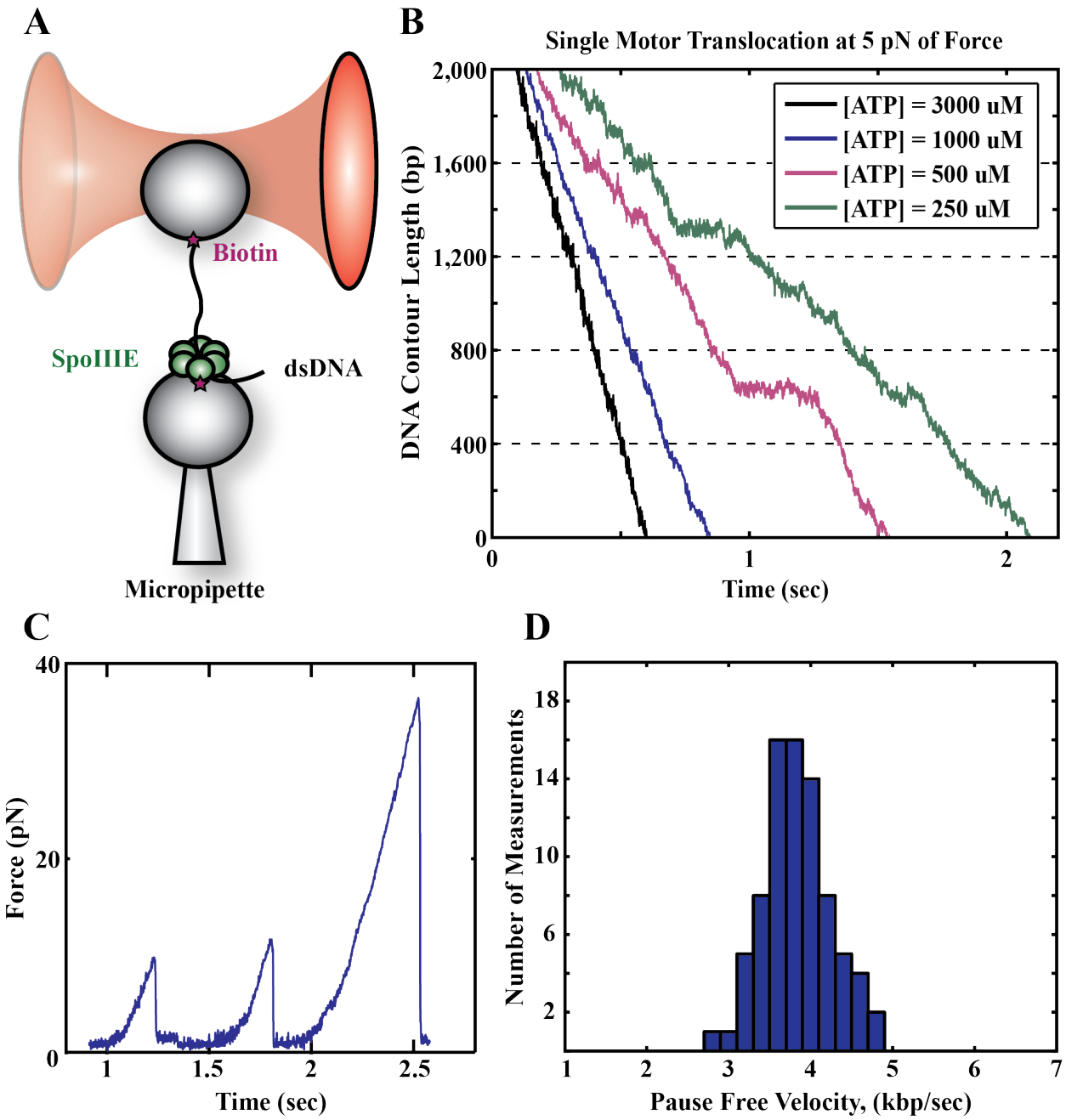

Figure 1.7 Single Molecule Assay of SpoIIIE

(A) Optical tweezer geometry used for single-molecule assays. A SpoIIIE hexamer (green spheres) with an N-terminal biotin (purple star) is immobilized onto a bead which is held in a micropipette. A biotinylated piece of DNA is immobilized on another bead and held in an optical trap.
(B) Representative traces of SpoIIIE translocation at 5 pN of constant opposing force.
(C) SpoIIIE pulling events measured in passive mode at [ATP] = 3 mM.
(D) Histogram of translocation velocity at 5 pN constant force and [ATP] = 3 mM. Velocity was calculated by fitting a line to pause-free regions in 1 kb bins of translocation distance.

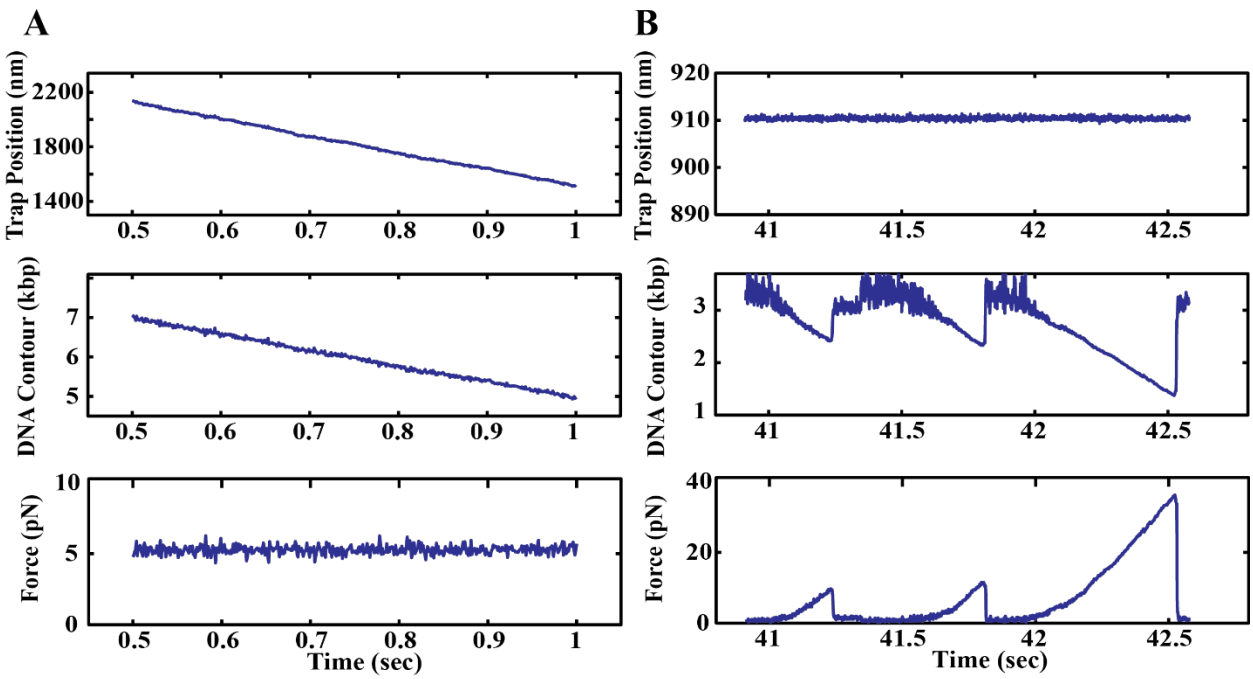

Figure 1.8 Constant Force vs. Passive Mode

(A) Example trace of data taken in constant force mode. The force is held constant at 5 pN (bottom panel) with an active feedback mechanism for the trap position (top panel). The change in DNA contour length is a simple unit conversion (middle panel).

(B) Example trace of data taken in passive mode. The trap position is held constant, SpoIIIE can be seen pulling on the DNA attached to the trapped bead which manifests as an increase in force (bottom panel). A reciprocal change in DNA contour length is calculated via the WLC equation (middle panel).

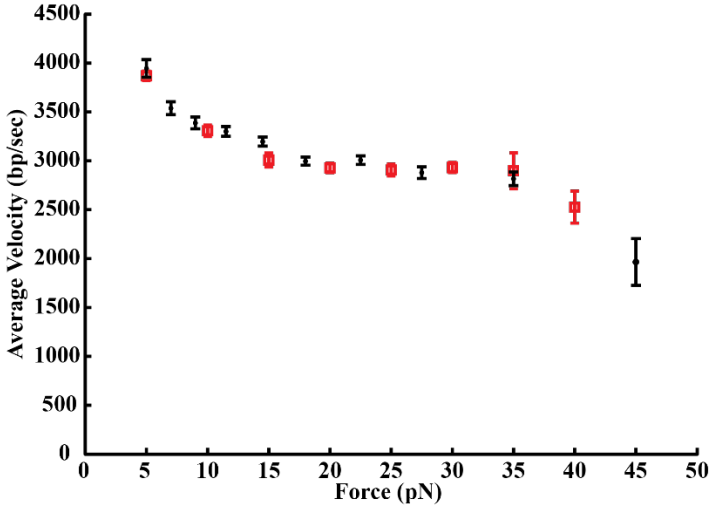

Figure 1.9 Force-Velocity Comparison

A force velocity curve calculated from passive mode (black). Overlayed is a force-velocity curve calculated from constant force mode (red). [ATP]=3mM. Error bars are s.e.m.

1.4 Previous Single-Molecule experiments

Traditionally, simple DNA translocation has been difficult to quantify because there is no chemical signature that accompanies DNA movement. SpoIIIE was first determined to be an ATP dependent DNA translocase by observing the degree of induced supercoiling on a DNA plasmid (*8*). Previous single-molecule experiments on the FtsK/SpoIIIE family of DNA translocases have primarily been done on magnetic tweezers, focusing on sequence recognition and directionality of DNA transport (*12*, *23–25*). The magnetic tweezers set-up for these experiments has a DNA molecule tethered and held under tension between a glass coverslip and a magnetic bead. Free protein is then flowed into the chamber along with ATP and other reagents needed for activity, which is defined by a decrease in the height of the bead. However, simple translocation of a motor protein along a DNA tether would not decrease the height of bead; a free protein moving along DNA has no attachment point to anchor itself on. The result of a bead height decrease is interpreted as the formation of a DNA loop, requiring the motor protein to make at least two points of contact on the DNA tether. These experiments have demonstrated that specific 8-mer sequences on the DNA can impart directionality to DNA translocation, thus allowing the motor protein to move the DNA in the proper direction. The two 8-mer sequences characterized thus far are Fts**K** **O**rienting **P**olar **S**equence (KOPS) for FtsK and **S**poIIIE **R**ecognition **S**equence (SRS) for SpoIIIE (*12*, *23*). The recognition sequences are recognized by the γ domains of both FtsK and SpoIIIE and are specifically recognized only by their respective protein. Amazingly, Ptacin et al. has demonstrated that the γ domain is a modular domain by replacing the SpoIIIE γ domain with the γ domain from FtsK, creating a chimeric SpoIIIE protein that was now capable of recognizing KOPS but not SRS (*12*).

In the process of determining sequence recognition, these experiments have also characterized some basic mechanical properties of these motor proteins, including velocity of translocation and force generation, which will be discussed in greater detail later. A distinguishing feature of this class of DNA translocases is its incredible speed of translocation, on the order of 4-6 kb/sec, and ability to work against 40-50 pN of force (*12*, *24*, *28*). In comparison other DNA translocases typically translocate DNA on the order of hundreds of basepairs/sec (*47*, *48*). The kinesin motor has been shown to walk at high speeds, on the order of 500 nm/sec with a stall force of about ~5 pN (*49*). It would be of great interest to understand the mechanism by which SpoIIIE accomplishes this remarkable mechanical task. Given the conserved structural core of ring NTPases, the mechanisms of SpoIIIE translocation could potentially be widely applicable to other members of the ASCE family.

1.4.1 Open questions – Mechanochemistry

All motor proteins generate force during its mechanochemical cycle. During translocation each subunit of SpoIIIE undergoes repeated cycles consisting of a well-defined sequence of chemical events such as ATP binding, ATP hydrolysis, phosphate and ADP release. To ensure processive DNA translocation, these chemical events are coupled to a sequence of mechanical events such as engaging the DNA substrate, executing the power-stroke motion to push DNA, dis-engaging the DNA substrate, and resetting the subunit in preparation for the next cycle. Determining the location of the force generating transition is a basic first step towards understanding motor function. Since the generation of force requires a physical motion of the protein, at least one of the kinetic events mentioned is coupled to a conformational change of the

protein that generates force. Conversely, applying an opposing force will slow the motor down in one of two ways. Opposing force can decouple a chemical transition from mechanical motion, ie. A force dependent coupling efficiency, or slow down the rate of the mechanochemical transition, ie. A force dependent rate constant. The functional dependence of the motor velocity on the applied force and chemical concentrations can be used to identify the relative locations of ATP binding, product release, and force generation – the outline of the mechanism for translocation (*7*, *50*) .

A preliminary force velocity curve was obtained for FtsK (*28*) and showed that at saturating ATP concentration, velocity was force-insensitive at a low force regime (8-15 pN) and displayed a force-sensitive transition at a force >15 pN. The velocity continued to decrease up until 40 pN which was the limit of the force range tested. Interestingly, no such transition was seen when ATP concentration was lowered to 1 mM. The force insensitive regime suggested that there was a rate-limiting biochemical step in the mechanochemical cycle that was not the force-generating step. However, the actual force generating step was not able to be determined as only two ATP conditions were tested.

A more complete set of force velocity curves was obtained for a related DNA translocase, the bacteriophage φ29-gp16 packaging motor (*51*). Experiments were performed on an optical tweezers set-up where the prohead-motor-DNA complex was attached to a polystyrene bead and the other end of the DNA was attached to another bead that is placed in an optical trap. Introducing ATP induces DNA packaging, shortening the DNA between the two beads. Initial single-molecule work determined that the φ29 motor can package DNA up to a force of ~60 pN (*47*), one of the highest stall forces recorded for a motor protein. Later work done by Chemla and Aathavan et al. (*51*) built a thorough set of force velocity curves at varying [ATP], [ADP] and [Pi] concentrations. Briefly, the authors found that the phage was force sensitive at a high [ATP] regime and force insensitive at low [ATP]. Since ATP binding rate should not be rate limiting at saturating ATP, the force-generating step is not coupled to the ATP binding step. Furthermore, the force behavior of the various Michaelis-Menten constants showed that any step reversibly connected to ATP also cannot be the force generating step, which suggests that the location of the step occurs after the first irreversible transition following ATP binding. Supplementing this result, the authors further showed that ADP acts as a competitive inhibitor to velocity and that P_i has little effect. Since ADP can be reversibly bound to the motor and P_i release is irreversible, these results in conjunction suggest that the force generating step is coupled to Pi release for φ29. There are however, key differences between the phage motor and the SpoIIIE motor, chief among them is their oligomeric state. The φ29 motor has been shown to form a pentameric ring in cryo-EM studies (*52*), in addition its translocation rate is ~40 times slower than SpoIIIE (*47*). Both motors belong to the same family of DNA translocases, yet these extreme differences in translocation velocity and ring architecture highlight differing mechanical strategies that are employed by ring NTPases.

1.4.2 Open questions – Intersubunit Coordination

Inter-subunit coordination is a critical component of the mechanism of ring NTPases. While generation of mechanical work is a common feature of molecular motors, the timing and order of individual power strokes applies this work in a nuanced manner to better suit particular biological tasks. Like most ring NTPases, SpoIIIE's active form is a homomeric ring of six individual subunits (*10*), with each subunit capable of binding and hydrolyzing NTP. Since each ring is composed of six identical subunits, a natural question to ask is whether there exists any

intersubunit coordination. Literature on subunit coordination in homomeric ring NTPases have increased steadily for the past 10 years with three basic models being proposed (*31*).

1. Sequential – In a sequential model, NTP hydrolysis would proceed in a clockwise or counterclockwise fashion around the ring, NTP hydrolysis events must be coordinated spatially. A subunit cannot begin its NTP hydrolysis cycle until a previous subunit has reached a certain part of its NTP cycle. The most common model in the literature, examples of sequential have been shown for many helicases (*53–55*), the φ29 packaging motor (*56*), and F1-ATPase (*57*) (Figure 1.10 A, B).
2. Concerted – In a concerted model, all subunits bind and hydrolyze ATP in an all-or-nothing fashion. Concerted models would require both spatial and temporal coordination between the disparate subunits within a ring. The SV40 large T-antigen has been proposed to work as a concerted model (*58*) (Figure 1.10 C).
3. Stochastic – A stochastic model would not display any sort of coordination. The activity of each subunit would be independent of other subunits within the ring. Targeted mutagenesis experiments on the protein translocase ClpX have shown that ring activity decreased linearly with the number of subunits inactivated, suggesting a stochastic model of ring activity (*59*). Recent results have changed the view of ClpX to show that individual subunits do display a partially coordinated mechanism (*5*, *6*) (Figure 1.10 D).

These three models serve as generalized starting points to describe subunit coordination. One can imagine more exotic variations of the three models listed above. It is not difficult to postulate on different degrees of subunit coordination that are better suited to particular biological tasks. For example, phage packaging motors must package DNA against a large internal pressure, thus a coordinated mechanism would help the motor maintain a constant grip on its DNA substrate, preventing DNA leakage. The φ29 packaging motor displays coordination on multiple levels, containing elements of concerted, sequential, and even a departure from the three 'canonical' models with a special subunit that does not participate in translocation (*33*). Semi-concerted models for protein translocases/unfoldases have been proposed to strike a delicate balance between the flexibility required for translocating a heterogeneous polypeptide track and the coordination required for robust protein unfolding (*6*). However, there is no detailed analysis of intersubunit coordination for fast dsDNA translocation. What strategies SpoIIIE might employ to accomplish this task of fast (~4 kb/sec) translocation is an open question.

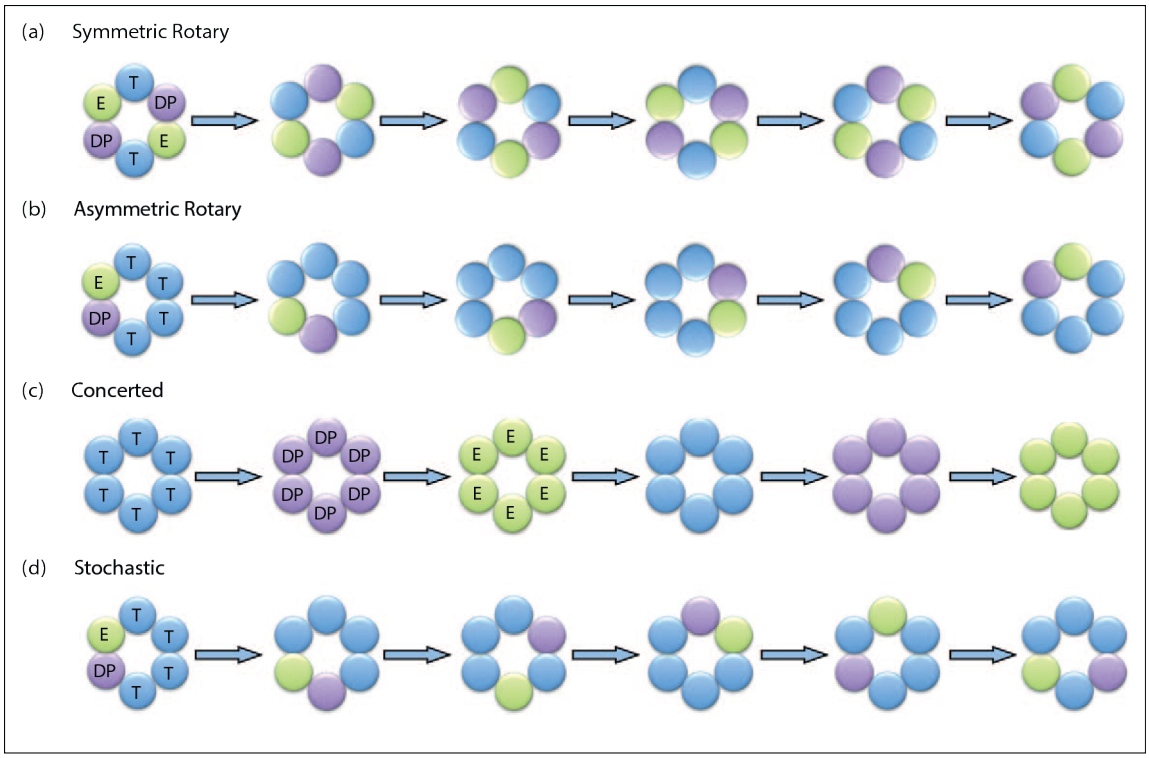

Figure 1.10 NTP Hydrolysis Models for Ring NTPases

NTP states are labeled as E: empty (green), T: NTP bound (blue); DP: NDP + P_i (purple)
(a) Symmetric rotary model where two hydrolysis events proceed sequentially around the ring.
(b) Asymmetric rotary model
(c) Concerted or 'all-or-nothing' model
(d) Stochastic or an uncoordinated model.
Figure reprinted from Lyubimov et al. (*31*) with permission from Elsevier © 2011.

Chapter 2 Mechanochemistry of SpoIIIE

Background

Force generation is a fundamental aspect of molecular motors. Within a single chemical cycle of NTP binding, hydrolysis, and product release, at least one step is coupled to force generation. Determining the chemical transition responsible for generating mechanical work is termed mechanochemistry and is a crucial step towards understanding the mechanisms powering molecular motor function. Recently there has been several studies published on ring motor mechanochemistry in exquisite detail. The φ29-gp16 bacteriophage packaging motor published an exhaustive set of single-molecule experiments demonstrating that inorganic phosphate (P_i) release is tightly coupled to the force generating step (*51*). Further experimentation has also revealed that ATP binding and ADP release events are interlaced, adhering to a strict one to one correspondence of ATP binding followed by ADP release (*33*). P_i release was found to be the rate limiting step for several related ring translocases, including the T7 DNA helicase (*60*), the NS3 RNA helicase (*61*), and Rho helicase (*62*) using rapid mixing pre steady-state kinetics. The force-generating step for these helicases is proposed to be nucleotide binding for T7 and Rho (*60*, *62*), and Pi release for NS3 (*61*). Fluorescent measurements of the F1-ATPase mechanochemical cycle revealed a unique cycle where a single 120 degree rotation is comprised of two substeps; with ATP binding providing the energy for the first 80 degree rotation and last 40 degrees coupled to P_i release (*63*).

Motor mechanochemistry can broadly be classified as either a Brownian ratchet or a power stroke. Generally speaking Brownian ratchets function by utilizing chemical energy from NTP hydrolysis to rectify or bias large thermal fluctuations of the motor, whereas power strokes couple the conformational changes induced by NTP hydrolysis to mechanical work (*64*). These definitions however, are not mutually exclusive as all molecular motors operating in an environment dominated by thermal fluctuations will contain elements of both (*65*). Imprecise as these labels are, identifying a motor as a Brownian ratchet or power stroke motor is still an important first step towards a basic characterization of motor mechanochemistry.

2.1 Single-Molecule Force-Spectroscopy

2.1.1 P_i Release is coupled to the Force-Generating Transition

To identify the location of the force generating step, the functional dependence of SpoIIIE translocation against opposing force was determined under various concentrations of ATP, ADP, and P_i. At a low opposing force of 5pN the average SpoIIIE translocation velocity as a function of ATP was well described by a Michaelis-Menten dependence, with V_{max} = 4700±140 bp/s, and K_m = 505±50 μM (Figure 2.1 C). A fit to the generalized Michaelis-Menten Hill equation

$$v = \frac{V_{max}[S]^n}{K_M^n + [S]^n} \tag{2.1}$$

yielded a Hill coefficient of $n = 1 \pm 0.5$ at 5 pN of external force. A Hill coefficient of 1 does not necessarily mean that a hexameric ring can only bind one ATP at any given time, rather it suggests ATP binding events are independent from one another (*51*). The ATP dependence of the mean translocation velocity was well fit by the simple Michaelis-Menten equation across the entire range

of external forces. During translocation each subunit of SpoIIIE undergoes repeated cycles consisting of a well-defined sequence of chemical events such as ATP binding, ATP hydrolysis, phosphate and ADP release. To ensure processive DNA translocation, these chemical events are coupled to a sequence of mechanical events such as engaging the DNA substrate, executing the power-stroke motion to push DNA, dis-engaging the DNA substrate, and resetting the subunit in preparation for the next cycle. The following kinetic scheme illustrates a generalized mechanochemical cycle of a ring ATPase that includes the transitions listed above.

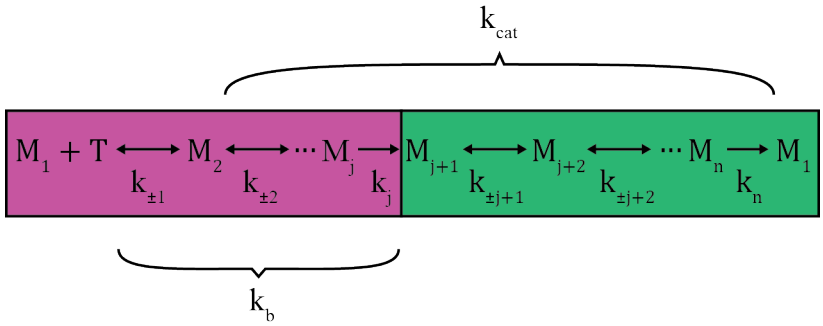

(2.2)

The above kinetic scheme can roughly be divided into two kinetic 'blocks', the first block consists of all rate constants $k_{\pm1}$, $k_{\pm2}$… up to the first irreversible transition k_j (purple rectangle). The second block comprises the remaining rate constants after k_j (green rectangle). It has previously been shown that the net rate of ATP binding, k_b, is a function of individual ATP binding rates as well as any transitions that are reversibly connected to ATP binding ($k_{\pm1, 2, ...}$) for each subunit. The Michaelis-Menten parameter V_{max} is shown to be dependent on all rate constants except the ATP binding rate $k_{\pm1}$ and the ratio of V_{max}/K_m is equal to k_b, thus V_{max}/K_m is comprised of rates in the first kinetic block. An external opposing force applied to the ring can act as an inhibitor to the force-generating transition (*50*). The force dependency of V_{max}/K_m can then be used to determine whether the force generating transition resides in either the first or second kinetic block (*7*, *50*, *51*). The observed force independence of V_{max}/K_m (Figure 2.1 B) for SpoIIIE indicates that ATP binding or any subsequent transition reversibly connected to ATP binding does not power the force-generating transition. Therefore the power-stroke must occur past the first irreversible transition after ATP binding (i.e. kinetic block 2) (*7*, *50*). The identity of the first irreversible transition is generally believed to be the tight binding of ATP, as has been shown for other ATPases (*51*, *63*, *66*).

To investigate the role of product release in the mechanochemical cycle, I titrated in free ADP and P_i. Passive-mode experiments were performed at different ADP and ATP concentrations (Figure 2.2 A). The pause-free DNA translocation velocity decreased significantly as [ADP] was titrated from 75 µM to 1 mM and [ATP] was kept constant at 3 mM (Figure 2.2 B). For a given [ADP] and opposing force, the translocation velocity dependence on [ATP] was well fit by a simple Michaelis-Menten dependence. At a low external force of 5 pN, the V_{max} remained constant as a function of [ADP] while the apparent K_m increased linearly with [ADP], consistent with ADP acting as a competitive inhibitor to ATP binding (Figure 2.2 C). Fits to a competitive inhibition model yielded a dissociation constant K_d = 129 µM for ADP release from the SpoIIIE complex. Titrating in P_i had little effect on translocation velocity. Even at the highest Pi concentration of 10 mM the pause-free DNA translocation velocity decreased by only ~12% (Figure 2.2 D), indicating that Pi release is largely irreversible with a K_d>>10mM. To determine whether ADP or P_i release

is coupled to the force-generating step, I estimated the free energy changes for both of the product release events based on the K_d values. The estimated the step size of SpoIIIE is 2 bp as will be shown in Chapter 3. The maximum force that I have seen SpoIIIE pull against is 50 pN, therefore the SpoIIIE motor must generate at least 50 pN · 0.68 nm or $\Delta G = 8.2\ k_BT$ of work per step. To calculate the free energy produced from product release, we first start off with a basic enzymatic reaction

$$E \cdot P \rightarrow E + P \tag{2.3}$$

where the enzyme product complex $E{\cdot}P$ releases its product P. The Gibbs free energy of product release is then

$$\Delta G = k_B T ln\left(\frac{[E]}{[EP]}\right) \tag{2.4}$$

Where k_B is Boltzmann's constant. We define the dissociation constant K_d as

$$K_d \equiv \frac{[E][P]}{[EP]} \tag{2.5}$$

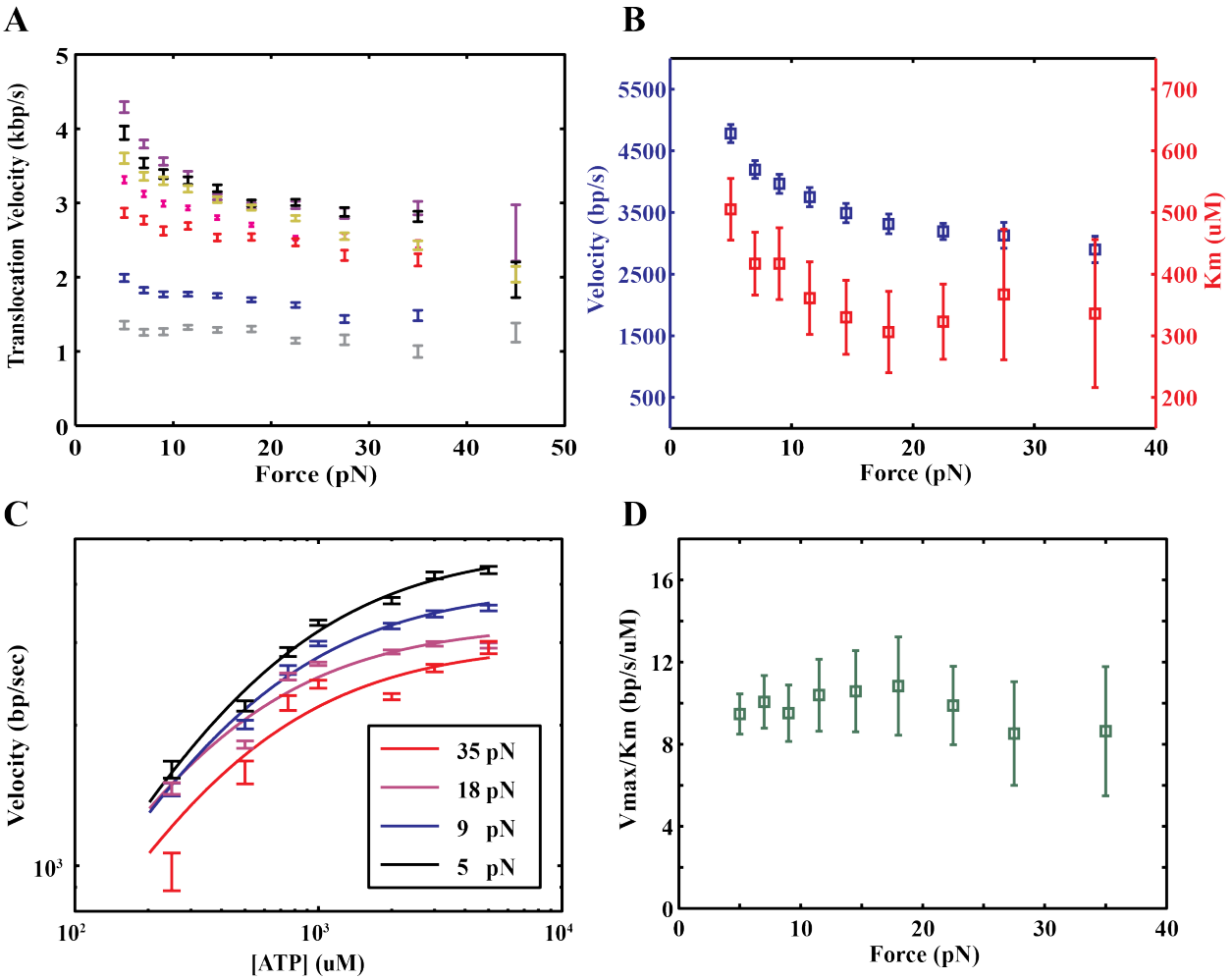

Figure 2.1 Effects of Opposing Force on Vmax and Km

(A) Force velocity curves for SpoIIIE gathered under passive mode for [ATP] = 5, 3, 2, 1, 0.75, 0.5, 0.25 mM (purple, black, yellow, pink, red, blue, gray, respectively). Error bars are s.e.m.
(B) Calculated K_m and V_{max} behavior from fits to Michaelis-Menten equation. Error bars are standard error of the fits
(C) Michaelis-Menten fits at different opposing forces.
(D) Vmax/Km ratio plotted over opposing forces. Error bars are obtained from fits.

Substituting in to Eq. (2.4) will give an expression for the free energy with respect to K_d and product.

$$\Delta G = k_B T ln\left(\frac{K_d}{[P]}\right) \tag{2.6}$$

With a K_d of 129 μM for ADP, the change in free energy from ADP release is $\Delta G_D = k_B T \ln(129/5) = 3.2\ k_B T$ (at [ADP]=5 μM). Conversely the free energy change for P_i release is $\Delta G_P >> 7.6\ k_B T$. Based on energetic considerations, we can assign P_i release as the identity of the force-generating step.

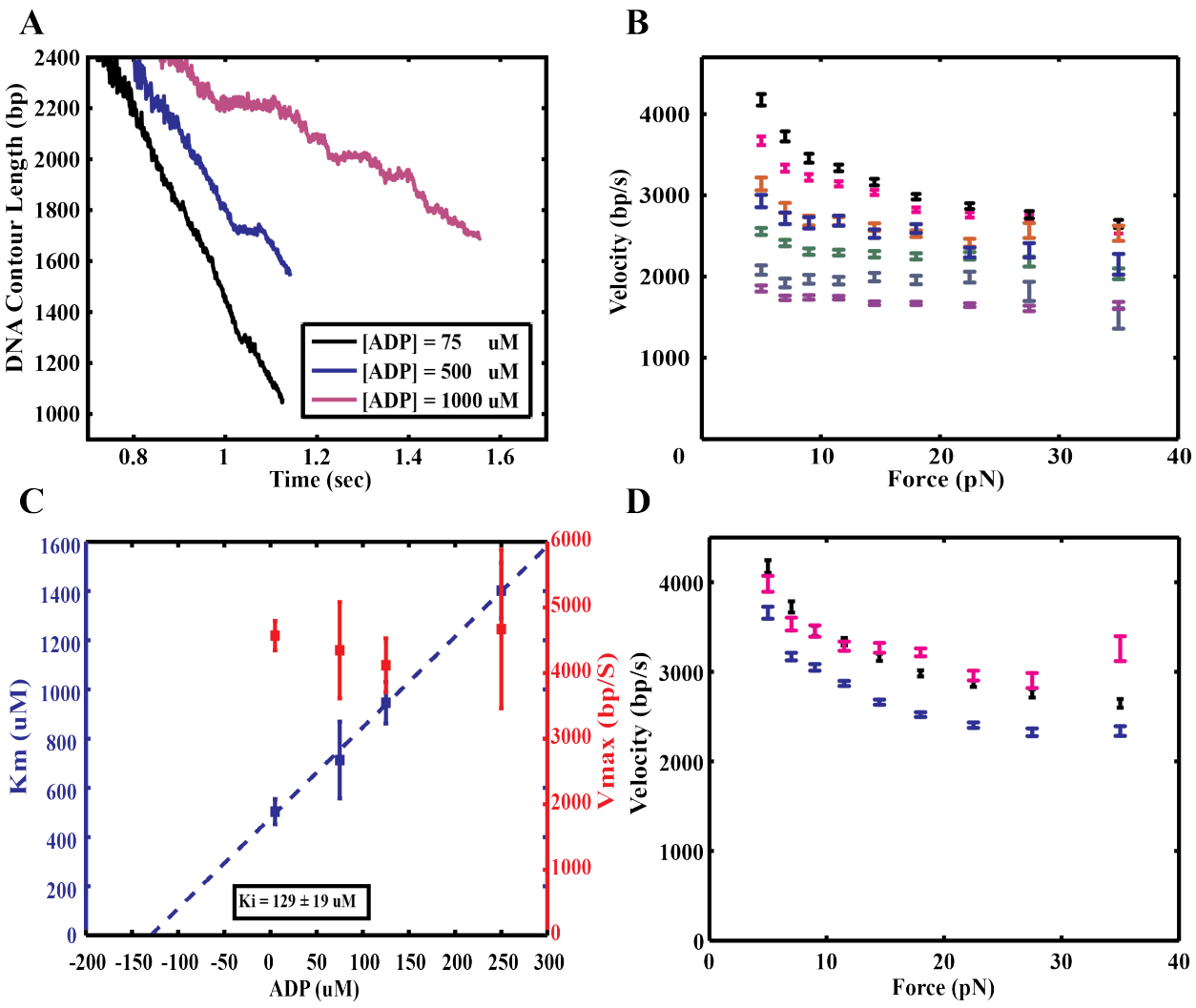

Figure 2.2 ADP and Pi Titrations

(A) Representative SpoIIIE traces at various [ADP] and [ATP] = 3 mM. Traces were gathered in passive mode.

(B) Force-velocity behavior of SpoIIIE at [ADP] = 5, 75, 125, 250, 500, 750 and 1000 uM (Black, pink, red, blue, green, cyan, purple) at 3 mM ATP. Traces were collected in passive mode. Error bars are S.E.M.

(C) V_{max} and K_m plots from simple Michaelis-Menten fits of pause free SpoIIIE velocity at 5 pN of opposing force at [ADP] = 5, 75, 125, 250 uM. Error bars are standard error. Dotted line is a linear fit to a competitive inhibition model.

(D) Force velocity behavior when [Pi] = 5, 3000, 10000 uM (black, pink, blue) at 3 mM ATP.

2.1.2 Possibility of a secondary force generating step

As shown in Chemla et al. (*51*) and proved in Derrida (*67*), an *N* state kinetic cycle with microscopic rate constants $k_{\pm 1}, k_{\pm 2}, \ k_{\pm j} \ and \ k_{\pm n}$,

$$M_1 \underset{k_{\pm 1}}{\longleftrightarrow} M_2 \underset{k_{\pm 2}}{\longleftrightarrow} \cdots M_j \underset{k_{\pm j}}{\longleftrightarrow} \cdots M_n \underset{k_{\pm n}}{\longleftrightarrow} M_1 \tag{2.7}$$

is equivalent to a one-dimensional hopping model. The steady-state velocity *v* is then

$$v = \frac{d}{\sum_{i=1}^{n} \frac{1}{u_i}} \left[1 - \prod_{i=1}^{n} \frac{k_{-i}}{k_i} \right] \tag{2.8}$$

where *d* is the step size and u_i is given by

$$\frac{1}{u_i} = \frac{1}{k_i} \left[1 + \sum_{l=i+1}^{n+i-1} \prod_{m=i+1}^{l} \frac{k_{-(m-1)}}{k_m} \right] \tag{2.9}$$

For simplicity, let us consider a kinetic scheme where there are two irreversible steps, as is shown in Eq. (2.2). We can now set k_{-j} and k_{-n} to 0 and ignore the second term for Eq. (2.8), furthermore all terms where $l > j$ will vanish. The equation for velocity is now

$$v = \frac{d}{\sum_{i=1}^{n} \frac{1}{u_i}} \tag{2.10}$$

and the binding rate constant k_b for ATP will depend on the docking rate $k_{\pm 1}$, as well as all rates up to the first irreversible step k_j. The catalytic rate k_{cat} is the sum of all rate constants except the ATP docking step $k_{\pm 1}$, as is shown in Eq. (2.2). To relate Eq. (2.8) to Michaelis-Menten kinetics, consider a simple enzymatic reaction where

$$E + S \underset{k_{\pm 1}}{\longleftrightarrow} E \cdot S \underset{k_2}{\rightarrow} E + P \tag{2.11}$$

the solution to Eq. (2.8) is then

$$v = \frac{d}{\frac{1}{k_1[S]} + \frac{k_{-1}}{k_1[S]k_2} + \frac{1}{k_2}} \tag{2.12}$$

where k_1 is considered a second order binding rate constant for *S*. For ensemble systems, the step size *d* is replaced with total enzyme $[E_T]$ giving

$$v = \frac{[E_T]}{\frac{1}{k_1[S]} + \frac{k_{-1}}{k_1[S]k_2} + \frac{1}{k_2}} \tag{2.13}$$

A judicious rearrangement of terms will yield the equation

$$v = \frac{k_2[E_T][S]}{\frac{k_{-1}+k_2}{k_1}+[S]}; v = \frac{V_{max}[S]}{K_M+[S]} \tag{2.14}$$

where we introduce $V_{max}=k_2[E_T]$ and $K_M=(k_{-1}+k_2)/(k_1)$ to arrive at the expected Michaelis-Menten dependence. This can be extended to any *N* state kinetic model as long as there is an irreversible transition in the enzymatic cycle.

It has already been demonstrated that P_i release is the likely identity of the force-generating step and is irreversible. A simplified kinetic model including this force-generating step is as follows,

$$M_1 + ATP \underset{k_{\pm 1}}{\longleftrightarrow} M_2 \underset{k_2}{\rightarrow} M_3 \underset{k_{\pm 3}}{\longleftrightarrow} M_4 \xrightarrow[k_4(F)]{} M_5 + P \underset{k_5}{\leftrightarrow} M_1 + D \tag{2.15}$$

where *P* is phosphate, *D* is ADP and M_N are kinetic states of the motor. It is generally believed that phosphate release occurs before ADP release as phosphate makes far fewer hydrogen bonds than ADP (*60*). While this assumption is not true for all motors, I will show later in the chapter that the long lifetimes of ADP induced pauses do suggest ADP release as rate-limiting. Note also that the release of phosphate is considered irreversible and ADP release is reversible. A velocity equation in terms of [ATP], [ADP] and opposing force can now be written as,

$$\frac{1}{v} = \frac{1}{d}\left[\frac{1}{k_b[ATP]}\left(1 + \frac{[D]}{K_D}\right) + \frac{1}{k_{cat}(F)}\right],\ k_{cat}(F) = \frac{k_{cat}^0}{\mathrm{p+q}\cdot e^{F\Delta x/k_BT}} \tag{2.16}$$

where K_D is the equilibrium dissociation constant for ADP, k_{cat}^0 is the catalytic rate constant at zero opposing force, Δx is the distance to the transition state and *p* and *q=1-p* are weighted values given to the biochemical and mechanical portions of the catalytic cycle respectively (*51*, *68*). The Boltzmann-like term $e^{F\Delta x/k_BT}$ arises from Kramer's rate theory which models chemical reactions as a one-dimensional energy landscape with parabolic energy wells (Figure 2.3). The rate of a reaction is then limited by diffusion across the activation barrier. If a force is applied in the same direction as the reaction coordinate, the height of the activation barrier and overall shape of the energy landscape can be tilted by force (*50*, *69*, *70*). Calculating the force-dependent rate of a reaction is equivalent to the first-passage time of a particle crossing a harmonic potential well under the effect of force (*70*). For a transition from state *A* to *B*, the force dependent rate constant is,

$$k_{A\rightarrow B}(F) = k_{A\rightarrow B}^0 \cdot exp\left(\frac{F\Delta x_{A\rightarrow B}^{\ddagger}}{k_BT}\right) \tag{2.17}$$

where $k^0_{A\to B}$ is the rate constant at zero force and $\Delta x^{\ddagger}_{A\to B}$ is the distance to the transition state along the reaction coordinate. At sufficiently high forces, the energy landscape can be tilted to the point where the reverse reaction is favored.

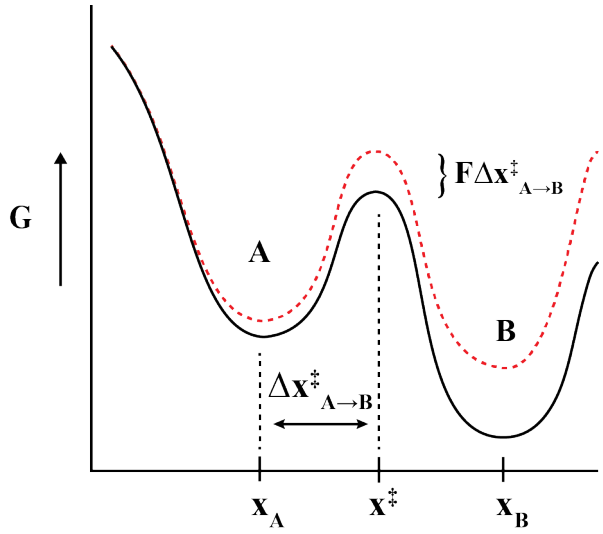

Figure 2.3 Force Tilts the Energy Landscape

An energy landscape under zero force (solid black line) where the enzyme in state A must cross an energy barrier to state B. An opposing force tilts the energy landscape (red dotted line), increasing the height of the activation barrier and thus slowing the rate of the reaction. Y axis is Gibbs free energy, X axis is the reaction coordinate.

At a given [ATP] and negligible [ADP], Eq. (2.16) can be simplified to

$$v(F) = \frac{d}{A + B \cdot exp\left(\frac{F\Delta x^{\ddagger}}{k_B T}\right)} \tag{2.18}$$

where *A* and *B* are now composite rate constants that correspond to the force insensitive and force sensitive parts of the mechanochemical cycle respectively. Note that this dependence implies a tight coupling between a chemical transition and the power stroke, in other words, one power-stroke is executed for every P_i molecule released in the case for SpoIIIE. Because of this tight coupling, one can slow down the power-stroke chemically – by maintaining a large Pi concentration in the buffer, which will reduce the net Pi release rate, or mechanically – by applying a large opposing force against the motor, which will slow down the power-stroke and therefore slow down Pi release.

The force velocity curves for SpoIIIE display an atypical behavior. It contains two force-dependent transitions and one force-independent transition. Similar force velocity curves were observed for the lambda phage packaging motor (*71*). The force-velocity curves for lambda phage were fit to a two exponential decay function, interpreted as two force-generating steps. A model with a single tightly-coupled force-generating transition cannot explain both the low-force sensitivity and the high-force insensitivity exhibited in the SpoIIIE velocity curves at near-saturating [ATP]. Fitting the force-velocity data at 3 mM ATP to Eq. (2.18) predicts a motor that highly insensitive to force, with the translocation velocity only approaching negligible rates (<100

bp/s) at ~400 pN (Figure 2.4 A). For a motor with an estimated step size of 2 bp, this stall force would require each step to generate 200 pN·nm of work, far greater than the estimated 100 pN·nm of free energy available from ATP hydrolysis in my experimental conditions. Because a single force-generating transition would require steps to produce more work than is available from a molecule of ATP, this model was discarded. A model with two tightly coupled force-generating transitions is also inconsistent with the data, as the force-dependency would be dominated by the rate-limiting force-generating transition, producing similar qualitative behavior to a single force-generating transition (Figure 2.4 B).

The most parsimonious model that can describe the results is a hybrid model with a tightly coupled force-generating transition with a step-size d_{TC} and a loosely coupled force-generating transition with a step-size d_{LC}. A loosely coupled transition is defined by its coupling ratio, the number of NTP molecules hydrolyzed that will lead to a productive mechanical transition. Tightly-coupled transitions have a coupling ratio $\varepsilon=1$ (ie. one to one correspondence of NTP hydrolysis and physical steps), loosely coupled would then have $\varepsilon\leq 1$. In the case of molecular motors, the coupling ratio is force-dependent (*50*, *72*, *73*). The kinesin and myosin steppers have been proposed to be a loosely-coupled motor (*49*, *74*, *75*), though for kinesin this view has changed to a tightly coupled one (*68*, *76*). This hybrid model predicts a velocity dependence on force

$$v_1(F) = \frac{d_{TC}+d_{LC}\cdot\varepsilon(F)}{A+B\cdot exp\left(\frac{F\Delta x^{\ddagger}_{TC}}{k_B T}\right)} \tag{2.19}$$

where $\varepsilon(F)$ is the force-dependent coupling of the loosely coupled state. The decrease in SpoIIIE velocity at low-medium force is captured by a simple one-step decoupling process

$$\varepsilon(F) = exp\left(-\frac{F\Delta x^{\ddagger}_{LC}}{k_B T}\right) \tag{2.20}$$

The velocity plateaus seen at 15-40 pN (Figure 2.1 A) and the subsequent drop in velocity at higher forces is captured by the ratio B/A, which must be very small (<0.001), suggesting a rate-limiting chemical transition in addition to the force-generating transition (*77*), as well as the distance to transition state for the tightly-coupled power-stroke $\Delta x^{\ddagger}_{TC}$. The calculated $\Delta x^{\ddagger}_{TC} \approx 1.0\,nm$, $\Delta x^{\ddagger}_{LC} \approx 0.8\,nm$, and $d_{LC}/d_{TC} \approx 1$. Interestingly, the predicted force where SpoIIIE translocation approaches negligible rates (i.e. stall force) is around 60 pN. It must be recognized that the calculated Δx from the fit is larger than the estimated step size of SpoIIIE. However, the calculated Δx assumes a one-dimensional energy landscape as described by Kramer's rate theory. It is possible that SpoIIIE must enter another energy minima orthogonal to the classic energy landscape before taking a step. Another possibility is that Eq. (2.19) carries six free floating parameters and thus the fit is not well-constrained. In this case, it would be more meaningful to calculate the ratio of $\Delta x^{\ddagger}_{TC}$ and $\Delta x^{\ddagger}_{LC}$ instead of looking at the absolute numbers.

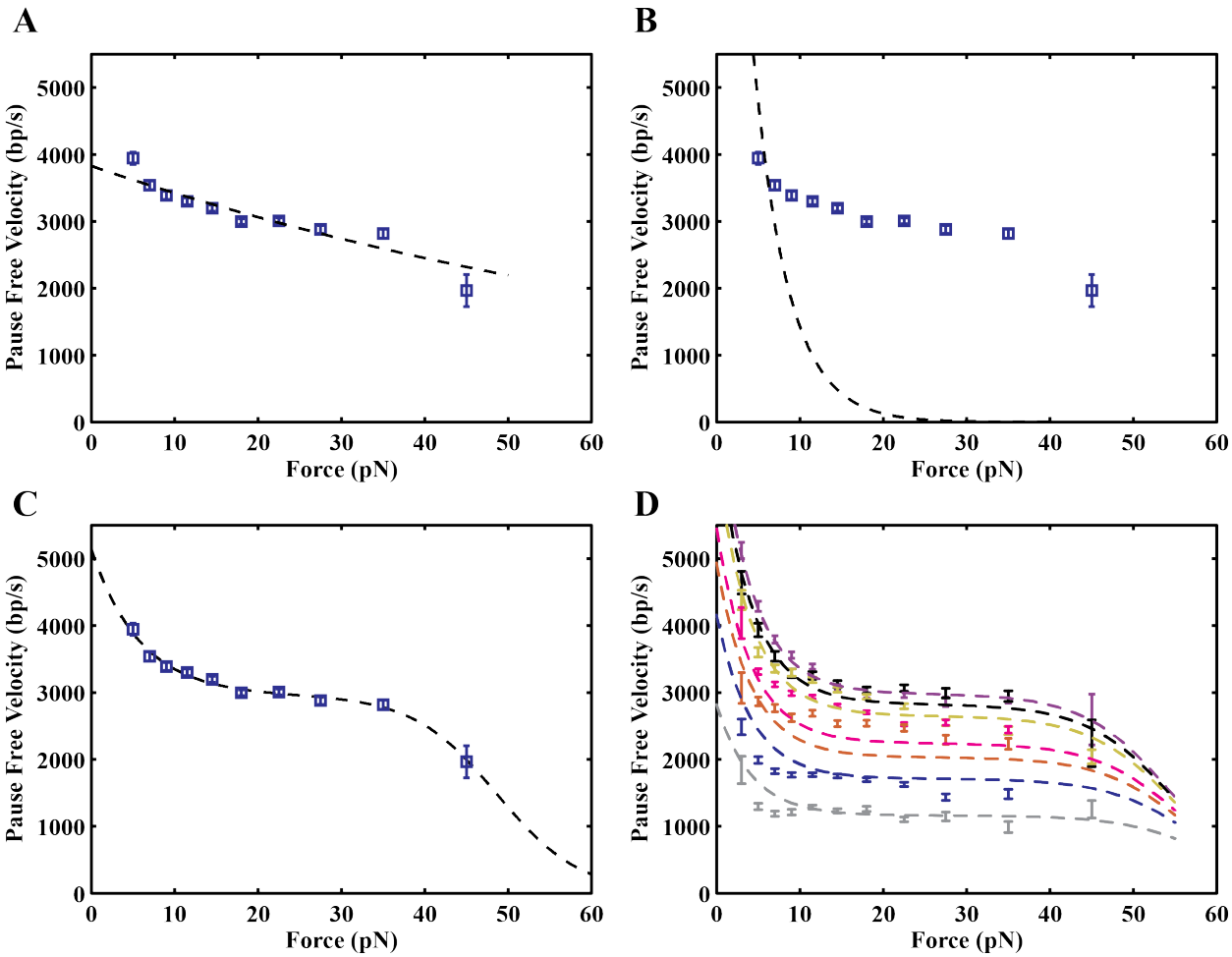

Figure 2.4 Fits of Force-Generating Transition Models

(A-C) The force velocity curve for 3 mM ATP is shown in blue. Fit to a single force-generating step is modeled by a dotted black line (A). Fit to two force-generating step model where one step is force-sensitive (B), and fit to a two force-generating step model where one step is loosely coupled, and the other step is tightly coupled (C).

(D) Global fits of a two force-generating step model (dashed lines) with a loose and tightly coupled step across all tested ATP conditions. Color coding is same as Figure 2.1 A.

The tightly coupled transition works against higher forces and requires ~8 k_BT of work. Due to energetic constraints, Pi release is the only viable candidate to power the tightly coupled transition. What is the identity of the chemical transition that is loosely coupled to the secondary force-generating process? Either ATP binding or ADP release provides sufficient free energy (~2-3k_BT) to drive this secondary power-stroke with an estimated step-size of ~1 bp against external loads upwards of 10-15pN. We can only speculate about the nature of the "loose coupling" required in this model. It is possible that during the secondary power-stroke the motor can successfully engage DNA only at low external loads. It is also possible that the secondary power-stroke acts via a flexible pore loop which can transduce DNA movement only against low forces but bends under high loads, effectively decoupling the secondary force-generating step from DNA translocation at forces above 15pN. Crystal structures of a highly related DNA translocase FtsK,

does indeed identify several flexible pore loops that could potentially interact with the DNA substrate (*21*).

An illustration of how a hybrid model of loose and tight coupling force generating steps could generate the force velocity behavior seen for SpoIIIE is shown in Figure 2.5. The hybrid model of DNA translocation can be described as follows: At low forces (1-5 pN), the coupling ratio ε is essentially 1, both the loosely coupled step (Figure 2.5 blue ovals) and the tightly coupled step (Figure 2.5 green ovals) are productive. At medium forces (5-15 pN), the loosely coupled step becomes slightly decoupled; each step will then consist of the tightly coupled step and occasionally the loosely coupled step. This effect will manifest as an overall decrease in translocation velocity. At high forces (15-35 pN), the loosely coupled step is nearly completely decoupled from the mechanochemical cycle, leaving only the tightly coupled step responsible for translocation. Because the tightly coupled step is force-insensitive, this will manifest as a velocity plateau between 15-35 pN. Eventually, even the tightly coupled step can be inhibited with enough opposing force. At very high forces (35-55 pN), the tightly coupled step remains 1:1 coupled to the mechanochemical cycle, but takes a longer time to complete (Figure 2.5 elongated green ovals). This will also manifest as a decrease in translocation velocity but is only observable past 35 pN.

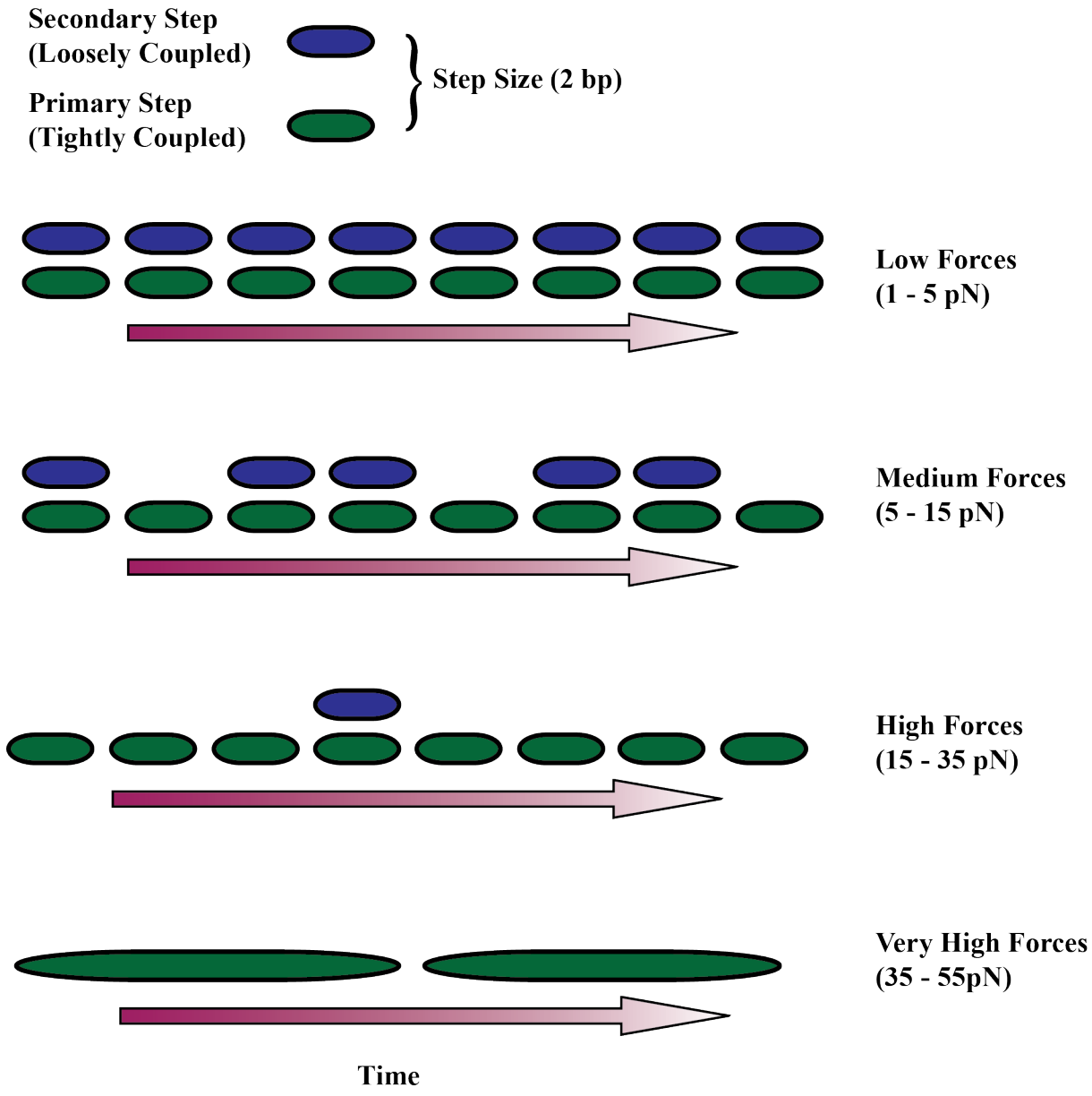

Figure 2.5 Cartoon of a Hybrid Translocation Model

A hybrid translocation model where a single step is comprised of a loosely coupled (blue oval) and tightly coupled step (green oval). The loosely coupled step becomes decoupled at higher forces, whereas the tightly coupled step takes longer to complete at higher forces.

2.2 SpoIIIE Displays Off-pathway Pausing Behavior

2.2.1 Off-pathway pauses emerges at low [ATP] conditions

As shown in (Figure 1.7 B), SpoIIIE translocation is punctuated by transient pausing events. To investigate the nature of these pausing events, a cross-correlation plot was calculated between pause frequency and pause-free velocity. I found that pausing is anti-correlated with pause-free velocity, suggesting that the pause state is off the main translocation pathway and is in

kinetic competition with translocation (Figure 2.6 A). Both the frequency and duration of pausing events was also found to be ATP-dependent (Figure 2.6 B, D) and force-independent (Figure 2.6 E, G). All pauses durations were well fit by a single-exponential decay (Figure 2.6 C), suggesting that pause recovery is governed by a single rate-limiting event. Due to signal-to-noise issues, a hard cutoff was set at 30 msec, as these are the shortest pauses that can be reliably detected (Chapter 5.4.2). Based on these results, we can propose a minimal kinetic model that includes an off-pathway pause state (Figure 2.6 F), where pause entry is force independent and pause recovery is dependent on ATP. Pausing behavior can also be induced by titrating in ADP, though the frequency of pausing displayed only a modest increase even at [ADP] = 1 mM (Figure 2.6 H). Surprisingly, the lifetime of ADP induced pauses is independent of [ADP] (Figure 2.6 I), averaging around a mean value of ~20 msec. Note that the lifetime of ADP induced pauses is longer than the expected completion time of an entire ATP cycle at saturating ATP (at 2 bp/ATP and 4 kbp/sec, an ATP cycle will be completed in 0.5 msec for the hexameric ring and ~3 msec for one subunit). This suggests that the recovery from ADP induced pauses is not a simple on-pathway ADP release mechanism; rather, the pauses induced by ADP must also be off-pathway. It is also possible that ADP release is coupled to the overall NTP binding state of the ring, as has been proposed for other ring NTPases (*33*, *54*, *78*). Introducing a large amount of ADP will bias the ring towards a more ADP bound state, thus forcing the ring to enter an off-pathway pause state.

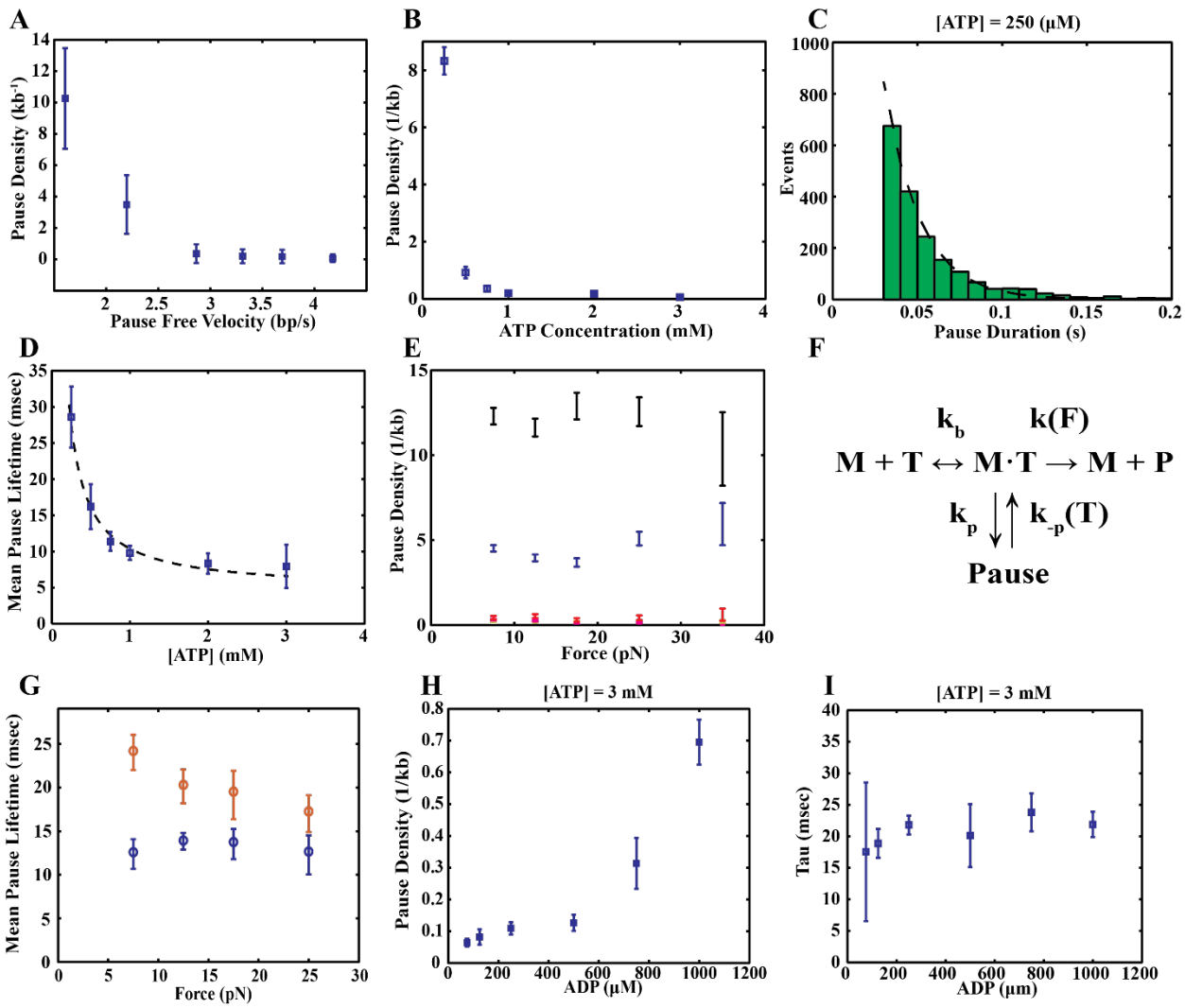

Figure 2.6 Pausing is a Random Off-Pathway Event

(A) Pause density is anti-correlated with pause-free velocity. Indicating that pausing is in kinetic competition with translocation.

(B) Pause density increases rapidly as [ATP] < 500 μM. Error bars are square root of number of pausing events measured.

(C) Pause duration histogram at ATP = 250 μM. The distribution was well fit by a single-exponential (dashed black line).

(D) Mean pausing lifetime calculated from the fit decreases as [ATP] increases. Dashed line is fit to a model where one ATP is required to recover the motor from a pause. Error bars are 95 percent confidence intervals of fits.

(E) Pause density behavior vs. opposing force at [ATP] = 3, 2, 1, 0.75, 0.5, 0.25 mM (purple, yellow, pink, red, blue, black points respectively). Pausing events become increasingly rare at [ATP] > 750 μM, pausing data gathered at [ATP] > 750 μM would not be visible at this scale. Error bars are square root of the number of pausing events measured for each force bin.

(F) Off pathway pausing model for SpoIIIE. The rate of entering a pause is force independent, pause recovery is dependent on ATP (T).

(G) Mean pause lifetimes calculated from single-exponential fits as a function of opposing force. [ATP] = 250 μM and 500 μM (orange and blue respectively). Errorbars are 95% CI. Other conditions of [ATP] yielded very few pausing events.
(H) Frequency of ADP induced pausing events at [ATP] = 3 mM. Error bars square root of number of events.
(I) ADP induce pause lifetimes are independent of [ADP]. Errorbars 95% CI of fits.

2.2.2 Investigating the nature of the pause state

What is the physical interpretation of an off-pathway pause? In most cases, interpretation of off-pathway states is dependent on the biological system. For RNA polymerase (RNAP), off-pathway pauses were found to be diffusive backtracked states (*79*), proposed to play a role in proofreading mechanism (*80*). For the T4 bacteriophage packaging motor, off-pathway pauses were shown to be part of a dynamic unpackaging process (*81*). What would be the nature of off-pathway pauses for SpoIIIE? There is little structural data that could help illuminate this question. However, we can speculate on the nature of the off-pathway pause by considering a few key facts. A pause is by definition a translocation-incompetent state, thus even though ATP is present in the buffer, the motor has adopted some conformation that is incapable of hydrolyzing ATP or coupling hydrolysis to mechanical work. I have shown that entry and recovery from the pause state is dependent on ATP but not force, suggesting that ATP binding helps to bias the motor back towards the translocation competent state.

An aside should be mentioned for a recently developed method of extracting kinetic information from lifetime distributions. Unfortunately, there are unique conditions of SpoIIIE pausing behavior that prevent the use of this method. In 1994, Schnitzer and Block introduced a kinetic parameter which characterizes the ratio between the variance and mean squared of dwell time measurements (*76*, *82*, *83*). In the context of a motor stepping between individual dwells, the ratio termed n_{min} sets a firm lower limit on the number of kinetic events taking place within the dwell. Mathematically, this is described as

$$n_{min} \equiv \frac{\langle \tau \rangle^2}{\langle \tau^2 \rangle - \langle \tau \rangle^2} \tag{2.21}$$

and

$$n_{min} \leq N \tag{2.22}$$

where τ is the dwell time and N is the actual number of kinetic states. The remarkable inequality described in Eq. (2.22) is simple to understand and carries distinct advantages of being model independent and free of any fitting parameters. The full breadth of the utility of n_{min} has been extensively reviewed in several publications (*84–87*).

While the utility of n_{min} is undeniable, there are critical conditions that must be satisfied in order for the inequality in Eq. (2.22) to be true. The first condition is that the visitation time for each kinetic state is memory-less, the kinetic pathway must be comprised of distinct Markov states with exponentially distributed lifetimes. For most enzymatic systems, this is a reasonable assumption. Secondly, there cannot be any dynamic disorder or off pathway events from the main kinetic pathway of interest (*88*). This condition is not necessarily true in every enzyme system though it is sometimes difficult to characterize off-pathway states. Interestingly, some ring NTPases require a certain number of nucleotides to bind to the ring before a step is taken (*6*, *33*).

Depending on whether these binding events happen in series or in parallel, the calculated n_{min} value will change. For example a three-step kinetic event, each step occurring in series prior to translocation will produce the expected n_{min} value of 3; whereas a three-step kinetic event, each with an exponentially distributed lifetime and occurring in parallel will produce an n_{min} of ~2.4 (Figure 2.7). Likewise a two-step event in series will produce an n_{min} of 2, whereas in parallel will produce an n_{min} of ~1.8. Parallel kinetic events are especially relevant for homomeric ring NTPases as multiple subunits are capable of hydrolyzing NTP and in some cases have been shown to act somewhat independently from one another (*59*, *89*, *90*). Therefore, non-integer values of n_{min} should not be ignored; nor do they necessarily suggest off-pathway states or dynamic disorder (*88*), but could represent a more subtle kinetic pathway than a simple linear nearest neighbor model. In the case for the ClpX protein translocase, it was proposed that the measured n_{min} value of ~2 corresponded to a minimum of 2 kinetic events that must occur prior to translocation (*6*). However, the model was based on the assumption that ATP binding and subsequent kinetic events happened sequentially. A 2-3 step kinetic event, with each step occurring in parallel, could also potentially give rise to an n_{min} of ~2.

There is another, more practical consideration; in order to obtain an accurate n_{min} measurement, the full range of dwell times must be measured, especially the shorter, more populous ones. While this statement seems trivial, there is a special case for apparent single-exponential distributions that prevent accurate measurements of n_{min}. As seen in (Figure 2.6 C), the pause time distributions appear to follow a single-exponential distribution. However, there is a measurement dead-time as the noise in the system prevents accurate scoring of pauses shorter than 30 msec. The pause scoring algorithm's accuracy is discussed in greater detail in Chapter 5.4.2. An interesting feature of single-exponential distributions is that removing a portion of the shorter lifetimes will obviously change the mean, but the overall shape of the remaining distribution is still a single-exponential, which means the variance stays constant. Naturally this behavior will create artifacts in n_{min} calculations. Methods to assume certain shapes for incomplete distributions to account for systematic errors arising from dead-times have been described in reviews (*85*), but is contingent on assumptions of the shape of the peak, or kurtosis of the distribution. Assuming a single-exponential distribution will ultimately lead back to an n_{min} of 1, defeating the purpose of n_{min} analysis in the first place. For the reasons stated above, n_{min} analysis is not a viable option to analyze pause time distributions for SpoIIIE.

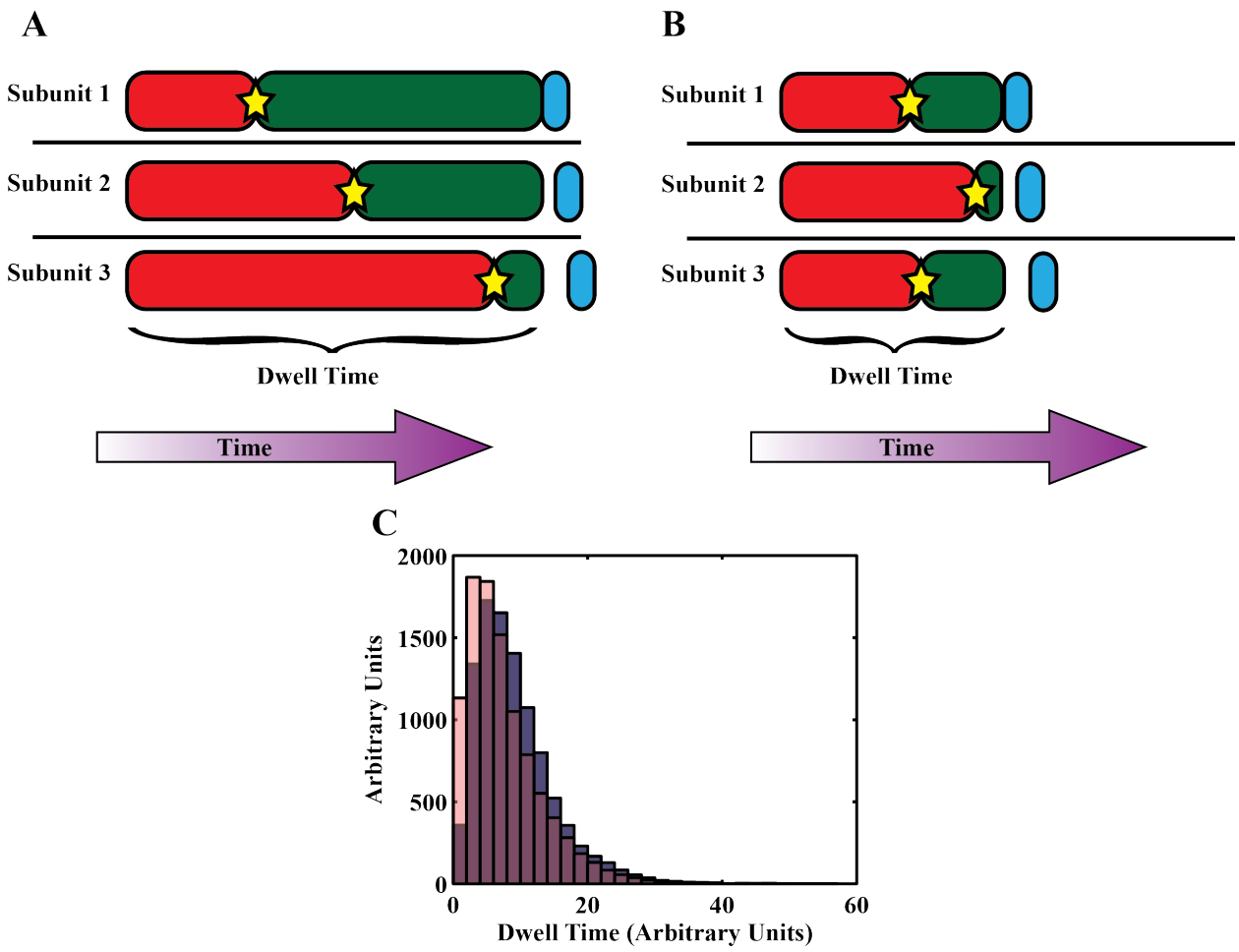

Figure 2.7 Theoretical Dwell Time Distributions

(A) Scenario in which 3 NTP molecules bind sequentially before stepping events. A subunit spends time in an empty state (red rectangle) until an NTP (yellow star) binds and remains NTP bound (green rectangle) until hydrolysis and translocation occurs (cyan ovals). The dwell time is represented as the total length of time before hydrolysis/translocation.
(B) Scenario in which 3 NTP molecules can bind in parallel. Color scheme is the same as (A). Each binding event is independent of events that occur in other subunits.
(C) Simulated dwell time distributions for scenario A (blue) and scenario B (transparent red).

2.3 Conclusions and Discussion

In this chapter, I have conducted an exhaustive set of single-molecule experiments on SpoIIIE in order to better understand motor mechanochemistry. It is apparent that the predominant mechanism of translocation for SpoIIIE is a power stroke. This can be reasoned from the large energy release of the primary force-generating step, phosphate release, is over 7 k_BT. This amount of energy is far greater than the energy available in a thermal bath, making a Brownian ratchet mechanism unlikely. Furthermore, the SpoIIIE motor is highly processive even at large opposing loads. A Brownian ratchet mechanism is predicted to have an exponential decay of processivity vs. load force, contrary to my results.

I have also demonstrated that phosphate release is irreversible and is the most likely candidate for the force generating step. It is interesting to note that several dissimilar motors, a pentameric dsDNA packaging φ29 motor (*51*), a hexameric protein translocase ClpX (*6*), and the hexameric dsDNA translocase SpoIIIE all utilize an irreversible phosphate release step as the force-generating transition. Irreversible phosphate release would likely be vital towards motor function as the concentration of intracellular phosphate is generally quite high (1-10 mM). One can easily imagine that if phosphate release was reversible, the high concentration of intracellular phosphate would likely inhibit motor function.

Finally, I have proposed a possible secondary force-generating step that is loosely coupled in order to explain the force-velocity behavior of SpoIIIE. Motors with two force-generating steps have been proposed for the F1 ATPase (*63*), though a hybrid model involving a loosely coupled and tightly coupled step is a unique departure from standard motor mechano-coupling. While a tightly coupled step capable of generating high forces would be useful for SpoIIIE to displace protein roadblocks on the DNA (*11*), it is unclear what advantages a secondary loosely coupled step might provide. The loosely coupled step is shown to be completely decoupled at ~20 pN. Interestingly, a loosely coupled step with a stall force of 20 pN is ideally suited for addressing the issue of spontaneous knotting when translocating ssDNA through a narrow channel such as a nanopore (*91*) or in this case, a ring ATPase. I do not believe that this loosely coupled step would serve the same purpose for SpoIIIE *in vivo* as the topology of the bacterial genome would be tightly controlled. Instead, it is possible that this loosely coupled step may be an evolutionary relic of single stranded translocases that likely would have encountered spontaneous knotting of ssDNA or ssRNA. Like most dsDNA translocases, SpoIIIE shares a universal common ancestor with ssDNA or ssRNA translocases (*17*).

Chapter 3 Probing Inter-subunit Coordination

Background

Inter-subunit coordination within a multimeric ring is a critical component of the overall mechanism of ring operation. As mentioned previously in Chapter 1, three generalized schemes of subunit coordination have been proposed: rotary sequential, concerted, and stochastic. Distinguishing between these three coordination models is a difficult task, especially if a ring NTPase contains elements of more than one coordination mechanism.

Ideally, subunit coordination is best probed by slowing the motor sufficiently enough to directly observe it work in discrete increments, i.e. the step size. An analogy can be drawn to the strategy that Eadweard Muybridge developed in 1872 to observe the timing of individual steps in a horse's gallop. A popular debate of the day was whether there was a point in a horse's gallop where all four legs were off the ground. However, a horse's legs moves too quickly during a gallop for the human eye to follow. To address this issue of time resolution, Muybridge invented motion picture photography to capture the individual motions of the legs of the horse, effectively looking at the step size of a horse. Muybridge's experiment yielded one picture frame where all four legs of the horse were indeed off the ground, settling the debate. A 'step size' for a ring motor is defined as the distance the motor translocates its substrate within a single productive NTP cycle. Observing the timing of individual steps yields intimate details on intersubunit coordination. This strategy of observing individual steps has been used to elucidate the details of subunit coordination for the φ29 packaging motor (*56*), the kinesin, myosin, and dynein motors (*92–95*), and the ClpX protein translocase (*5*, *6*).

Another powerful method of dissecting subunit coordination is crystallization of the ring NTPase at various stages of its catalytic cycle. In the case of the E1, Rho, and DnaB helicases the ring was co-crystallized with its single-stranded substrates (*54*, *55*, *96*, *97*), revealing not only detailed structural information of the ring, but also a highly coordinated sequential mechanism of translocation. However, crystals are by definition static structures, thus any temporal coordination (e.g. taking 'n' steps in a fixed amount of time) a ring NTPase might employ would be lost.

Other methods to probe ring coordination involve mixing mutant and wild-type subunits and observing the rate of activity decrease (*98*). While some information on subunit coordination can be gleaned from mutant mixing, this experiment suffers from a heterogeneous population of mutant and wild-type mixes. The issue of ring heterogeneity can be addressed with the expression of a single-chain ring, as in the case for the ClpX protein translocase (*59*) or conducting experiments on rings with six unique subunits such as the MCM2-7 replicative helicase (*99*). In these constructs, targeted mutagenesis can be employed to inactive specific subunits within a ring.

An indirect way of probing subunit coordination would be to observe substrate rotation or motor processivity. In the case of the φ29 packaging motor and the FtsK/SpoIIIE dsDNA translocase, these motors can induce supercoiling during the course of DNA translocation. By attaching a 'rotor bead' to the side of a DNA molecule, the φ29-gp16 motor was observed to introduce a consistent negative twist ahead of its DNA substrate (personal communication: Craig Hetherington). For the T7 helicase, motor processivity as a function of [NTP] was used to determine a coordinated mechanism of hydrolysis, based on the logic that coordinated hydrolysis should hand off the ssDNA substrate from one subunit to the next, leading to a larger increase in processivity at higher [NTP] when compared to uncoordinated models (*100*). A noteworthy aside should be mentioned for the F1-ATPase motor, which contains a γ-subunit that rotates within the

αβ-hexamer. In this case subunit coordination for the F1-ATPase was directly observed by attaching a fluorescent actin molecule to the γ-subunit and observing a consistent rotation powered by ATP hydrolysis (*57*).

The high velocity of SpoIIIE's DNA translocation (~4 kbp/sec) presents unique challenges towards probing intersubunit coordination. Sufficiently slowing the motor to observe individual steps is a daunting task that is currently beyond the scope of this thesis work. This high velocity of translocation also prevents the use of a rotor bead assay as the drag forces imparted on the bead would quickly become rate-limiting and introduce higher order effects on the DNA, such as strand melting or plectoneme formation. In this chapter, I will focus on two alternative methods using a non-hydrolysable ATP analogue, ATPγS, to probe intersubunit coordination and modified DNA experiments to measure the step size of SpoIIIE.

3.1 Single-Molecule Experiments in the Presence of ATPγS

3.1.1 ATPγS Induces Pausing Event

For a homomeric ring such as SpoIIIE, a pause in translocation indicates that no subunit is actively translocating DNA; thus determining how many subunits must be inactivated in order to induce a pause would serve as an indicator of subunit coordination. Pausing for SpoIIIE was induced by addition of a non-hydrolysable analogue of ATP, ATPγS, in the reaction buffer (Figure 3.1 A). Experiments including ATPγS were all conducted at a saturating concentration of [ATP] = 3 mM. At saturating ATP conditions, pausing events for SpoIIIE were extremely rare; thus all pauses seen with the addition of ATPγS analogue can safely be assigned as an analogue induced pause.

Pause frequency was shown to increase nonlinearly with ATPγS and best described by a third power law dependence, $P_{freq} = a \cdot [ATP\gamma S]^n$ where 'a' is a fitting parameter and $n = 2.9 \pm 0.5$ (Figure 3.1 B). A nonlinear dependence of pause frequency vs. [ATPγS] is evidence against a strictly concerted or sequential model; in these models, a single γS molecule is sufficient to induce a pause and pause frequency would be linearly proportional to [ATPγS]. While a linear relationship between pause frequency and [ATPγS] has a fairly straightforward interpretation, higher order relationships are not as straightforward. In the case for the measured third power law dependence for SpoIIIE, this means that an 'n' value of 3 *does not* automatically lead to the conclusion that 3 ATPγS molecules are required to induce a pause. Two representative examples demonstrate why this is true.

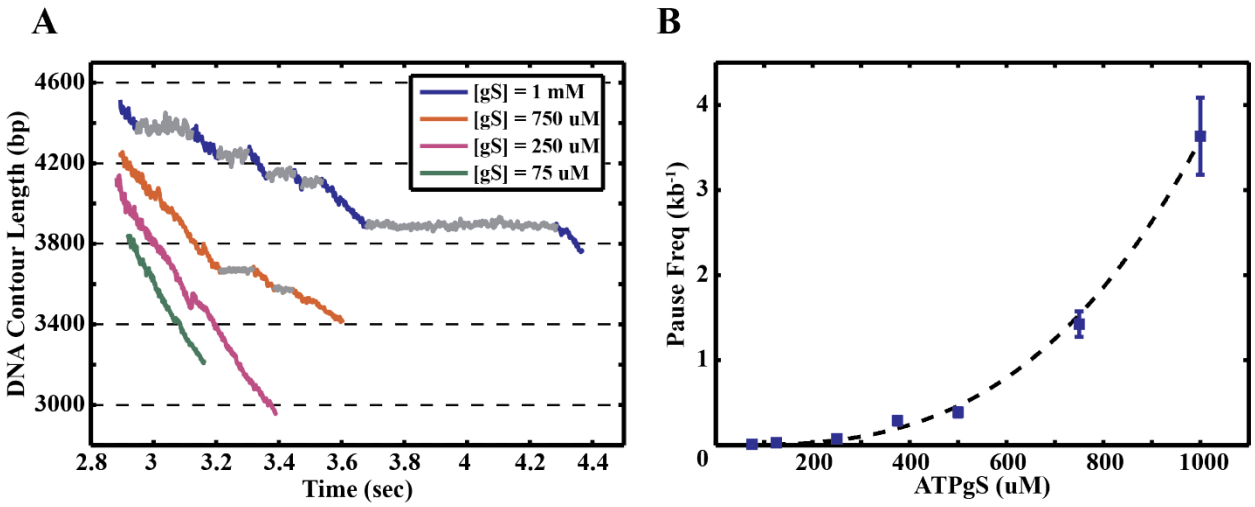

Figure 3.1 ATPγS Induces Pausing Events

(A) Representative traces following SpoIIIE translocation in the presence of ATPγS and [ATP] = 3mM. Pausing events are highlighted in gray.
(B) Pause frequency increases non-linearly with [ATPγS]. Dotted line is fit to a third power law. Error bars are square root of number of pausing events measured for each condition. [ATP] = 3mM.

In the first scenario, imagine a hexameric ring that must bind 4 ATPγS molecules in order to pause. The likelihood of a hexameric ring binding 4 ATPγS molecules is a classic problem in combinatorics which can be represented as

$$f = \frac{N!}{K_{\gamma S}!(N-K_{\gamma S})!} p^{K_{\gamma S}} (1-p)^{N-K_{\gamma S}} \tag{3.1}$$

where N is number of binding sites, $K_{\gamma S}$ is number of sites bound to ATPγS, f is the fraction of the population bound to $K_{\gamma S}$ ATPγS molecules and $p = \frac{[ATP\gamma S]}{[ATP]+[ATP\gamma S]}$
Surprisingly, plotting pause frequency vs. [ATPγS] at a given concentration of [ATP]=3 mM would yield a third power law dependence over the range of [ATPγS] = 0.1-1 mM (Figure 3.2 A). Intuitively, this result can be rationalized by the fact that a hexameric ring has 15 different ways of binding 4 ATPγS molecules. This would increase the likelihood of a ring having 4 ATPγS molecules and inducing a pause. This highly simplified scenario demonstrates degenerate binding states alone can convolute a power law dependence

A more complete expression for fraction of subunits bound to ATPγS takes into account both empty subunits and the different affinities of SpoIIIE towards ATP or ATPγS. For the SpoIIIE motor (M), it can either bind ATP (A) or ATPγS (B). This can be represented as

$$MB \leftrightarrow B + M + A \leftrightarrow MA \tag{3.2}$$

Since the total number of motor subunits must comprise of empty, ATP bound and ATPγS bound, it follows that

$$[M]_T = [M] + [MA] + [MB] \tag{3.3}$$

The fraction of motors bound to ATP or ATPγS and their dissociation constants can be written as

$$f_A = \frac{[MA]}{[M]_T};\ K_d^A = \frac{[M][A]}{[MA]} = \frac{(1-f_A-f_B)[A]}{f_A} \tag{3.4}$$

and

$$f_B = \frac{[MB]}{[M]_T};\ K_d^B = \frac{[M][B]}{[MB]} = \frac{(1-f_A-f_B)[B]}{f_B} \tag{3.5}$$

We now have terms for K_d^B, K_d^A, $[A]$ and $[B]$. We want to reconstruct the expressions for f_A and f_B in terms of the four terms listed previously. Rearranging will yield:

$$f_A = \frac{K_d^B[A]}{K_d^A K_d^B + K_d^B[A] + K_d^A[B]} \tag{3.6}$$

and

$$f_B = \frac{K_d^A[B]}{K_d^A K_d^B + K_d^B[A] + K_d^A[B]} \tag{3.7}$$

The K_d^B for ATPγS was measured to be ~ 75 μM (Figure 3.5 B). The K_d^A for ATP is not as straightforward to measure, hydrolysis of ATP will obviously convolute the measurement and binding assays performed with mutant enzyme may not reflect the true K_d^A value. Nevertheless, we can set the K_M of 500 μM to be the upper bound estimate for K_d^A. The likelihood of N ATPγS binding to a hexameric ring is then represented as

$$\binom{6}{N} p^N q^{6-N} \tag{3.8}$$

where $p = f_B$, $q = 1 - f_B$, and $\binom{6}{N}$ is the binomial coefficient shown in Eq. (3.1). We can see from Eq. (3.8) that both degenerate binding states and the unequal affinities of the motor towards ATP vs. ATPγS can affect the likelihood that the ring is in a certain ATPγS bound state and therefore affect the pausing probability.

The effect of different affinities of the ring towards ATP and ATPγS on subunit coordination can be simulated in the second scenario. Imagine a hexameric ring must bind 6 ATPγS molecules in order to pause, i.e. a stochastic ring mechanism. However, ATPγS binds more tightly to the ring than ATP and therefore stays bound to the ring for several ATP hydrolysis cycles (Figure 3.2 B). Assuming ATPγS stays bound to the ring for a factor of ~5 times longer, Monte Carlo simulations reveal that this scenario would also produce a third power law. In fact, depending on how tightly ATPγS binds to the ring, it is possible to produce any number of power law dependencies. Intuitively, one can think of a ring with one subunit analogue bound as a slightly slower (5/6 initial velocity) translocating ring with only five binding sites available, thus lowering the required number of ATPγS molecules needed to bind to the ring in order to induce a pause. Simulations were written in MATLAB, the complete code can be found in the methods section.

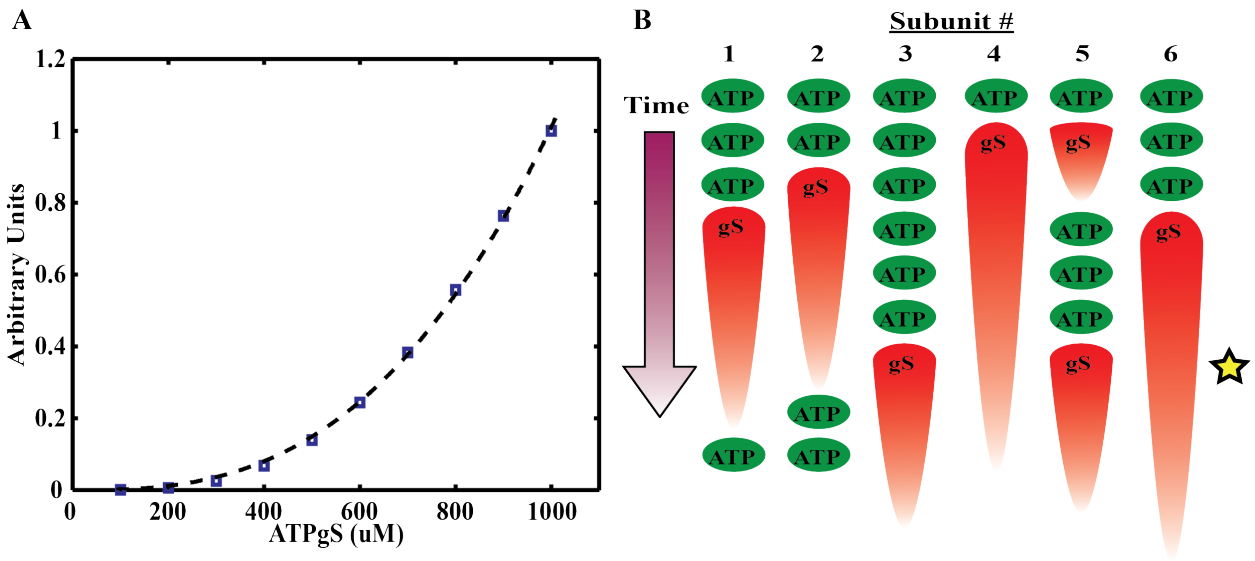

Figure 3.2 Simulations of ATPγS Induced Pausing

(A) Pausing behavior of a hexameric ring if four subunits must bind to ATPγS in order to induce a pause. Dotted black line is a power law fit with n=2.8. [ATP]=3 mM.
(B) Cartoon of a simulated ring where six subunits are required to bind to ATPγS in order to pause (yellow star). The long residence time of ATPγS (red ovals) is represented by a long tail.

These two scenarios demonstrate that multiple factors can convolute a power law dependence, how then should one interpret such a plot? By itself, a power law dependence can only give a strict lower bound on the number of subunits required to induce a pause. Given the error of the fit in Figure 3.1 B, this would mean that 2-3 subunits must bind to ATPγS in order for the SpoIIIE motor to pause, therefore a strictly coordinated model of subunit coordination can be ruled out. Ideally this information should be used with other pieces of data in order to build a more detailed model for subunit coordination.

3.1.2 ATPγS induces long pausing events

The lifetime of ATPγS was also measured by plotting a histogram of pause durations for various [ATPγS]. The pause durations were well described by a single-exponential decay with a fitted mean lifetime of ~27 msec (Figure 3.3 A), about 5 times longer than the mean pausing events with [ATP] = 3 mM alone. This lifetime is interpreted as the time necessary for a single gS molecule to come off the ring and recover the motor from the pause state. Interestingly, the lifetime of γS induced pauses is independent of [ATPγS] (Figure 3.3 C). Intuitively, we would expect that a higher proportion of subunits would be ATPγS bound at higher [ATPγS] and the pause duration would lengthen as the ring waits to release more ATPγS molecules. The independence of the pause duration can be interpreted to indicate that only one configuration of a γS bound ring will enter into a pause, and the release of a single gS molecule will recover motor translocation. To better understand the state of the ring, we can plot the expected population of rings with 0-6 subunits bound to ATPγS using Eq. (3.8). The result shows that even at [ATPγS] = 1 mM and [ATP] = 3 mM, the majority of gS bound rings would only have 1-2 ATPγS molecules bound (Figure 3.3 D). It is likely that the majority pauses induced by ATPγS are from rings with only a partial ATPγS

occupancy. It is important to note that at [ATPγS] = 1 mM, a second longer pause lifetime of ~200 msec begins to appear (Figure 3.3 B). This second pause only contributes to approximately 3 percent of the total pauses measured. Interestingly, the calculated fraction of rings that have four subunits bound to ATPγS is also about 3 percent.

While it is tempting to assign the identity of the longer pause to a ring with 4 ATPγS bound molecules, the lifetime of the second pause is nearly a factor of 8 longer than the other γS induced pauses, suggesting that pause recovery from this extra-long pause is not a simple matter of releasing 3 or 4 ATPγS molecules from the ring. Furthermore, I also cannot exclude the possibility that multiple pausing events have been combined into one long pause. A more thorough description of the behavior of pause recovery in the presence of ATPγS would be better addressed with high resolution measurements where individual steps, or power strokes, are punctuated by ATPγS induced pauses. In this regime I would be able to estimate the number of kinetic events required to take place prior to a pause recovery.

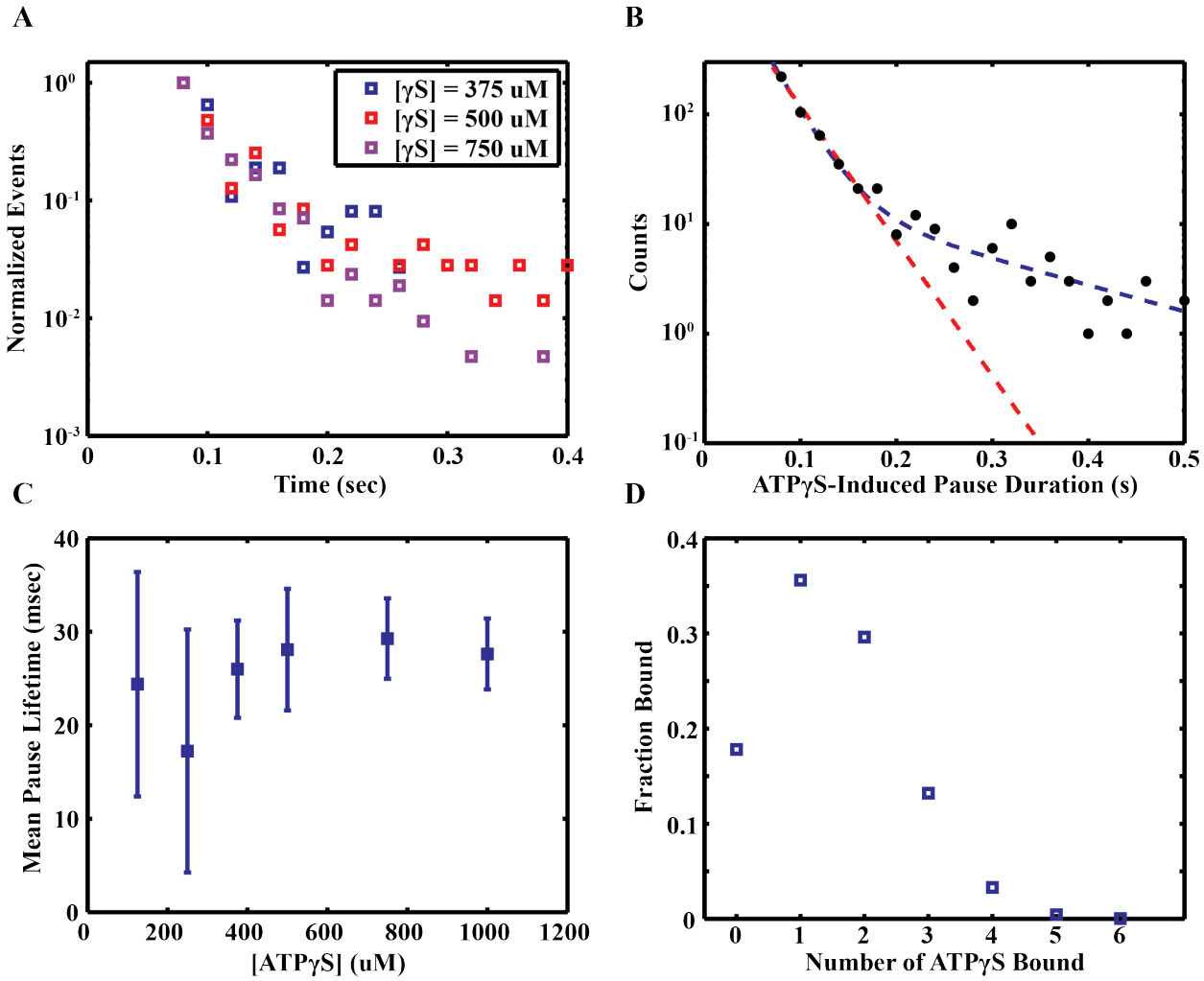

Figure 3.3 ATPγS Pause Durations

(A) Pause duration histograms at three different [ATPγS] concentrations. All distributions follow a single-exponential decay. [ATP] = 3 mM for all conditions.
(B) Pause duration histogram at [ATPγS] = 1 mM. Dotted red line is fit to a single-exponential decay. Dotted blue line is a fit to a double exponential.
(C) Mean pause lifetimes from exponential fits across all [ATPγS] tested. Error bars 95% CI.
(D) Calculated fractional occupancy of the ring when [ATPγS] = 1 mM and [ATP] = 3 mM.

3.1.3 ATPγS pausing events are independent of force

The experiments in the presence of ATPγS were conducted in passive mode and the pausing behavior at each force bin has also be measured. Figure 3.4 shows that ATPγS induced pausing behavior for both frequency and duration are independent of the amount of opposing force applied. This result has an important implication for the location of the force generating step in the motor. If ATP binding acted as a force generating step in the motors mechanochemical cycle, then an opposing force would favor unbinding of the nucleotide. Applying this logic to ATPγS induced pausing events, opposing force would promote unbinding of ATPγS in the mechanochemical scenario described previously and therefore lower the mean duration of ATPγS induced pauses. In the absence of these results, ATP binding is likely not a force-generating transition, in good agreement with the results found in Chapter 2.1.1. Finally, because pausing behavior is independent of force, we can also safely combine pauses measured in different force bins in a single histogram in order to bolster the statistics of measured pauses.

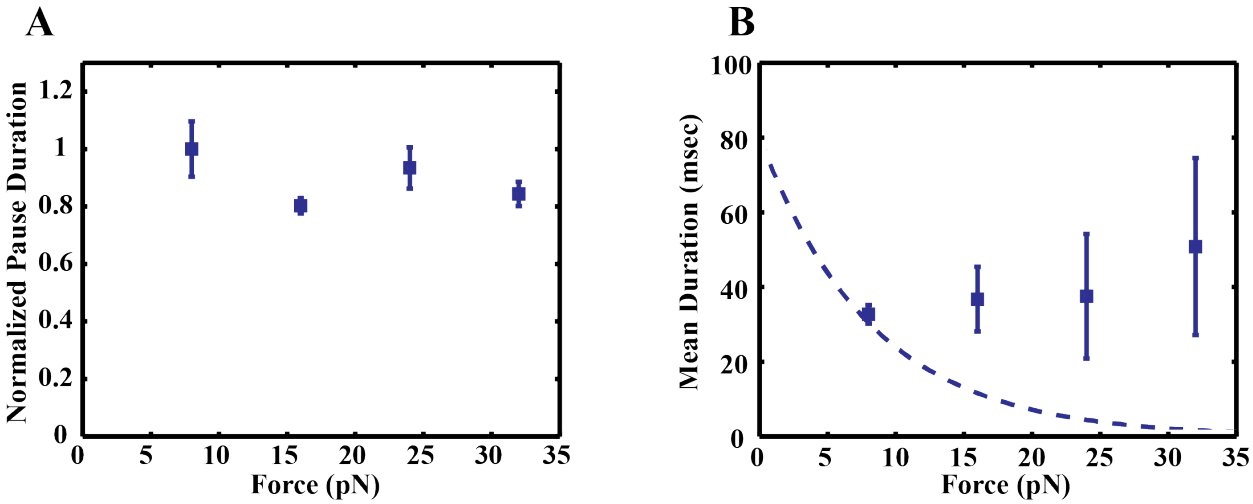

Figure 3.4 ATPγS Pausing Behavior is Independent of Force

(A) Normalized pausing duration at [ATPγS]= 75 uM and [ATP]= 3 mM. Error bars are 95% CI of the fit.
(B) Mean pause durations from fit at [ATPγS]= 1 mM and [ATP] = 3 mM. Error bars are 95% CI of the fit. Dotted line is predicted force dependence of pause durations if motor mechanochemistry comprised of a single force-generating step coupled to nucleotide binding. Pausing data for both [ATPγS] conditions were separated by 10 pN bins and fitted to a single-exponential.

3.1.4 ATPγS behaves as a simple competitive inhibitor

The length and frequency of an ATPγS induced pause could potentially be affected by the slow hydrolysis of ATPγS or by cooperative binding events. To investigate the possibility of slow ATPγS hydrolysis, SpoIIIE-DNA stalled complexes were formed in the tweezers in the presence of ATPγS. The SpoIIIE ring could bind to DNA in the presence of ATPγS but did not demonstrate any translocation for ~20 min (data not shown). The issue of possible cooperative binding events was addressed by observing the inhibitory effect of ATPγS on SpoIIIE pause-free velocity. The equation for a simple competitive inhibitor in a classic Michalis-Menten enzyme is

$$v = \frac{V_{max}[S]}{K_m\left(1+\frac{[I]}{K_i}\right)+[S]} \tag{3.9}$$

where $[I]$ is concentration of inhibitor and $K_i = \frac{[E][I]}{[EI]}$

Rearranging the terms, we can reconstruct Eq. (3.9) in terms of percent inhibition (i)

$$i = 1 - \frac{v_i}{v_0} = \frac{[I]}{[I]+K_i\left(1+\frac{[S]}{K_m}\right)} \tag{3.10}$$

where v_i is inhibited velocity and v_0 is uninhibited velocity (*101*). In the presence of ATPγS, we can see that plotting percent inhibition as a function of [ATPγS], the inhibition curve is well described by a simple competitive inhibition model with a K_i = 76 ± 12 uM for ATPγS (Figure 3.5 B).

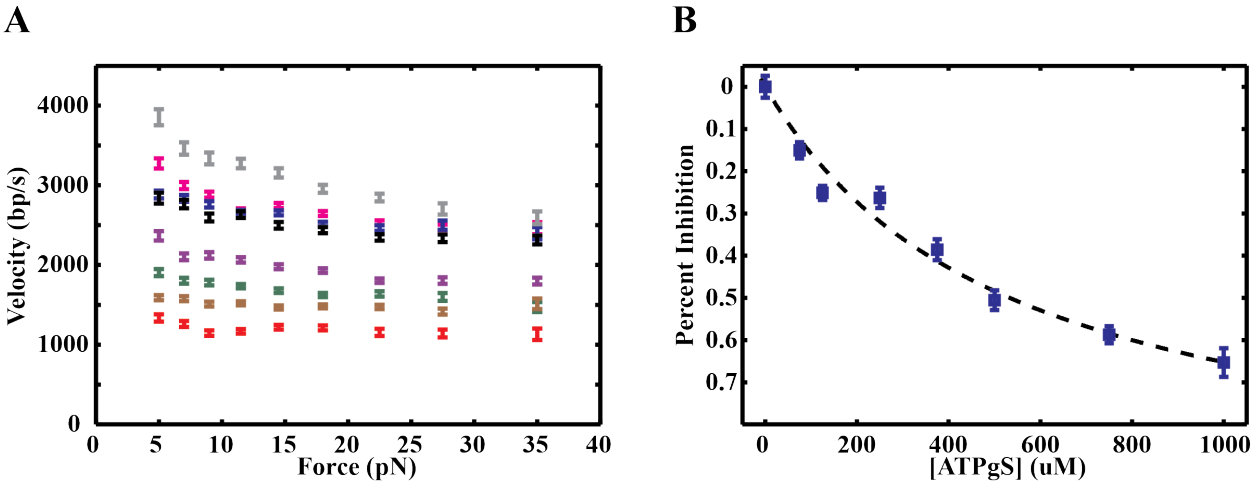

Figure 3.5 ATPγS Behaves as a Competitive Inhibitor to ATP Binding

(A) Pause free velocity with respect to opposing force in the presence of [ATP] = 3 mM and [ATPγS] = 0, 75, 125, 250, 375, 500, 750, 1000 uM (grey, magenta, blue, black, purple, green, brown, red curves respectively).

(B) Percent inhibition of SpoIIIE pause-free velocity with increasing [ATPγS] and 5 pN of opposing force. Dotted black line is a fit to a competitive inhibition model yielding a K_i = 76 ± 12 uM. Error bars are s.e.m.

3.1.5 Additional experiments with AMP-PNP

ATPases tend to have different binding affinities for different ATP analogues, thus the choice of analogue may affect the single-molecule results measured for the motor. To address this issue, I conducted experiments using another available non-hydrolysable ATP analogue, AMP-PNP. Force-velocity behavior, pause duration and frequency were assessed in comparison to ATPγS (Figure 3.6). All three criteria displayed quantitatively similar results to ATPγS.

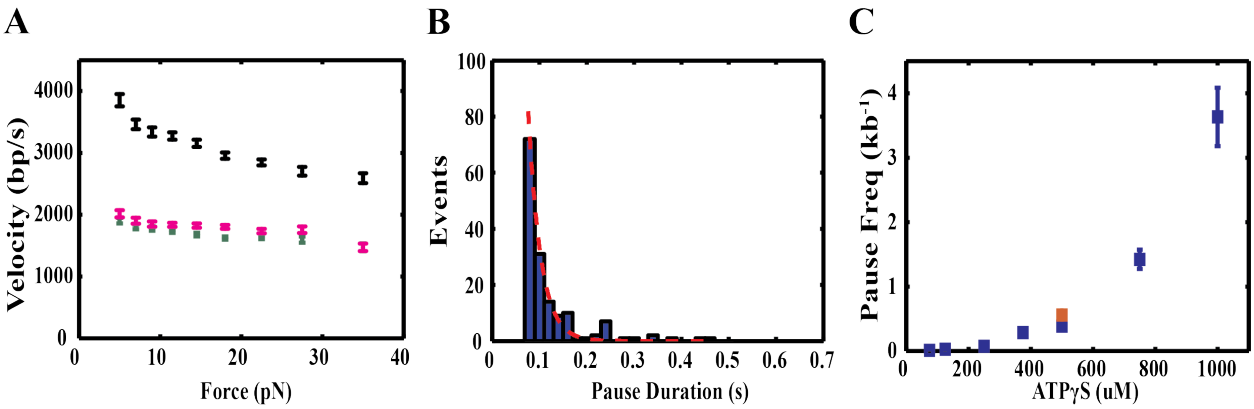

Figure 3.6 Pausing Statistics with AMP-PNP

(A) Pause free velocity vs. force in the presence of [ATP] = 3 mM. and 0 μM ATPγS (black), 500 μM ATPγS (green), or 500 μM AMP-PNP (magenta).
(B) Pause duration histogram with [ATP] = 3 mM and [AMP-PNP] = 500 μM. Dotted red line is a fit to a single exponential with a mean lifetime of 27 ± 4.7 msec. Error is 95% CI.
(C) Pause frequency in the presence of [ATP] = 3 mM and ATPγS (blue) or AMP-PNP (red)

3.2 Challenging the Motor with Neutral DNA

3.2.1 Necessity of alternative methods to measure step size

Direct observation of a motor taking a step would be the ideal method of measuring the step size. This however is not possible for SpoIIIE given its high velocity of translocation. We can consider the difficulty of measuring a step with a simple signal-to-noise ratio (SNR) calculation. As is shown in Chapter 5, the measured position noise in the system at 5 pN of tension has a standard deviation of ~15 bp. We can also calculate the maximum theoretical step size of SpoIIIE based on the available energy of ATP hydrolysis. The maximum force that the motor has pulled was measured to be ~50 pN (Figure 4.1 B). Given the estimated amount of free energy available from ATP hydrolysis in the buffer solution (~100 pN·nm), the maximum step size allowed would be about 2 nm, or ~ 5.8 bp. For simplicity, we will approximate the maximum step size to 5 bp. The equation to calculate SNR is

$$SNR = \frac{\Delta x}{\sigma} \tag{3.11}$$

where Δx is the expected signal and σ is the standard deviation of the noise; we can see that the SNR is less than ideal with $\Delta x = 5\ bp$ and $\sigma = 15\ bp$. A standard method of improving SNR is to time average uncorrelated data points between discrete stepping events, the positional accuracy will then improve as $\sqrt{N}$ where N is the number of data points. Certain step detection algorithms can be used with a SNR of 2 (*102*), though a SNR of 4 is recommended (*102*, *103*). To achieve a SNR of 4, we must time average at least 144 data points between each stepping event. At a sampling frequency of 1 kHz, this will translate to a dwell of 144 msec between each step and a velocity of ~35 bp/sec for the motor. There is a subtle difference between bandwidth and sampling frequency due to signal aliasing that will not be explored in this thesis, suffice to say that $f_{sample} = 2 \cdot Bandwidth$ (*104*). Note that sampling at a higher frequency in order to obtain more data points within the dwell will not improve the SNR. The positional accuracy of the bead will ultimately be limited by the corner frequency f_c and autocorrelation time of the bead[1], $t = 1/(2\pi f_c)$ (typically around 1-4 kHz) (*105*). Since the bead is placed in a thermal bath, its motions are overdamped, acting as a low-pass filter past the corner frequency. Another way of interpreting this damping effect is that the motion of the bead will become correlated past the corner frequency. As mentioned earlier, SNR will only improve as $\sqrt{N}$ by time averaging uncorrelated data points. This signal attenuation effect can be observed in the power spectrum analysis shown in Chapter 5.

The V_{max} of the SpoIIIE motor is ~4.7 kb/sec under low opposing force (5 pN) and room temperature. In order to directly measure steps, the motor must be slowed down by over a factor of 100. As shown in (Figure 2.1 A), SpoIIIE is fairly insensitive to opposing force, slowing by at most a factor of 2 even at high opposing forces. Lowering the concentration of ATP will also slow the motor down. If we follow the Michaelis-Menten dependence of the motor, we can see 4 μM of ATP is needed to achieve the required velocity, over 100 times lower than the K_m. However, at such low concentrations of ATP, I have found that SpoIIIE will not even bind to its DNA substrate (data not shown). It should now become clear that standard methods of slowing down the motor is not a feasible option. In order to measure the step size of SpoIIIE, an alternative approach must be taken which will be discussed below.

3.2.2 SpoIIIE makes specific phosphate contacts with the DNA.

All translocases must interact with their substrate in order to accomplish mechanical work. Furthermore, these interactions must occur in a cycle to satisfy motor processivity. Understanding the chemical identity and periodicity of these motor-DNA interactions provides critical information on a motor's minimum operating cycle. In other words, measuring the periodicity of motor-DNA interactions allows for an indirect measurement of the step size. For dsDNA, SpoIIIE's substrate, the most prominent repeating chemical moiety is the negatively charged phosphate backbone, providing an attractive target for protein-DNA interactions. Several related helicases have been shown to make phosphate contacts every base, with the disruption of a single charge interaction halting translocation (*106–108*). In contrast, the dsDNA packaging motor φ29-gp16 has been shown to form critical phosphate contacts every 10 bp (*109*).

[1] There is also uncertainty in the instantaneous tension applied to the DNA due to tether compliance. However, over long time scales it can be assumed that $\langle F_{Bead} \rangle = -\langle F_{DNA} \rangle$.

I tested the role of the phosphate backbone charge in SpoIIIE motor-DNA interactions by inserting methyl-phosphonate (MeP) DNA into the DNA tether. MeP DNA has the negative oxygen group in the phosphate backbone replaced with an uncharged methyl group (Figure 3.8 A), neutralizing the negative charge of the phosphate backbone while still preserving the overall B-form structure of DNA (*110*, *111*). Custom oligos containing these MeP modifications (Genelink) were then ligated to a DNA tether and placed 4 kb away from the biotin tag. The overall experimental set-up is identical to Figure 1.7 A with the addition of a MeP patch (Figure 3.7 A).

I first tested dsMeP patches ranging in length from 2-30 bp. Figure 3.7 C shows examples of SpoIIIE challenged by various lengths of double-stranded MeP (dsMeP) at 5 pN of constant opposing force and saturating (3 mM) ATP. When the length of dsMeP exceeds 4 bp, translocation proceeds normally until SpoIIIE reaches the 4 kb mark where the dsMeP patch resides and pauses for an extended period of time (> 5 s). It is worth noting that in the absence of MeP, pauses on the order of seconds are an extreme rarity for SpoIIIE under saturating ATP conditions (Figure 2.6 C). Note that the pauses induced by MeP are not the same kind of off-pathway pauses intrinsic to SpoIIIE translocation. SpoIIIE is still mechanically competent for translocation in the presence of MeP, translocation is only prevented because MeP eliminates the grip that SpoIIIE requires to pull and translocate DNA. Several slipping, re-translocation, and pausing events can be seen in representative traces which illustrate this behavior (Figure 3.11). With the longest dsMeP patch tested (30 bp dsMeP), the crossover probability (number of traces that crossed the MeP patch placed at the 4kb mark) is less than 4 percent. The low crossover probability of dsMeP clearly demonstrates that SpoIIIE must make crucial phosphate contacts during translocation (Figure 3.7 B).

We have now established the negatively charged phosphate groups are critical motor-DNA contacts. Given the natural periodicity of the phosphate backbone on DNA, we can successively shorten the length of neutral DNA and observe the maximum length of neutral DNA SpoIIIE can cross over. Challenging the motor with different lengths of modified DNA provides essential information on the periodicity of motor-DNA interactions, the maximum crossover length serves as an indicator of the step size of SpoIIIE. Figure 3.7 C demonstrates representative samples of SpoIIIE's response when it encounters 2, 3, 4, and 5 bp of dsMeP. We can see that 5 bp of dsMeP presents a significant challenge for the SpoIIIE motor with a crossover probability of ~50%. Moreover, incidences of when the motor did crossover were always preceded by a long pause (>1 sec) at the 4 kb mark. Shortening the dsMeP patch by 1 basepair allowed a near 100% crossover efficiency (Figure 3.7 B), furthermore nearly all crossover events across 4bp dsMeP occurred with pauses less than one second in duration. The difference between 4 and 5 dsMeP is significant for two reasons. Firstly, the large increase in traversal probability when the dsMeP patch is shortened from 5 to 4 bp suggests that the step size of SpoIIIE is $\leq$ 5 bp. Secondly, traversals across a 5 bp dsMeP patch are always preceded by a long pause (>1 sec). This long pause is interpreted as the length of time SpoIIIE requires to successfully traverse the dsMeP patch. However, the long pause also suggests that a 5 bp dsMeP patch is sufficiently long enough to always force SpoIIIE to "land" on an MeP DNA when it tries to step across, further suggesting that the step size of SpoIIIE is $\leq$ 5 bp.

Upon initial inspection, the fact that SpoIIIE can cross a 4 bp stretch of neutral DNA suggests that the step size of SpoIIIE is ~5 bp. This is unlikely for several reasons. As mentioned earlier, the maximum step size allowed by a single ATP molecule is ~5.8 bp. A 5 bp step size would require the motor operate at ~85% thermodynamic efficiency. Furthermore, crystal structures and single-molecule studies of other ring NTPases demonstrate that a ring NTPase can

make more than one contact with DNA substrate (*55*, *96*, *109*), leading to several models that can explain how the SpoIIIE motor can cross over a 4 bp dsMeP patch. Figure 3.8 B lists four possible scenarios in which SpoIIIE can cross 4 but not 5 bp dsMeP. The first model listed is the simplest one in which only one subunit of SpoIIIE makes a single contact with the DNA at any given time. In this model SpoIIIE would be required to take a 5 bp step in order to cross a 4 bp dsMeP patch. The second model depicts a single subunit making two contacts with the DNA substrate, similar to what has been shown for the φ29 packaging motor, and the DnaB helicase (*96*, *109*). In this model the two contacts can "straddle" the interface between unmodified and MeP modified DNA, allowing the SpoIIIE motor to only take a 4 bp step to cross a 4 bp dsMeP patch. The third model involves 2 adjacent subunits each making one contact with the DNA substrate. Because the periodicity of a hexameric ring is 60^0 and a single basepair rise in dsDNA is ~34^0, the DNA contacts are spaced apart by one base between the two subunits in order to minimize the twist of the DNA substrate. This model is equivalent to a coordinated escort model in which the DNA substrate is sequentially handed off from one subunit to the next; each motor-DNA contact is then guided through the ring by a spiral staircase of DNA interaction loops protruding into the central channel (*54*, *55*, *90*).

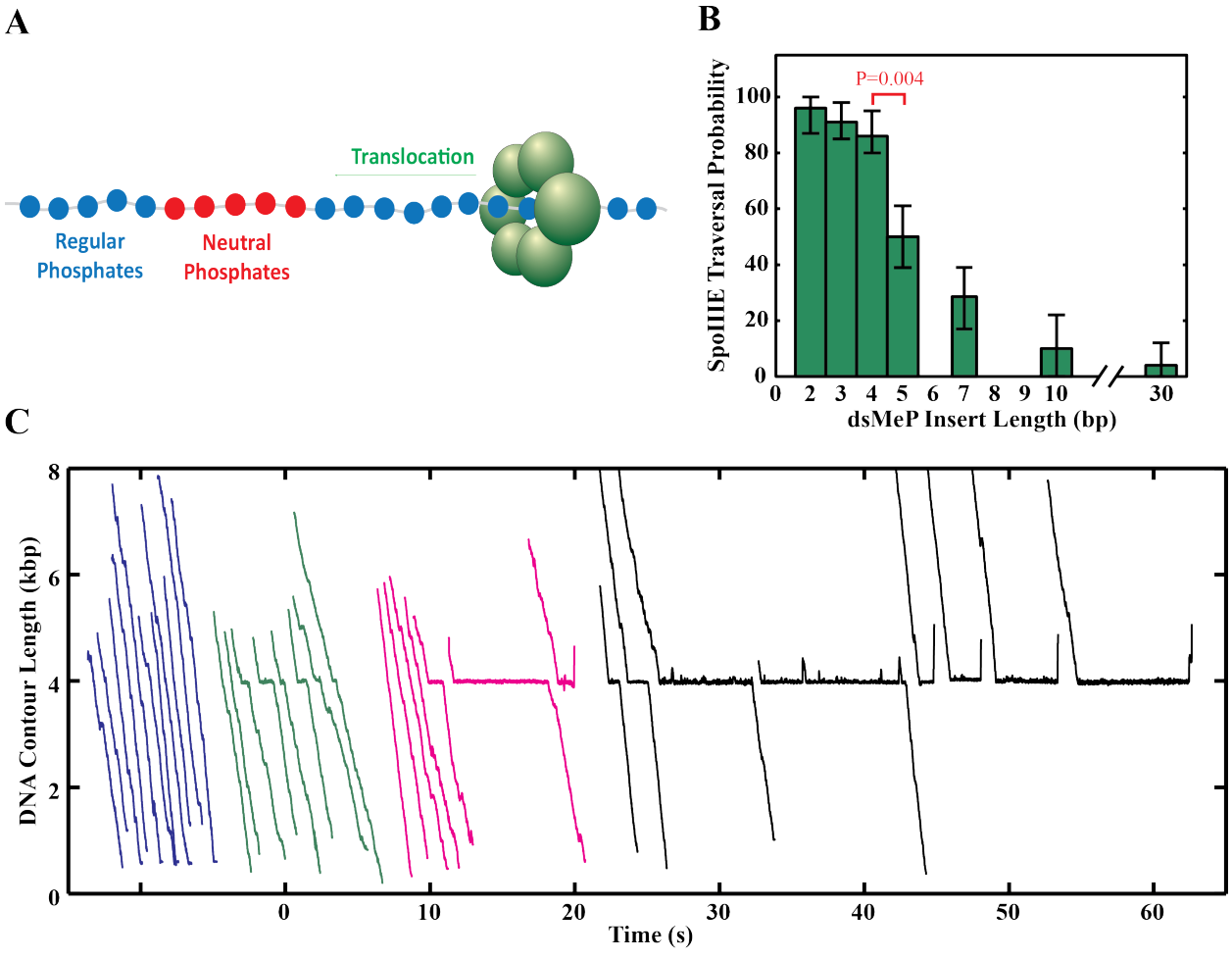

Figure 3.7 SpoIIIE Translocation is Halted by Neutral DNA

(A) Cartoon depicting a SpoIIIE hexamer (green spheres) moving towards the left and approaching a patch of DNA with the methyl-phosphonate modification.
(B) Traversal probabilities of SpoIIIE across various lengths of dsMeP. Error bars are 68% CI from bootstrapping. P value (two-tailed Fisher exact test) between 4 and 5 bp dsMeP is indicated in red.
(C) Examples of SpoIIIE response to 2, 3, 4, and 5 bp of dsMeP (blue, green, pink, black respectively) at 5 pN of opposing force and [ATP] = 3 mM. The dsMeP patch is placed at the 4 kb mark.

The final model is a combination of model 2 and model 3. This particular model has two adjacent subunits each making two contacts with the DNA, for a total of four adjacent phosphate contacts. With four adjacent phosphate contacts, the ring only requires a 2 bp step to cross a 4 bp dsMeP patch. The logical continuation of these models would end with a ring making five adjacent phosphate contacts and only taking a 1 bp step to cross a 4 bp dsMeP. However, five adjacent phosphate contacts cannot be evenly distributed around a hexameric ring without significantly distorting the dsDNA structure; due to structural constraints, this model was discarded. It should now be clear that in order to eliminate certain models of SpoIIIE stepping, further probing with MeP is required.

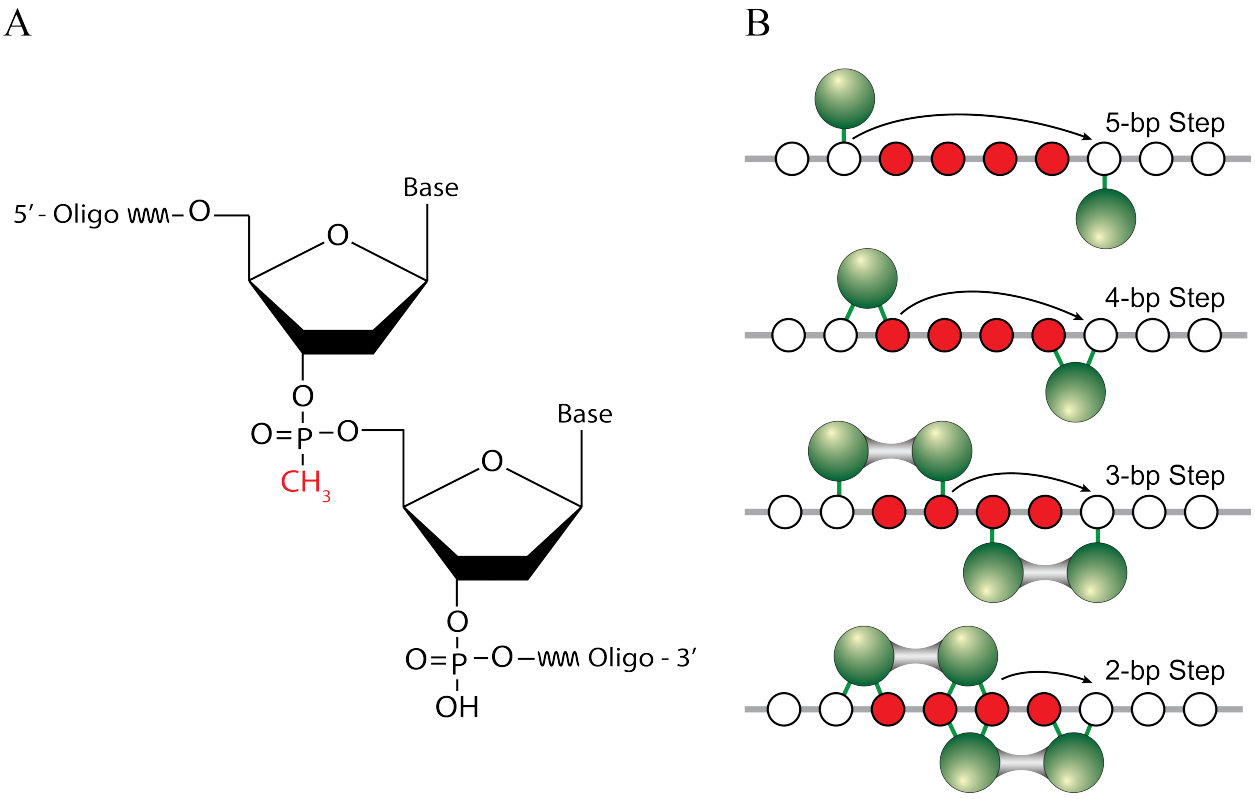

Figure 3.8 Multiple Models of SpoIIIE Crossing MeP

(A) Chemical structure of a methylphosphonate modification of DNA. The methyl group is highlighted red.

(B) Various models of how SpoIIIE can cross 4 but not 5 bp dsMeP. Possibilities include the first model at the top depicting a single SpoIIIE subunit (green sphere) making a single contact (green line) with an unmodified phosphate backbone (white circle) and stepping by 5 bp across the MeP modified DNA (red circles). Or a single SpoIIIE subunit making two contacts with the DNA, one contact on the unmodified phosphate and one on the MeP DNA and stepping by 4 bp (second model from the top). Or two adjacent subunits making contacts separated by one base and stepping by 3 bp (third model from the top). Or two adjacent subunits making two contacts each, for a total of four contacts, and stepping by 2 bp (fourth model from the top).

3.2.3 Stepping stone MeP design reveals a 2 bp step size for SpoIIIE

The previous MeP experiments have set an upper limit of 5 bp for the step size of SpoIIIE. In order to refine our measurement of the step size, I placed an MeP "Probe" spaced one basepair past an initial 4 bp dsMeP "Primer" (Figure 3.9 A). The selection of 4 bp dsMeP as the so-called primer is based on two criteria. Firstly, SpoIIIE has demonstrated a high traversal probability and low traversal time across a 4 bp dsMeP patch. Secondly, increasing the MeP patch by one basepair to 5 bp significantly decreases the traversal probability, furthermore traversals are always preceded by pauses that are at least one second long. These second long pauses are interpreted as SpoIIIE attempting to cross over a 5 bp dsMeP patch. However, SpoIIIE is hindered in its crossover attempts by consistently landing on a MeP modified DNA.

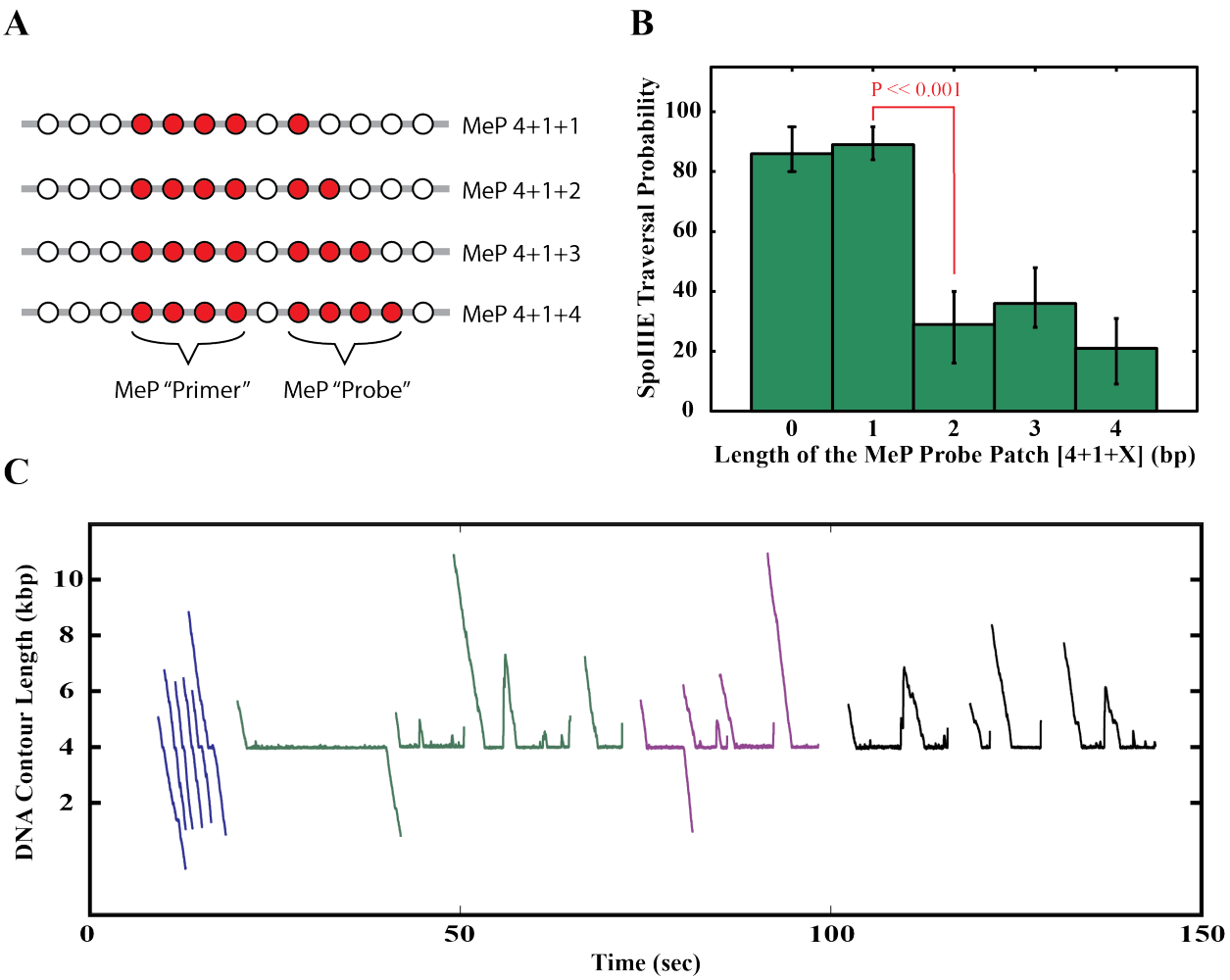

Figure 3.9 MeP Stepping Stone Experiments

(A) An MeP stepping stone design in which an MeP "Probe" (red circles right side) of lengths varying from 1-4 bp are spaced one basepair away from an MeP "Primer" (red circles left side).
(B) Traversal probabilities of SpoIIIE across all MeP stepping stone constructs. Error bars are 68% CI from bootstrapping. P value between MeP 4+1+1 and 4+1+2 is indicated in red.
(C) Representative traces of SpoIIIE attempting crossover of MeP 4+1+1 (blue), 4+1+2 (green), 4+1+3 (purple), 4+1+4 (black). The MeP patch is placed at the 4 kb mark.

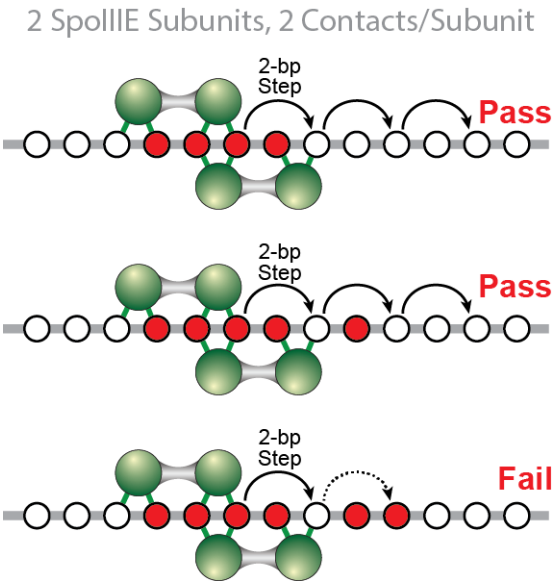

Figure 3.10 SpoIIIE Translocation Model

A cartoon summarizing the overall MeP results. SpoIIIE has 2 subunits each making 2 contacts with the DNA. With a 2 bp step size, this model allows traversal of 4 bp dsMeP, MeP 4+1+1, but does not allow traversal of MeP 4+1+2. Figure courtesy of Gheorghe Chistol.

Given the large difference in both traversal probability and traversal time between 4 and 5 bp dsMeP, 4 bp is likely to be the maximum length of MeP that SpoIIIE can cross efficiently. Furthermore, SpoIIIE must only be able to cross 4 bp dsMeP in a certain phase with respect the location of the MeP patch. The long pauses seen at 5 bp dsMeP indicates that no matter what phase SpoIIIE is in, it will always land on an MeP DNA when attempting to cross. Thus the initial 4 bp dsMeP primer acts to force the SpoIIIE motor into this particular phase and the following MeP probe then tests whether SpoIIIE can continue its traversal activity. For example, if SpoIIIE does indeed make 5 bp steps, then it should be able to cross all MeP stepping stone designs shown in Figure 3.9 A. If the step size was 4 bp, then SpoIIIE would not be able to cross MeP 4+1+4 but it would be able to cross the remaining constructs etc… The results show that SpoIIIE cannot cross a stepping stone construct where the MeP probe is 2-4 bp in length (Figure 3.9 C). Once the MeP probe is shortened to 1 bp, the traversal probability is near 100% and is within error of 4 bp dsMeP alone (Figure 3.9 B). These results clearly indicate a step size of 2 bp for the SpoIIIE motor. Given a step size of 2 bp, the most likely model of SpoIIIE translocation would be the fourth model in Figure 3.8 B. A step size of 2 bp is also in good agreement with the proposed step size of the related dsDNA translocase FtsK as determined from crystal structure conformation changes (though absent the dsDNA substrate) and stopped-flow ATP hydrolysis assays (*21*, *112*). Interestingly, the DnaB helicase structure was also shown to make 2 adjacent nucleotide contacts per subunit with its ssDNA substrate with a proposed physical step size of 2 bp (*96*). A summary of the MeP results and SpoIIIE translocation model is shown in the Figure 3.10.

3.2.4 SpoIIIE tracks one strand of the double helix

Many ring NTPases of the ASCE family have demonstrated a strand polarity when translocating along its substrate. Furthermore, the related dsDNA φ29 packaging motor makes preferential contacts with one strand of the DNA and packages DNA with a 5’→3’ polarity (*109*). To determine whether SpoIIIE adopts a similar mechanism of DNA translocation, methyl-phosphonate (MeP) modifications were introduced on a 30 base stretch of DNA. The modifications were placed on either the 3’→5’ strand or the 5’→3’ strand.

When SpoIIIE encountered the 3’→5’ MeP DNA, translocation was unimpeded. Surprisingly when the MeP modification was introduced on the 5’→3’ strand, SpoIIIE could not cross (~15%) (Figure 3.11). We can immediately draw two important conclusions from this result. Firstly, SpoIIIE favors contacts on one strand and translocates DNA with a 5’→3’ polarity.

Secondly, the efficient traversal of the 3'→5' modified strand suggests that SpoIIIE maintains preferential strand contact with the 5'→3' strand through several rounds of ATP hydrolysis, at least 15 rounds of ATP hydrolysis given a step size of 2 bp. A 5'→3' translocation polarity is a common mechanism for the RecA-like family of NTPases (*31*), of which SpoIIIE is a member.

Strand polarity also presents implications on the order of firing for individual subunits of SpoIIIE. We have already established that the motor makes crucial contacts with the phosphates on the DNA backbone for translocation, these contacts are only made on one strand of the DNA and the step size of SpoIIIE is likely 2 bp. If phosphate-motor interactions proceed along one strand of dsDNA during translocation every 2 bp, the helical pitch of the DNA strand would cycle the interactions between the DNA backbone and the closest subunit within a ring in a clockwise fashion, highly suggestive of a sequential model of translocation. However, a strictly sequential model (ie. Activity proceeds in an ordinal fashion of 1,2,3 etc…) does not agree with the pausing behavior of SpoIIIE shown in Figure 3.1 B. In a strict sequential model, once the hydrolysis order reaches the affected subunit, a single subunit that is bound with ATPγS would stall the entire motor. This would translate to a linear dependence of pausing frequency as a function of [ATPγS] at saturating ATP.

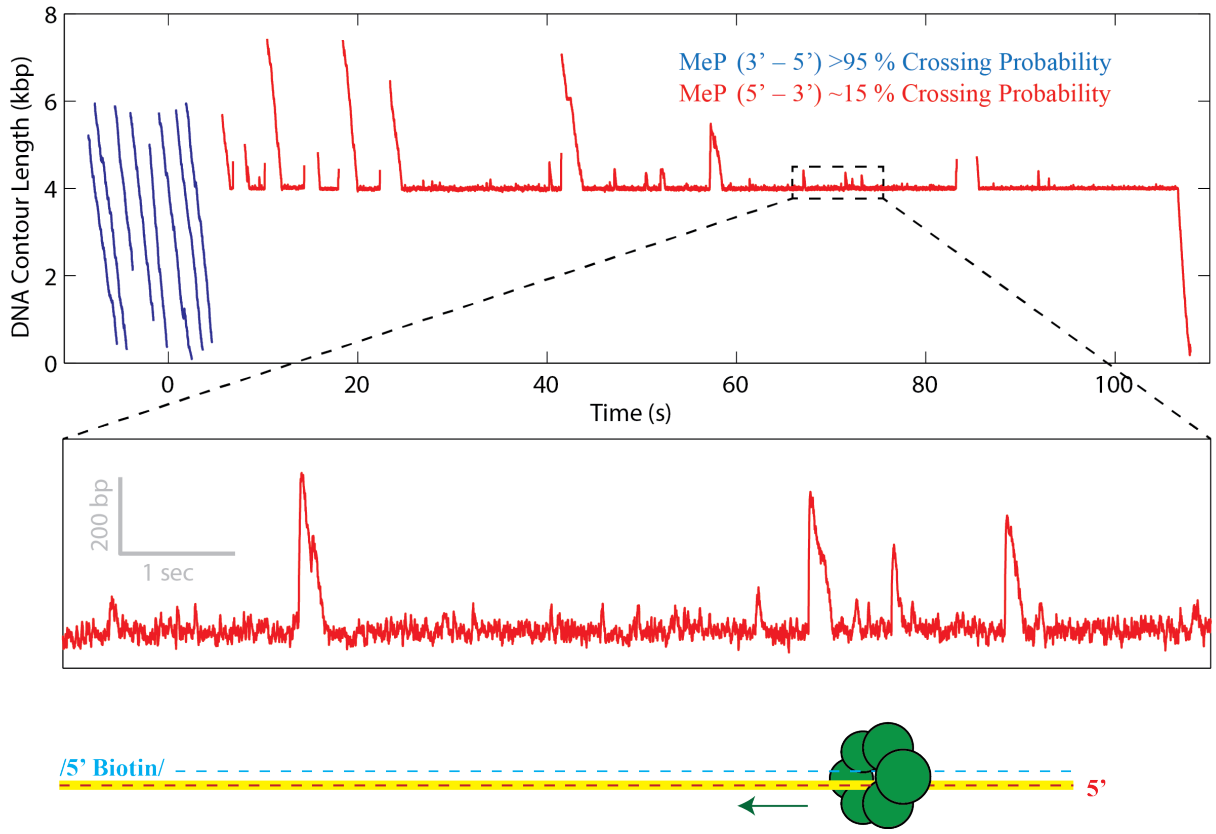

Figure 3.11 SpoIIIE Tracks the 5'→3' Strand of dsDNA

Representative SpoIIIE traces where phosphates were neutralized on either the 3'→5' (blue) or the 5'→3' (red) strand. A zoomed in box shows the SpoIIIE motor halting translocation at the 4 kb mark, slipping and reattempting translocation (dotted box). The cartoon at the bottom of the figure depicts the DNA tether used in these experiments. The SpoIIIE hexamer (green spheres) is shown

translocating towards the biotin tag and favors interactions on the 5'→3' strand (highlighted dotted red line).

These two seemingly contradictory pieces of data can be resolved one of two ways. The first possibility is that the ring does indeed follow a strictly coordinated mechanism of hydrolysis but each individual subunit has a fast binding equilibrium with ATP and ATPγS. This means that if a sequential firing order encounters an ATPγS bound subunit, the ring will not have to wait very long until the ATPγS molecule is replaced by an ATP molecule. Ultimately this model would require multiple ATPγS molecules to bind to the ring in order to lengthen an ATPγS induced pause into an observable time window. This is a rather insidious possibility that would be difficult to characterize given the minitweezers time resolution. A second possibility would be if the ring carries a small degree of flexibility to the sequential model. One extra degree of flexibility in a sequential ring would involve the ability to skip inactive subunits in the ring or have adjoining subunits rescue translocation activity. For example, the model presented in Figure 3.10 has two subunits contacting the DNA throughout a translocation cycle. It is possible that if one subunit is inactive, the other adjacent subunit can re-bind another ATP molecule and continue translocation, pulling the DNA through the central channel and aligning the phosphate backbone with the next available subunit. Such a model would allow both sequential ATP hydrolysis around the ring but also provide some flexibility when the ring encounters inactive subunits. It is interesting to note that some ring NTPases have been shown to tolerate catalytically inactive subunits (*59*, *89*, *90*), leading to coordination models that are neither strictly sequential nor fully stochastic.

3.3 Implications of SpoIIIE Translocation

3.3.1 SpoIIIE positively supercoils the DNA

A motor that tracks one strand of a dsDNA and translocates by 2 bp per step must address one outstanding issue; the periodicity of the phosphate backbone does not match the periodicity of a hexameric ring. Because of the helical pitch of dsDNA, simple translocation will result in a 'pseudo-rotation' of the DNA when viewing the motor head-on. In fact there is no integer step size that will always bring the phosphate backbone in perfect register with the subunits. The change in pseudo-rotation per rise in dsDNA is about ~34^0 per bp, thus producing a pseudo-rotation of ~69^0 every 2 bp. This will produce a ~9^0 discrepancy between the phosphate backbone and the nearest subunit within a hexamer, which has a structural periodicity of 60^0. This ~9^0 discrepancy can be resolved if we allow the SpoIIIE motor to twist the DNA and bring the phosphate backbone into register. Depending on which direction SpoIIIE translocates the DNA relative to its central channel, this will either be positive or negative supercoiling.

Previous results and current work have established SpoIIIE as a DNA exporter, translocating DNA across a division septum in *Bacillus subtilis* during sporulation, with only the SpoIIIE on the mother cell side functioning as DNA pumps to translocate DNA into the daughter cell (*113*). The DNA exporter mechanism would then require DNA to be translocated towards the viewer when viewing the ring top-down from the N-terminal domain. Given the strand tracking mechanism demonstrated earlier and the right-handed helical pitch of B-form DNA, this would also require the ATP hydrolysis cycle to proceed in a clockwise direction when viewing the ring top down. Ultimately, a clockwise direction of subunit firing will lead to a positive (+) 9^0 of supercoiling per 2 bp translocated, resulting in one positive supercoil per ~80 bp translocated.

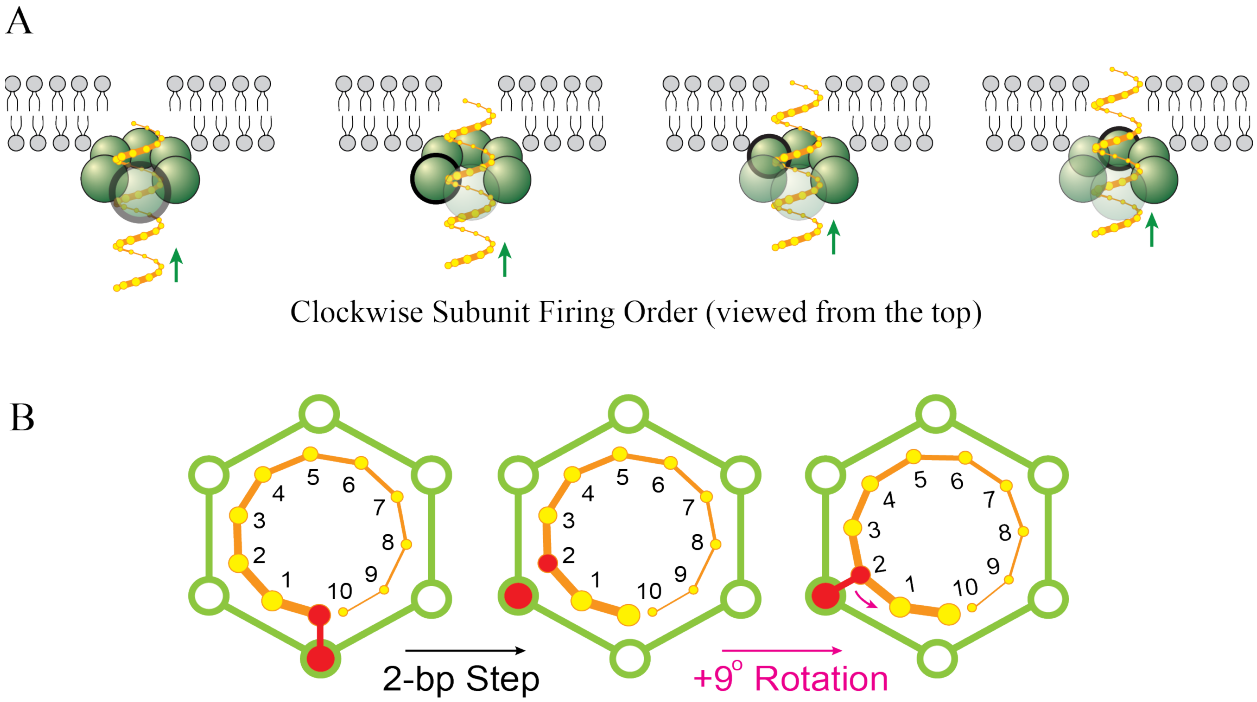

Figure 3.12 Rotation of DNA by SpoIIIE

(A) Cartoon depicting one strand of a right-handed DNA passing through a SpoIIIE hexamer (green spheres). The lipid membrane is separating the mother cell (lower half) from the daughter cell (upper half). DNA is being translocated upwards towards the daughter cell compartment. Hydrolysis proceeds in a clockwise fashion.

(B) The SpoIIIE hexamer outlined by a green hexagon would translocate DNA towards the viewer and out of the page (only one strand is shown for clarity). A 2 bp step would be out of register with the closest subunit of SpoIIIE, leading to a ~9^0 twist of DNA. The DNA would be positively supercoiled in the mother cell side and negatively supercoiled in the daughter cell side.

Figures courtesy of Gheorghe Chistol.

The degree of supercoiling has been measured for the FtsK translocase (*114*) and SpoIIIE (unpublished work) using magnetic tweezers and measuring the ability of the motor to relieve twists introduced into the DNA tether prior to motor translocation. The FtsK motor was found to induce one (+) supercoil every 150 bp of DNA translocated. The degree of supercoiling indicated that FtsK is not a strict groove tracking motor, as a groove tracking mechanism would be expected to introduce one (+) supercoil every 10.5 bp (*115*). The ability of FtsK to fine tune its supercoiling was proposed as a mechanism of addressing the native topology of *E. coli* DNA. Because bacterial genomes are circular and topologically closed, simple translocation will not change the linking number of the DNA, thus a motor that introduces positive supercoils ahead of translocation will also produce reciprocal negative supercoils in its wake. Note that the *E. coli* genome contains about one negative supercoil every 150 bp, thus FtsK translocation would introduce a positive supercoil to relieve the negative supercoil at a one to one ratio and then reintroduce the same degree of negative supercoiling in its wake. In other words, FtsK translocation is superbly tuned to maintain the native topology of the *E. coli* genome during translocation.

The degree of supercoiling was also measured for SpoIIIE in the magnetic tweezers and was found to induce one positive supercoil every 100 bp (Personal Communication: Jerod Ptacin, Marcelo Nollman), close to the expected degree of supercoiling from a motor that takes steps of 2 bp. While the sign of supercoiling measured for SpoIIIE is the same as FtsK, the degree of supercoiling is slightly higher. Why would two highly similar dsDNA translocases have different degrees of DNA supercoiling? To answer this question, it is important to place the role of SpoIIIE in a biological context. The role of SpoIIIE is slightly different than FtsK, SpoIIIE is responsible to translocating DNA into a developing forespore in *B. subtilis*. The degree of supercoiling in the *B. subtilis* mother cell is around one negative supercoil per 130-150 bp, similar to *E. coli*. However, the degree of supercoiling of the DNA in the forespore is believed to be around one negative supercoil every 95 bp as determined by measuring the superhelicity of plasmids purified from the forespore (*116*). This value is close to the magnitude of supercoiling measured for SpoIIIE in the magnetic tweezers. The high degree of negative supercoiling in the forespore is believed to play a role in the high UV resistance of forespore DNA. Recall that SpoIIIE acts as a DNA exporter, operating on the mother cell side of the division septum. This orientation for SpoIIIE would result in the ring inducing positive supercoils on the mother cell side and negative supercoils on the forespore side, thus resulting in DNA translocation that helps maintain the native topology of *B. subtilis* in the context of sporulation.

A quick note should be mentioned on the small discrepancy between predicted SpoIIIE supercoiling and the measured result. The prediction that SpoIIIE would introduce one positive supercoil every 80 bp operates under the assumption that SpoIIIE consistently supercoils the DNA every time it takes a step. However, a reconstruction of the SpoIIIE hexamer with dsDNA modeled in the center shows that there are multiple locations within one subunit that could potentially interact with the DNA in the central channel (Figure 3.13). It is possible that these interactions can change mid-translocation and reposition the DNA, leading to an inconsistent supercoiling during translocation, possibly explaining the small 20^0 discrepancy between the predicted and measured results.

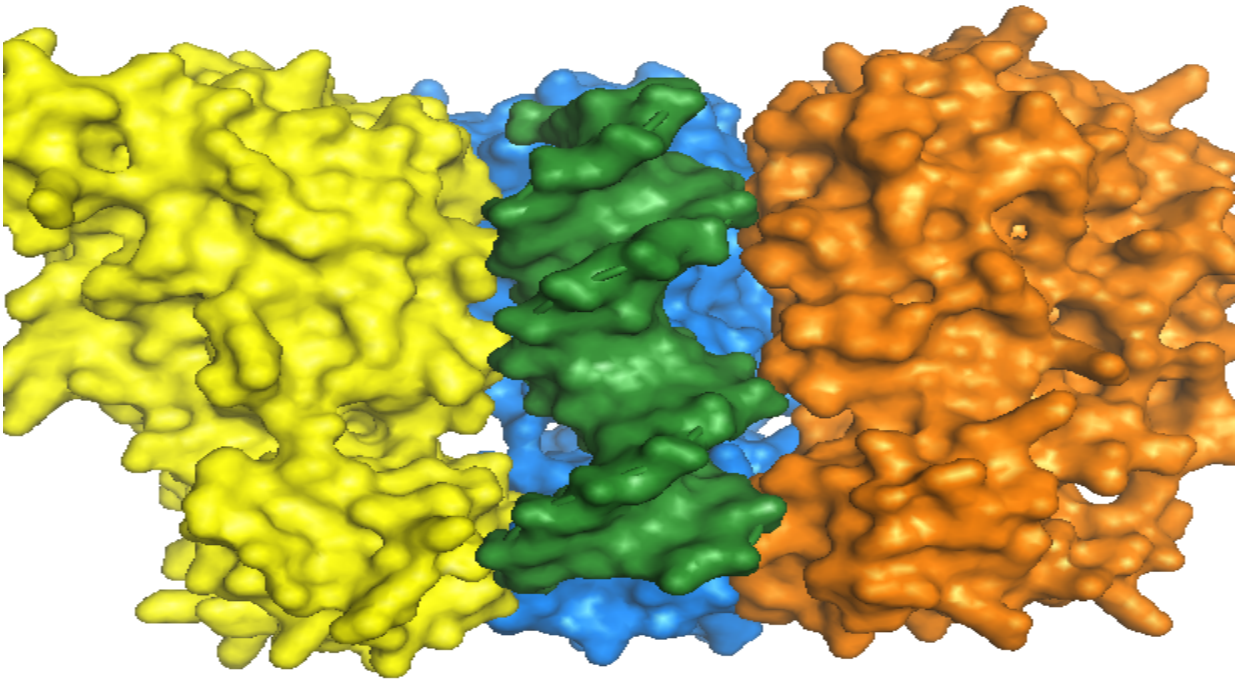

Figure 3.13 SpoIIIE Hexamer Reconstruction

A reconstruction of the SpoIIIE hexamer based on the FtsK crystal structure (*21*). Only 3 subunits of the hexamer are shown for clarity (yellow, blue, orange). The subunits in the structure only contain the alpha and beta subdomains. dsDNA is modeled in the central channel as a green surfaced filled double helix. Reconstructions were made using Phyre 2 (*27*) software by Gheorghe Chistol.

3.3.2 The mystery of the strand tracking mechanism

Previously it was mentioned that a 5'→3' polarity is a common mechanism of the RecA like family of ring NTPases. However, it is not entirely obvious why a dsDNA translocase would prefer interactions on one strand vs. the other or how it can recognize the correct strand during initial loading of the ring onto the DNA. Strand preference may force the ring to bind to DNA in a certain orientation, yet counter intuitively this would not provide directionality to the ring. Consider a thought experiment where a newly discovered motor protein binds to the DNA with the N-terminus proximal to the 5' end. This piece of information alone cannot tell you which direction the motor will go. On the other hand, information on the ring architecture does provide an indication of directionality. Case in point, the Rho and E1 helicases both bind to ssRNA and ssDNA respectively and in the same orientation with the 5' end proximal to the N-terminus, yet differing ring architectures have given the two helicases opposite translocation polarities, with Rho translocating in the 5'→3' direction and E1 translocating in the 3'→5' (*54*, *55*). One possible explanation for strand preference may be related to DNA supercoiling, a ring motor must preferentially interact with only one strand of the DNA in order to impart a consistent twist to the

DNA. Because SpoIIIE does have a biological role that involves supercoiling, evolutionary pressure would be placed on maintaining a strand preference. The 5'→3' strand preference for SpoIIIE would likely be the result of an evolutionarily conserved mechanism for all RecA like motors.

While SpoIIIE does have a biological reason for strand preference, it is not clear what mechanism SpoIIIE utilizes to recognize the 'correct' strand during initial loading and maintain this interaction across many ATP hydrolysis cycles. This is also an outstanding question in the field of ring NTPases in general, as helicases must also be able to recognize the correct strand during initial loading. Some possible mechanisms proposed for helicase loading include sequence specificity, such as the Rho helicase binding to the Rho Utilisation Site (rut) to help orient the ring in the 5'→3' direction (*117, 118*). Other mechanism also involve loading co-factors that are strand specific, recruiting helicase subunits and assisting in loading the ring onto the substrate (*37*). SpoIIIE has not demonstrated any sequence specificity nor does it require loading co-factors to assemble around the DNA. Further experiments would no doubt be illuminating on the mechanisms of this process.

DNA Construct	***Successful Crossing***	***Failed Crossing***	***Total Traces***
Double-Strand MeP Modification			
2 bp dsMeP	21	1	22
3 bp dsMeP	16	0	16
4 bp dsMeP	21	3	24
5 bp dsMeP	13	13	26
7 bp dsMeP	3	9	12
10 bp dsMeP	1	19	20
30 bp dsMeP	1	22	23
Single-strand MeP Modification			
30 base 3'→5' MeP	23	1	24
30 base 5'→3' MeP	6	22	28
Stepping Stone MeP			
4+1+4 dsMeP	7	16	23
4+1+3 dsMeP	9	16	25
4+1+2 dsMeP	6	18	24
4+1+1 dsMeP	33	4	37

Table 3-1 MeP Crossing Statistics

All MeP data was gathered under 5 pN of opposing force in constant force mode and [ATP] = 3 mM.

3.4 Conclusions and Future Directions

The ATPγS titration and MeP DNA experiments have revealed a complex mechanism of subunit coordination within SpoIIIE. Furthermore a step size of 2 bp has been determined without the need for an ultra-high resolution optical tweezer set-up designed to directly observe individual

steps of the motor. However, some information pertaining to subunit coordination would best be addressed by directly observing the timing of individual steps of the motor. For example, we can see from the ATP analogue titration experiments that SpoIIIE is not a strictly coordinated motor. A further investigation to dissect the details of this partial coordination would provide insights into the diverse mechanical strategies utilized by these classes of ring NTPases. One example of partial coordination is a pairs coordination mechanism proposed for an archaeal MCM helicase (*98*). If SpoIIIE were to operate by this mechanism we would see 'bursts' of 4 bp translocation subdivided into two 2 bp steps. Naturally, one can imagine many permutations of partial coordination that would best be studied by direct observation of stepping.

As mentioned earlier, in order to obtain enough data to average down the noise to see individual steps, this would require slowing down the motor to ~50 bp/sec (for a step size of 2 bp and the minimum required SNR of 2). Previously, I have attempted loading the motor with high force and titrating low concentrations of ATP to slow down SpoIIIE translocation. Unfortunately, at high forces and/or low ATP, SpoIIIE displays an increase in slipping frequency, to the point where the ring simply will not bind to its substrate. This situation can be rectified by forming stall complexes of SpoIIIE in the presence of ATPγS. Optical tweezer pulling experiments have confirmed that SpoIIIE can form stalled complexes. These stalled complexes can also be pulled to high forces (~20 pN), indicating that ATPγS increases SpoIIIE's affinity towards DNA. Once a stalled complex is formed with ATPγS, an arbitrarily small concentration of ATP can be flowed in to restart translocation. Using Eq. (3.9), we can calculate that a concentration of [ATPγS] = 5 mM and [ATP] = 25 μM would be the necessary conditions to sufficiently slow down the motor in order to observe individual steps. The high concentration of ATPγS required for this experiment might become prohibitively expensive, thus it is recommended that the tubing for the chamber should be designed to minimize the amount of void volume.

MeP modified DNA experiments have demonstrated that SpoIIIE makes critical phosphate contacts during translocation. Crystal structures of possible DNA interaction loops of FtsK suggest that motor-DNA interactions would likely be charged-charged, or polar-charged interactions (*21*). These are fairly stable noncovalent interactions, having bond dissociation energies on the order of 15 kJ/mol at room temperature in solution, or about 6 k_BT (*119*). As a fast and processive motor, SpoIIIE must be able to quickly form electrostatic interactions during DNA binding and then expend energy to break those same interactions after DNA translocation in order to reset the subunit for the next DNA binding event. The only energy source available in the reaction buffer is the chemical potential energy from ATP, thus SpoIIIE must utilize part of the ATP hydrolysis cycle to break these electrostatic interactions. The total estimated energy available from a single ATP molecule is about ~25 k_BT under my buffer conditions. About 10 k_BT must be used for translocating DNA (assuming a 2 bp step size and stall force of ~65 pN Figure 2.4 C). Some energy is likely used in twisting the DNA; the remainder is more than enough energy to break an electrostatic interaction. It is important to remember that this calculation gives no indication as to whether the electrostatic interaction is broken by the same subunit immediately after taking a 2 bp step, or by another subunit. Observing the order of DNA binding events would ideally be suited for co-crystallization of the ring with DNA and at different ATP hydrolysis stages. Alternatively, high-resolution experiments that are capable of resolving small slipping events can be used to interrogate the order of DNA binding in greater detail.

Neutralizing the charges on one strand of the DNA has shown that SpoIIIE tracks one strand of the double helix and maintains preferential contact on one strand throughout several translocation events. How does SpoIIIE recognize the correct strand upon initial binding? How

does it maintain its strand preference during translocation? These are outstanding questions that deserve further experimentation. SpoIIIE has not been shown to interact with any strand specific loading co-factors *in vivo* and there are certainly no co-factors present during *in vitro* experiments on the tweezers. Furthermore, SpoIIIE has not displayed a sequence preference when loading onto lambda phage DNA. Despite the lack of these co-factors, SpoIIIE is still competent to recognize and interact with the 5'→3' strand of dsDNA even when the substrate contains non-native lambda phage sequence. There are however, subtle differences between the two strands phosphate backbone structure in B-form DNA that SpoIIIE potentially could recognize. To test this hypothesis, I can challenge the motor with DNA substrates that slightly alter the orientation of the phosphate backbone. One experiment would involve the use of a chiral phosphate backbone to challenge the motor. Note that the MeP modifications made to DNA in Figure 3.8 A has introduced a chiral center in the phosphorous atom. Currently SpoIIIE is probed with MeP patches containing racemic mixtures of MeP DNA. It would be interesting to observe whether SpoIIIE displays different responses to chirally pure oligos of MeP. Alternatively, one could synthesize oligos that switch polarity midway and ligate restriction digested overhangs to a normal DNA tether. Observing how SpoIIIE can resolve the challenge when presented with strands of opposite polarity would provide deep insights into the partially coordinated mechanism of SpoIIIE.

Chapter 4 Motor-Substrate Interactions

Background

The stall force of a molecular motor is both a mechanical parameter and an indicator of the stability of motor-substrate interactions. The relatively large bond dissociation energy of electrostatic interactions that SpoIIIE makes with its DNA substrate is in good agreement with the high forces that the motor is observed to work against. A distinction must be made between thermodynamic stall force and effective stall force. The thermodynamic stall force is defined as the force which the motor reaches zero velocity and reverses translocation (*7*, *50*). This definition is somewhat misleading as a motor containing an irreversible transition will formally have an infinite stalling force, which is clearly artificial (*7*). Typically, motors sufficiently slowed down under high forces will eventually step backwards or the motor itself will deform. In some cases however, a motor under high forces will encounter secondary effects that force detachment before the thermodynamic stall force is reached (ie. DNA strand melting, motor-substrate interactions breaking etc…), this is what is called an effective stall force. This chapter will focus on the forces SpoIIIE is capable of working against and the stability of its DNA interactions.

4.1 Motor-DNA stability

4.1.1 SpoIIIE is capable of pulling to high forces

To determine the average force that SpoIIIE can work against, a histogram of slip forces was created using passive mode analysis. Passive mode takes advantage of SpoIIIE's ability to maintain DNA interactions even after a slip, allowing sampling of multiple slip forces within a single experimental trace (Figure 4.1 A).

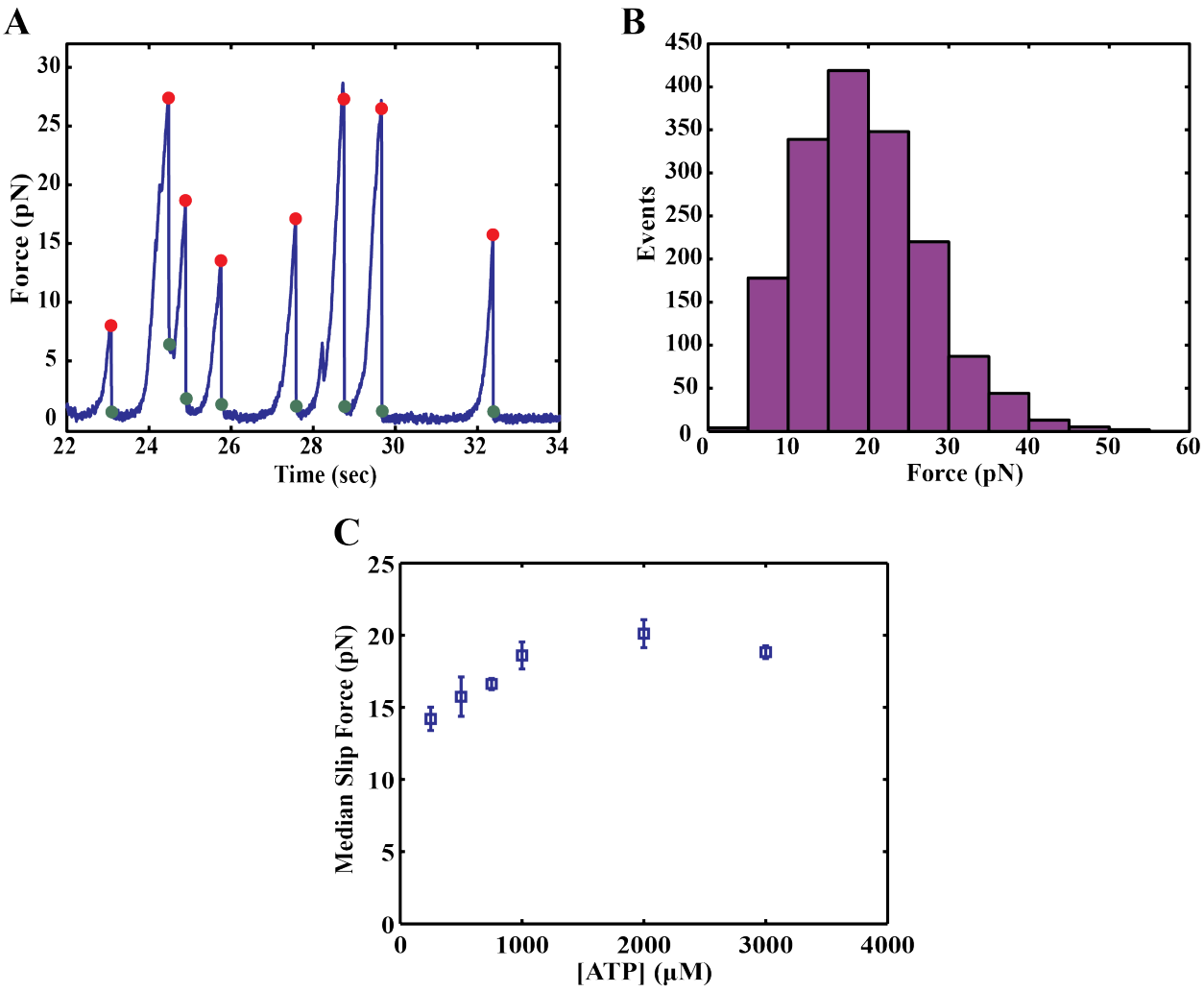

Figure 4.1 Slipping analysis

(A) An example passive mode trace at [ATP]=3 mM. A custom MATLAB script scores the slip location and force (red dot) as well as the recovery force (green dot).
(B) Histogram of slip forces at [ATP]=3 mM. Mean slip force is ~20 pN. Maximum force seen is 50 pN.
(C) Mean slip force as a function of [ATP]. Error bars are s.e.m.

Experimental determination of the SpoIIIE stall force has not yielded a clear result. At the highest force tested (45 pN), the motor did not display backstepping behavior. Furthermore, forward translocation still proceeded at a significant rate of ~2 kb/sec (Figure 1.9). Testing translocation velocity at higher forces was prevented due to increased slipping frequency, thus the slip forces histograms do not contain data higher than 50 pN (Figure 4.1 B). Given the high rate of translocation even at 45 pN, the thermodynamic stall force is likely even higher than 45 pN. Comparatively, the stall force of kinesin is shown to be ~ 5pN (*49*). We can calculate the maximum theoretical stall force based on the available free energy of ATP hydrolysis using

$$F_{stall} = \frac{\Delta G^0}{d} + \frac{k_B T}{d} \ln\left(\frac{[ADP][P_i]}{[ATP]}\right) \quad (4.1)$$

where ΔG^0 is the standard free energy of ATP hydrolysis and d is the step size of the motor (*7*, *50*). The standard free energy of ATP varies in the literature and is also dependent on pH and temperature (*120*). For the most part, ΔG^0_{ATP} lies within -20 to -25 k_BT (*70*). Under conditions where [ATP] = 3 mM, [ADP] = [P_i] = 5μM and pH 7.5, ΔG_{ATP} is ~ -27 k_BT, or about -110 pN·nm. Taking the measured step size of 2 bp and assuming 100% efficiency in energy conversion, we arrive at a maximum theoretical stall force of ~160 pN. Most molecular motors however, operate around a thermodynamic efficiency of 30-40% (*50*); applying this efficiency to the calculated maximum stall force will yield a new stall force of ~65 pN, close to the predicted stall force of the loosely coupled + tightly coupled translocation model (Figure 2.4 C).

Ring NTPases typically exhibit greater binding affinity towards their substrates in the presence of NTP. To test this hypothesis, the mean slip force of SpoIIIE can be used as a direct measurement on the stability of motor-DNA interactions. At near saturating ATP concentrations of 2 mM or greater, the mean slip force of SpoIIIE is ~20 pN, lowering the ATP below the K_m reduced the mean slip force to ~15 pN (Figure 4.1 C). The reduction in mean slip force at lower ATP concentrations suggests that ATP increase SpoIIIE binding affinity to its DNA substrate. Alternatively, lower ATP concentrations also reduce the pause-free velocity of SpoIIIE, the slower translocation velocity could potentially affect SpoIIIE's efficiency of handing off the DNA substrate to adjacent subunits during an ATP hydrolysis cycle around the ring.

4.1.2 ATPγS stabilizes SpoIIIE DNA interactions

To differentiate between ATP binding or translocation effects on the motor's affinity towards DNA, the non-hydrolysable analogue ATPγS was used again for pulling experiments with SpoIIIE. In the presence of only ATPγS, SpoIIIE demonstrated no translocation activity for at least 20 min (data not shown). To test whether ATPγS increases SpoIIIE binding to DNA, a manual pulling protocol was tested on DNA using SpoIIIE as the attachment point. In 1x reaction buffer without the presence of nucleotide, SpoIIIE was able to form weak complexes around DNA. Pulling curves demonstrate that these complexes could be broken at a force of ~4 pN (Figure 4.2 A), indicating that SpoIIIE binds to DNA with low affinity in the absence of nucleotide. Adding in 1 mM ADP or ATPγS significantly increased the mean pull forces, with ATPγS providing the largest increase (Figure 4.2 D). Taken together, these results show that SpoIIIE has a greater binding affinity towards DNA in the presence of nucleotide.

4.1.3 SpoIIIE slipping increases with force

The stability of motor-DNA interactions can be directly modulated with force. Slipping frequency as a function of opposing force was calculated in constant force mode. Slips in constant force mode and passive mode are roughly equivalent. However, constant force mode does provide more information on the force-dependent behavior of slipping. Figure 4.3 B shows that at saturating ATP conditions, slipping frequency is insensitive to force. At [ATP]≤K_m, slipping frequency increases with force, consistent with the hypothesis that ATP stabilizes motor-DNA interactions.

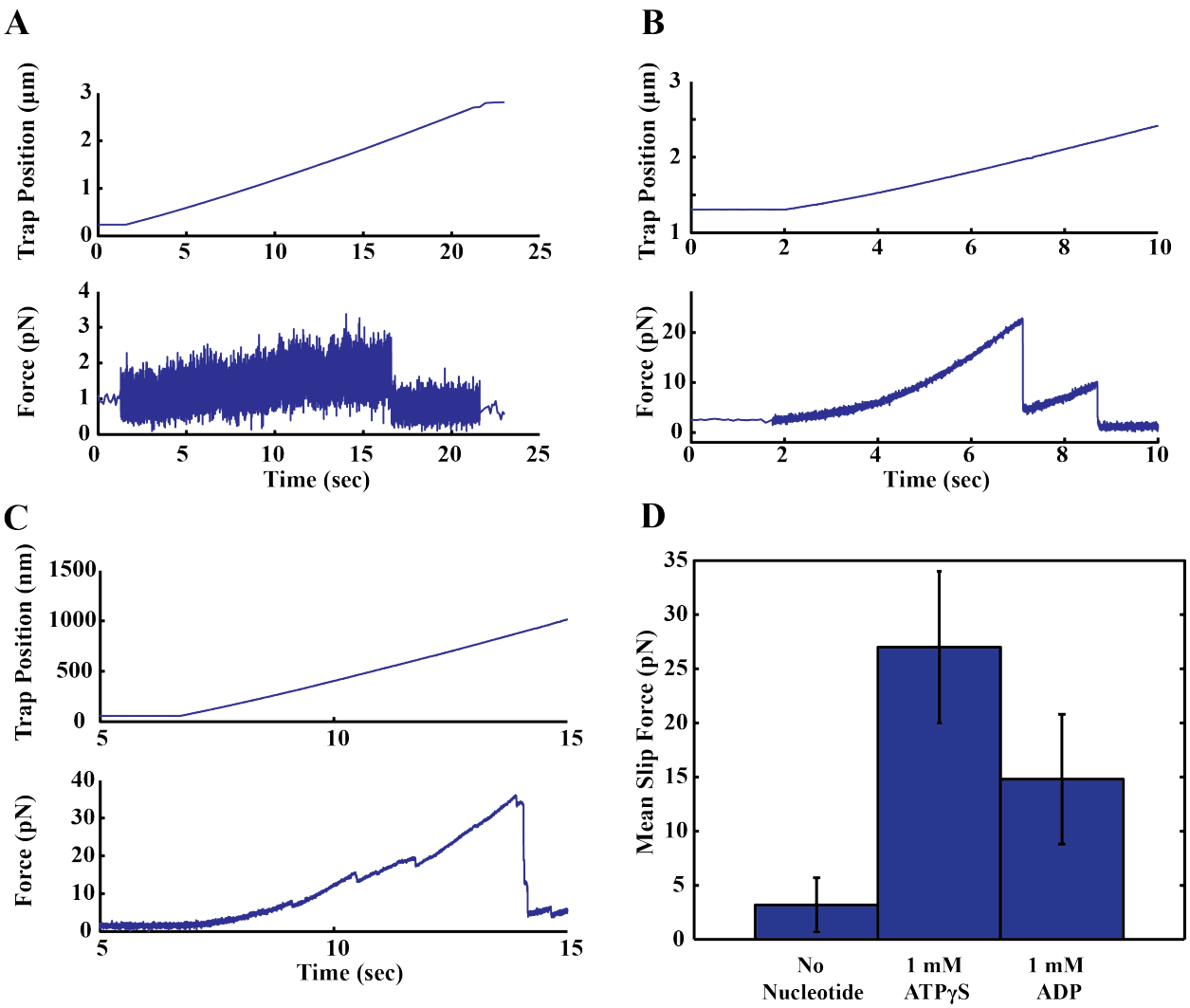

Figure 4.2 Pulling Experiments with SpoIIIE

(A) A pulling curve with only SpoIIIE and no nucleotides. The trap is moved further apart from the pipette bound bead at a constant rate of 100 nm/sec to create tension on the DNA tether.
(B) Pulling curve with SpoIIIE and 1 mM of ADP. The slip force is significantly higher than no nucleotide.
(C) Pulling curve with SpoIIIE and 1 mM of ATPγS.
(D) Mean slip forces for all 3 conditions tested. Error bars are standard deviation.

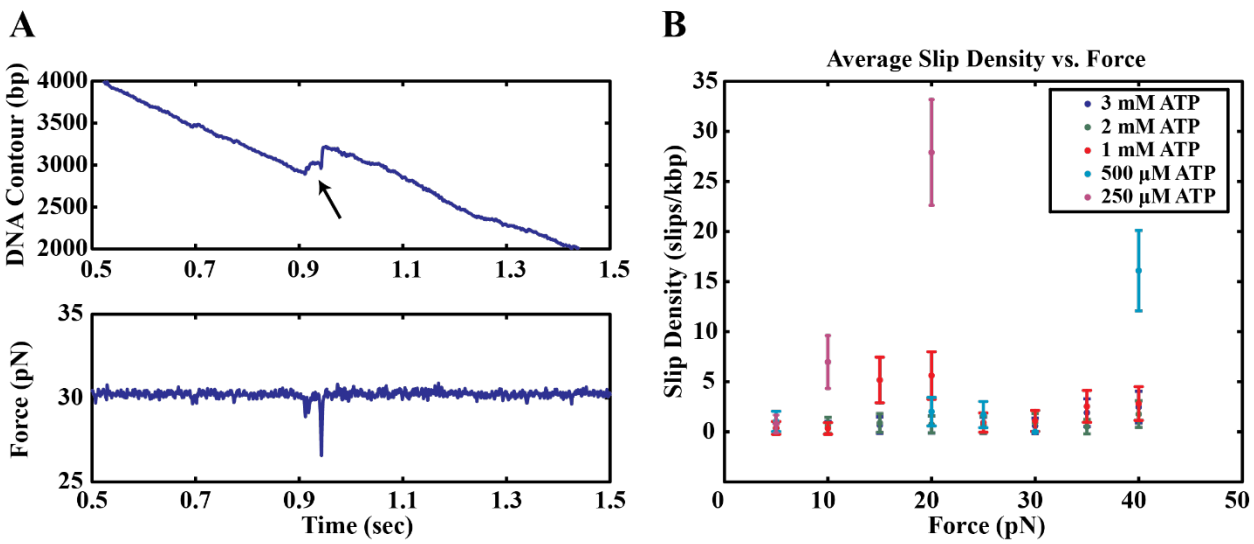

Figure 4.3 Slipping Frequency vs. Force

(A) Representative trace at [ATP] = 1 mM and 30 pN of force. A single slip is denoted by the arrow. Note that a reciprocal drop in force accompanies a slip.
(B) Slip density as a function of opposing force for ATP conditions 0.25-3 mM. Error bars are s.e.m.

4.2 Conclusions

In this chapter, I have demonstrated that SpoIIIE is capable of pulling DNA to high forces and that the stability of motor-DNA interactions is dependent on both nucleotide and force. I have previously shown in Chapter 3 that the SpoIIIE motor makes at least four electrostatic phosphate contacts with the DNA backbone. Given the stability of electrostatic interactions, the pulling experiments with SpoIIIE suggests that only an ATP or ADP bound subunit is capable of making electrostatic interactions. Figure 4.2 B shows motor-DNA interactions proceeding in order of decreasing affinity when the motor is ATPγS bound, ADP bound, and empty. The importance of cycling motor-DNA affinity in terms of processivity should not be lost on the reader.

Chapter 5 Materials and Methods

5.1 General Molecular Biology

5.1.1 Plasmid Construction

Biotinylated SpoIIIE constructs were created used the plasmid pJB103 (*8*) as a template. The biotin tag protein from PinPoint Xa-1 (Promega) vector was PCR amplified using flanking primers containing BamHI sites. The biotin tag was then ligated to the N-terminal location of the pJB103 plasmid to create the plasmid pNL3 (Figure 5.1).

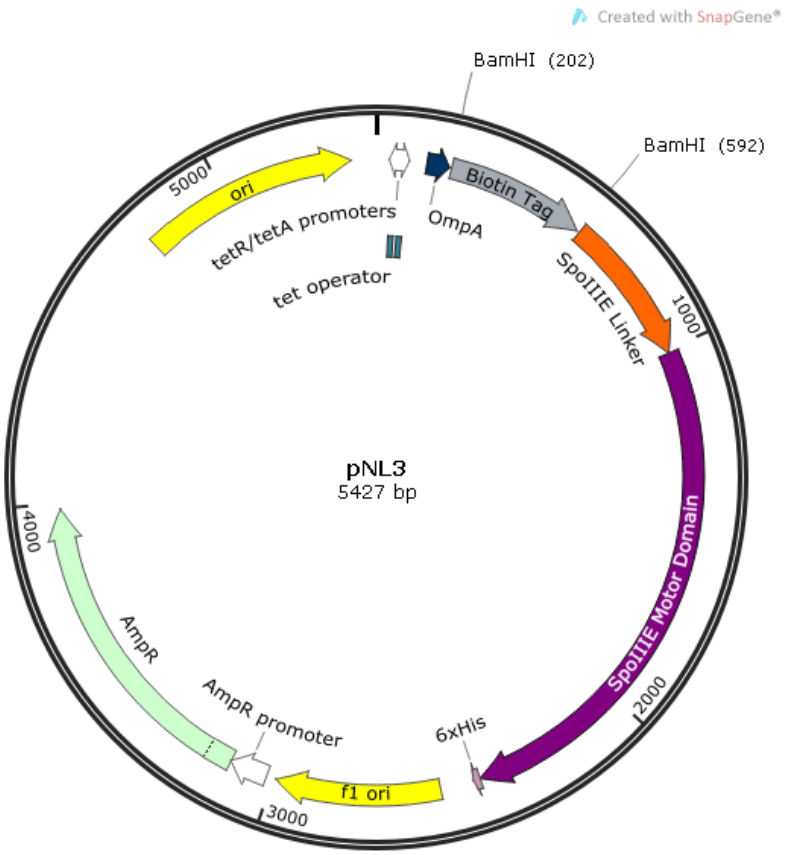

Figure 5.1 Plasmid Map of the pNL3 Biotinylated SpoIIIE Construct

The pNL3 plasmid is used to express the protein for the majority of the work presented in this thesis. The plasmid contains ampicillin resistance for selection and a 6x C-terminal His tag for nickel column purification. Plasmid cartoon created with SnapGene.

5.1.2 Protein Expression and Purification

Biotinylated SpoIIIE (pNL3) were expressed using established protocols (*12*) but with the addition of biotin to the liquid culture. Briefly, DH5α *E. coli* cells containing the pNL3 plasmid were grown overnight in a 50 ml Luria Broth (LB) starter culture in the presence of 1x (0.1 mg/ml)

ampicillin and 2 μM biotin. Overnight cultures were then inoculated into 1 L LB cultures and grown to OD_{600} ~0.6. The 1 L cultures must also be supplemented with 1x ampicillin and 2 μM biotin. Induction is done with 1 ml/L 4 mg/ml anhydrotetracyclin (Sigma CAS: 13803-65-1) dissolved in EtOH for 2 hours. The cells at this point will be bright yellow, do not be concerned as this is perfectly normal. Cells are then pelleted, washed with TBS buffer and frozen in the -80^0 freezer.

After expressing the protein, purification is a one step process with a Ni-NTA column (GE Healthcare, Figure 5.2 B). Cells are taken out of the freezer and resuspended in lysis buffer supplemented with Protease Inhibitor Cocktail VII (EMD Cat: 539138). Lysate is sonicated, spun down, filter sterilized, and run through a Ni-NTA column using an FPLC instrument. Protein is eluted with an imidazole gradient. The protein usually comes off the column around 250 mM imidazole. Fractions are observed on an SDS-PAGE gel (Figure 5.2 A), dialyzed overnight into 1x Dialysis buffer and stored in the -80^0 C freezer. Samples generally can be stored in -80^0 for six months before activity is negatively affected.

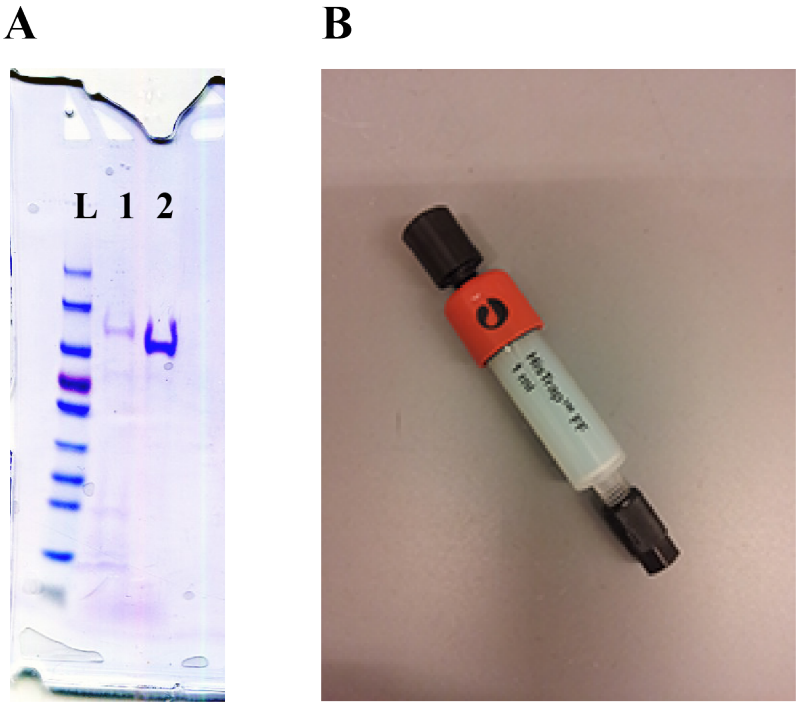

Figure 5.2 Protein Preps

(A) SDS-PAGE gel after SpoIIIE purification and stained with Commassie. Ladder (L) is a standard pre-stained ladder from Fermentas. The red stain in the ladder is the 70 kDa marker, SpoIIIE runs at an apparent molecular weight of ~110 kDa. Lane 1 is the biotinylated SpoIIIE purified from pNL3. Lane 2 is the SpoIIIE purified from pJB103.
(B) HisTrap FF column used in protein preps. Column is a product of GE healthcare.

5.2 Single-Molecule Experiments

5.2.1 Preparation of the chamber

The experimental chamber is composed of Nescofilm gaskets sandwiched between two No. 1 coverslips (VWR). The gaskets are laser cutted with a design to allow for 3 separate channels. Dispenser tubes connecting the 'top' and 'bottom' channel to the 'middle' channel are placed on to the Nescofilm. Finally a micropipette is also placed on to the middle chamber. Afterwards the chamber is mounted onto a chamber holder and installed into the instrument (Figure 5.3).

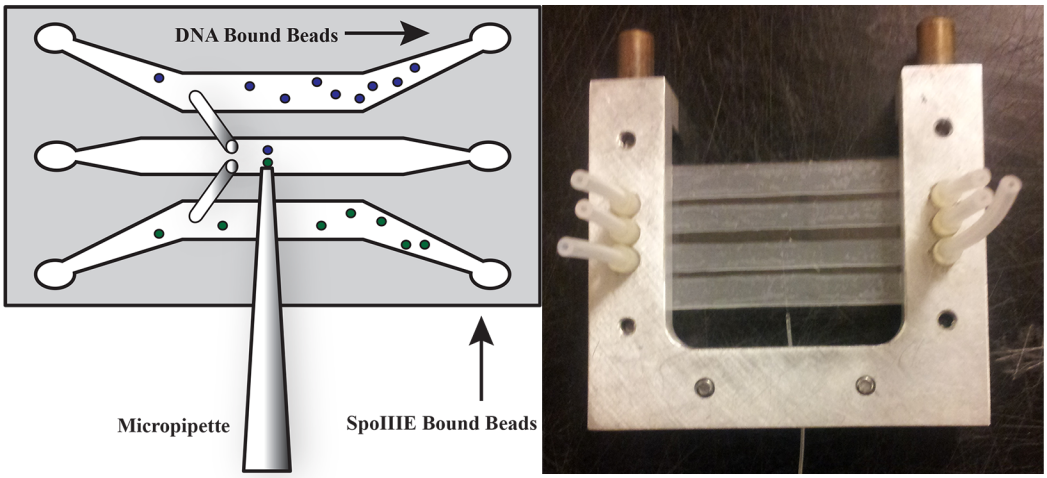

Figure 5.3 Chamber Design for Optical Tweezers Experiments

A cartoon of the chamber used is shown on the left. DNA bound beads (blue circles) and SpoIIIE bound beads (green circles) are flowed into separate channels and only brought to the middle experimentation area via dispenser tubes (shaded cylinders). The actual chamber mounted on to the metal chamber holder is shown on the right.

5.2.2 DNA tether preparation

DNA tethers used for optical tweezers experiments were PCR amplified using lambda DNA (NEB) as the template and 5' biotinylated primer (IDT). The PCR reaction product is 21 kb in total length, which requires the use of a specialized PCR extender system (5prime). Alternatively, DNA tethers can be prepared directly from lambda DNA stock itself. Briefly, lambda DNA is cut in half using the XbaI restriction enzyme (NEB). Biotin is added on one end of the DNA using a Klenow exo- reaction with biotinylated nucleotides.

The choice of using biotin as an attachment point for DNA is based on two criteria. The first is the stability of biotin-streptavidin interactions. As one of the strongest non-covalent interactions known, it is capable of maintaining bond cohesion up to 160 pN of force. The second criteria is more subtle; biotin contains a single bond about which the molecule can swivel freely. This is of vital importance for studying motor proteins as the swivel point relieves any supercoiling

effects introduced by motor translocation. A DNA tether that is torsionally unconstrained greatly simplifies data analysis further down the line.

5.2.3 Single-molecule experiments

Prior to single-molecule experiments, 2.1 micron streptavidin beads (Spherotech SVP-20-5) are blocked for 30 min at room temperature with 1x Bead Blocking Buffer. I have found that SpoIIIE can bind non-specifically to the streptavidin beads even in the absence of a biotin tag. This is likely due to the fact that the beads have exposed groups with a negative charge and SpoIIIE as a DNA binding protein would likely favor highly negative surfaces. Non-specific binding will eventually complicate data analysis further down the line, especially slip force analysis, thus blocking is a necessary step to prevent slipping artifacts. Separately, biotinylated DNA tethers are also incubated onto streptavidin beads, blocking is unnecessary for this incubation.

After incubation, the beads are diluted to a total volume of 1 mL in 1x Reaction Buffer. Each bead solution is then injected into either the top or bottom channel. Beads can then flow into the middle channel via a connecting dispenser tube. Note that in this set-up the experimental area is the middle channel. Furthermore, the SpoIIIE protein and DNA are spatially separated until they are manipulated into close proximity to one another via the optical trap. Previously, magnetic tweezers experiments involved flowing in free SpoIIIE protein to bind to the DNA (*12*). The disadvantage of such a set-up is that the experimentalist would not know where on the DNA tether SpoIIIE has bound. The new set-up presented here eliminates that ambiguity as the only SpoIIIE protein present in the middle channel is the protein bound to the bead. As shown in previous chapters, immobilizing SpoIIIE on the bead allows for experiments on modified DNA, pulling experiments, and more.

5.3 Data Analysis

5.3.1 Analyzing passive mode data

Passive mode traces were analyzed by dividing traces into regions of translocation or pauses. Translocation regions were binned together in force windows of 2 pN. A line was fit to the contour length data in the force window to calculate translocation velocity (Figure 5.4 B). Pauses were scored using a custom built MATLAB program by Gheorghe Chistol using the Schwartz Information Criterion (SIC) step finding algorithm (*102*). The SIC equation is

$$SIC(j_1, \cdots, j_k) = (k+2)\, log(n) + n \cdot log(\hat{\sigma}^2_{j_1,\cdots,j_k}) \tag{5.1}$$

where j_k are the location of the assumed steps, k is the number of steps, n is the number of data points, and $\hat{\sigma}^2_{j_1,\cdots,j_k}$ is the maximum likelihood estimator of the variance for k steps. The algorithm is an iterative procedure that attempts to minimize the SIC score (Figure 5.4 A). One can see from the equation above that the SIC score will increase if too many steps are fitted (left term), or if the variance of the fit is too high (right term). When the algorithm is applied to real SpoIIIE data, we found that the procedure tended to over-fit the data. To address this issue, an additional penalty factor (PF) was applied to the SIC equation to give $SIC(j_1, \cdots, j_k) = PF(k+2)\, log(n) + n \cdot log(\hat{\sigma}^2_{j_1,\cdots,j_k})$. A penalty factor of 2-3 was found to be sufficient for all conditions tested.

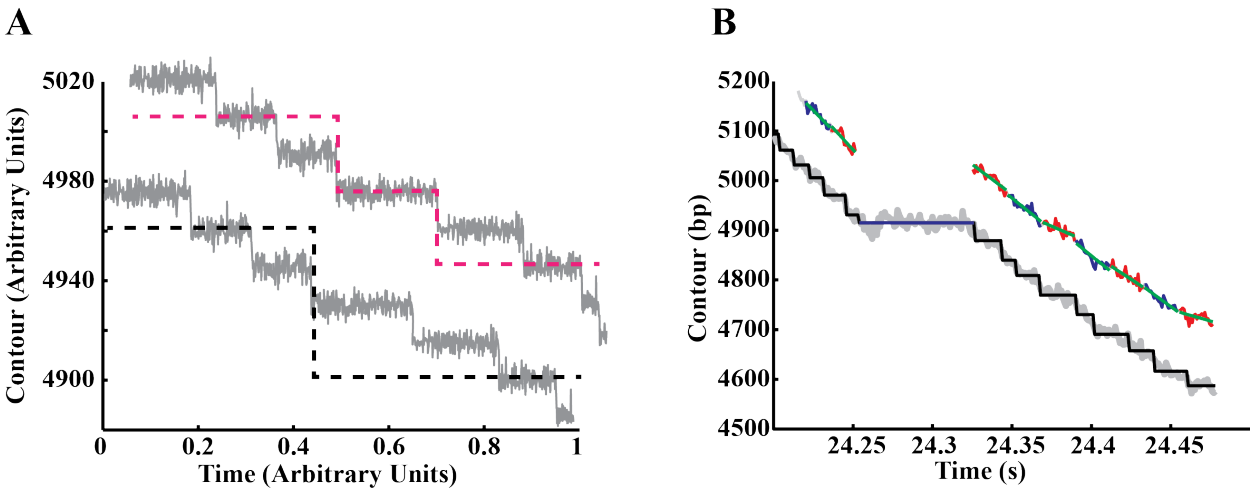

Figure 5.4 Examples of SIC Analysis

(A) Cartoon of how the SIC scores steps and dwells on a simulated trace. The two traces are offset for clarity. A first iteration (dotted black line) will place a step in the middle of the trace. The second iteration (dotted magenta line) will maintain the position of the first step and place a second step in the next most likely location.

(B) Example of SIC algorithm on SpoIIIE translocation data (grey lines). The two traces are identical and offset for clarity. The SIC fits steps and dwells to the entire trace (black line). A pause is scored based on a time threshold (blue line). The pause is then removed and the remaining trace is binned into 2 pN force windows (alternating red and blue regions) and fitted to a line (green line).

While it may seem strange to use a step-finding algorithm to find pauses, step finding algorithms perform equally well in scoring both pauses and steps. SpoIIIE moves too fast for individual steps to be resolved, thus the steps scored by the SIC are ignored. Pauses are scored based on a time threshold within the dwell regions of the SIC fit. The minimum time threshold used was 30 msec as this is the shortest pause than can be accurately detected given the signal to noise ratio of my experimental system. Generally speaking, the faster a motor moves, the easier it is to detect shorter pauses. The standard deviation of the positional noise in my system is about 15 bp, taking 5 times the standard deviation we get 75 bp. Given SpoIIIE's translocation velocity, the motor can traverse 75 bp in ~20 msec. In principle a 20 msec cutoff is a sufficiently long threshold for pause scoring. However, I have found that for simulated traces a 20 msec cutoff will still occasionally give false positives (Figure 5.7 B). Therefore the time threshold was tightened further to 30 msec.

The SIC algorithm does carry one disadvantage in its pause scoring algorithm, extremely long pauses (>1 sec) tend to get broken up into a series of shorter pauses (Figure 5.5). To correct for this over-count, another custom MATLAB script was written to combine disparate pauses.

```
CombPause = logical(~GoodTracePortions(p).PauseIndex);
DwellNumberL=[1:numel(GoodTracePortions(p).Dwells)];
DwellNumberL=logical(~DwellNumberL);

    for d=1:length(GoodTracePortions(p).PauseIndex)
```

```
        if      d>1     &&      abs(GoodTracePortions(p).PauseIndexLocation(d)-
GoodTracePortions(p).PauseIndexLocation(d-1))<PauseThreshold
            if DwellNumber(d)-DwellNumber(d-1) < 3  %Only Combine Pauses that
are adjacent.
                CombPause(d-1:d)=1;
            end
        end
    end
```

Briefly, the MATLAB code looks for adjacent pauses scored by the SIC and determines whether their position in the y axis is within the standard deviation of the noise. If they are within one standard deviation, a red line is drawn between the two pauses to indicate that it is a single pause.

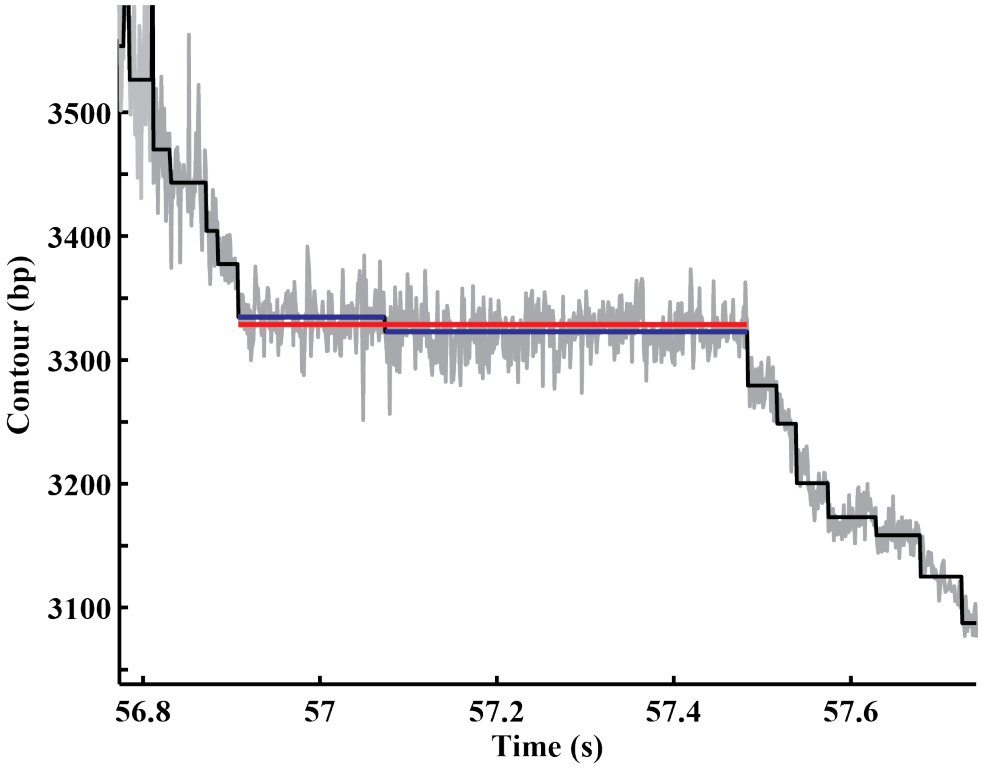

Figure 5.5 Combining Disparate Pauses

An example of the SIC algorithm scoring two pauses (blue lines) in the SpoIIIE trace (grey lines). A custom MATLAB script identifies that the two pauses are within error of the noise and combines them into a single pause (red line).

5.3.2 Analyzing constant force data

Single-molecule traces taken at constant force use an active feedback system to adjust the trap position in order to maintain a constant force on the trap. Since constant force mode is only looking at relative changes in distance, the WLC correction for DNA is a simple unit conversion. For example, at 5 pN a DNA tether is about 92% extended (*42*). Thus converting Δnm to Δbp is $\Delta bp = \Delta nm/(0.34\,nm/bp)/0.92$ at 5 pN of force. Raw data is collected at 1 kHz and boxcar

filtered down to 50 Hz. Pauses were identified as described previously. Pause-free translocation velocity was determined by fitting a line and calculating the slope for 1 kbp bins of translocation.

Active feedback systems however, will artificially reduce the bead position noise at the cost of increasing trap position noise (Figure 5.6 A). This noise can be addressed by adjusting the gain of the feedback. Looking at the minitweezers active feedback code, the relevant line of code is

```
Trapstep = C±(psdTargetY-psdY)*(ForceGain/64)
```

How far the trap moves per cycle is dependent on the difference between the measured force and preset force and the gain. For feedback systems with the gain set too high, the trap will overshoot the set value. Lowering the gain will prevent trap overshooting and eliminate trap position noise (Figure 5.6 B).

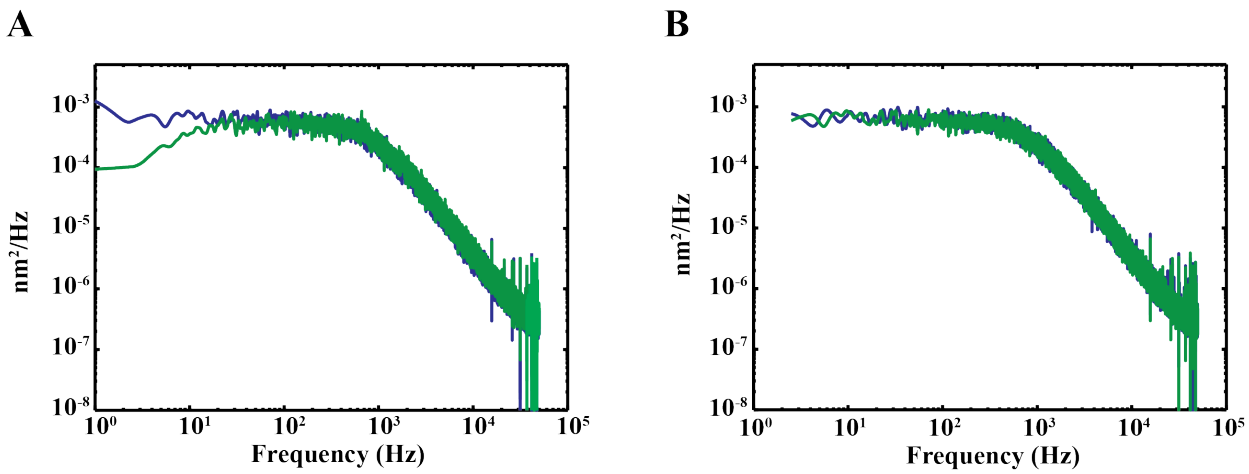

Figure 5.6 Power Spectrum Analysis of Feedback Gain

(A) Power spectrum of a bead held at 5 pN of force (blue), or held at 5 pN with an active feedback system (green). Note the dip in the power spectral density at long timescales is due to the feedback system reducing the apparent bead motion.

(B) Power spectrum of a bead held at 5 pN of force (blue), or at 5 pN with an active feedback system where the gain has been lowered (green). The power spectral density of the bead now behaves as one would expect for a bead held under tension without a feedback mechanism.

5.3.3 Analyzing slipping data

Slip forces were calculated for traces using a custom written MATLAB script shown below that identifies and bins together the slip forces.

```
difF = diff(Force);
slipindex = difF<-.5;
slip_location = find(slipindex>0);
for j=1:numel(slip_location)
    if slip_location(j)==0
        continue
    end
```

```
    for k=1:Span
        Unifiedslip = slip_location(j)+k;
        for l=1:numel(slip_location)-1
            if Unifiedslip == slip_location(l+1)
               slip_location(l+1)=0;
            end
        end
    end
end
if slip_location(1)<Span
    slip_location(1)=[];
end
slip_location=nonzeros(slip_location);
slip_location(end)=[];
```

Briefly, the code calculates the difference in force across the entire time trace. Slips generally have a large change in force over a short period of time which allows a threshold to be set. After the location of slips has been determined, the maximum force within a time window is calculated as the slip force. A user interface also allows for a visual assessment of the accuracy of slip scoring and if necessary, remove false positives before the data is saved (code not shown).

5.4 Simulations

5.4.1 Intersubunit Simulation

The simulation of intersubunit coordination were custom written in MATLAB. Simulations start off by calculating the percent occupancy of the ring in terms of ATP and ATPγS. Because ATPγS likely binds to SpoIIIE tighter than ATP, subunits that have bound to ATPγS will stay bound for a longer, exponentially distributed amount of time. The code to follow a ring in various nucleotide bound states is shown below.

```
for h=100:100:1000  %Run simulation for 100-1000 uM gS conditions
    Satp=zeros(10000,6);
    Fraction=h/(h+3000);
    gstau=5;   %Lifetime of gS molecule relative to ATP turnover.
    for i=1:6  %Run simulation for subunit 1-6
        j=0;
        mark=0;
        count=0;
        for j=1:10000  %Run simulation for 10000 time increments
            r=rand;
            if j<mark+count
                continue
            end
            if r<Fraction
                rgs=exprnd(gstau);
                count=round(rgs);
                Satp(j:j+count,i)=0;
                mark=j;
            end
            if r>=Fraction
                Satp(j,i)=1;
            end
```

```
            end
        end
    end
```

It is important to remember that the code is presenting a highly simplified version of what is happening at the molecular level. Off-pathway states and higher order effects are not considered here. The code will produce a 10000x6 array with a list of 0's and 1's, with 0 defined as ATPγS bound and 1 as ATP bound, each column represents a single subunit of SpoIIIE over time. The cartoon illustration of the code is shown in Figure 3.2 B. Various coordination models can now be imposed to better understand the nature of SpoIIIE translocation. For example, stochastic models would require all 6 subunits to be ATPγS bound in order to induce a pause, pairs models requires two adjacent ATPγS bound subunits to induce a pause.

5.4.2 Simulation of experimental noise

The accuracy of the pause detection algorithm was tested on a simulated trace containing pauses and obscured with normally distributed noise (σ = 15 bp, similar to experimentally measured noise). Simulated traces shows a translocase moving at 4 kbp/sec interspersed with 30 msec pauses. The pause detection algorithm succeeded in scoring all pauses of at least 30 msec in length (Figure 5.7 A). Relaxing the pause scoring algorithm to a 20 msec cutoff gave several false positives (Figure 5.7 B), demonstrating that a 20 msec threshold is too permissive. The minimum pause time threshold value for all single-molecule experiments was therefore set to 30 msec. Conditions with slower translocation will necessitate further tightening of the pause threshold.

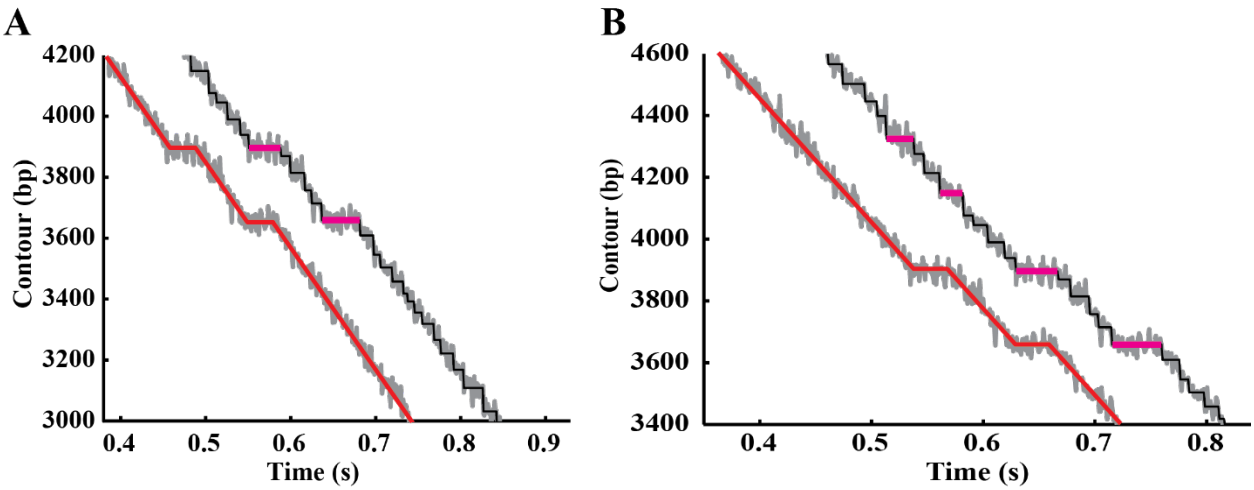

Figure 5.7 Simulated Translocation and Pausing Events

(A) Simulated trace containing 30 msec pauses. An idealized trace (red line) is obscured with normally distributed noise (grey outline). Simulated data is run through the pause scoring algorithm (black line) and scored for pausing events (magenta highlights) with a 30 msec time threshold. The two traces are offset for clarity.

(B) Simulated trace containing 30 msec pauses and run through the same pause scoring algorithm with a 20 msec threshold. Both actual pausing events were correctly scored but false positives were also introduced.

5.5 Optical Trap Calibration

5.5.1 Force and distance calibration

The most straightforward way to model an optical trap is as a Hookean spring with a stiffness of κ. The position-sensitive photodetectors in the optical tweezer instrument generate a photocurrent that is proportional to the intensity and position of the light hitting the sensor. In order to relate these voltage readings to force and distance, the readings are calibrated using a well-established method that relates the thermal fluctuations in position of an optically trapped bead to the measured voltages (*121*). According to the equipartition theorem, the average energy imparted to a particle in thermal equilibrium is $\frac{1}{2}k_BT$ for each degree of freedom. For a bead attached to a spring with stiffness κ, the average potential energy is $\frac{1}{2}\kappa\langle x^2\rangle$. Setting these two energies equal to each other yields a relationship between the stiffness κ to the variance in bead position.

$$\kappa = \frac{k_bT}{\langle x^2\rangle} \tag{5.2}$$

This fundamental relationship describes the expected variance of bead position if the trap stiffness is known. Eq. (5.2) contains two unknowns, solving for the expected variance requires an independent determination of the trap stiffness. For a bead constrained by an optical trap with stiffness κ, the potential well can be considered harmonic, and the one-dimensional motion of the bead is described with the following Langevin equation,

$$m\frac{d^2x}{dt^2}(t) + \gamma\frac{dx}{dt}(t) + \kappa x(t) = F(t) \tag{5.3}$$

where m is the mass of the particle, γ is the drag coefficient, κ is the trap stiffness and $F(t)$ is the time-dependent thermal force term.
Since micron-sized beads are operating in a low Reynolds number environment, the inertial term can be dropped, leaving

$$\gamma\frac{dx}{dt}(t) + \kappa x(t) = F(t) \tag{5.4}$$

Under equilibrium conditions, the $F(t)$ term will have zero mean and is uncorrelated in time (*122*), represented mathematically as

$$\langle F(t)\rangle = 0;\ \langle F(t_1)F(t_2)\rangle = \delta(t_1 - t_2) \tag{5.5}$$

where δ is the Dirac delta. The equation of motion can be rewritten as,

$$\gamma\frac{dx}{dt}(t) + \kappa x(t) = (2k_BT\gamma)^{1/2}F(t) \tag{5.6}$$

where $(2k_BT\gamma)^{1/2}$ is the expected Gaussian profile of a zero mean process for a bead (*121*, *123*). At equilibrium, Boltzmann's law must also be satisfied, leading to the Einstein relationship between the diffusion coefficient D and drag coefficient γ.

$$D = \frac{k_BT}{\gamma} \tag{5.7}$$

Substituting in to Eq. (5.6) and rearranging the terms yields

$$\frac{dx}{dt}(t) + 2\pi f_c x(t) = (2D)^{1/2}F(t) \tag{5.8}$$

where the corner frequency as a function of stiffness κ

$$f_c \equiv \kappa/(2\pi\gamma) \tag{5.9}$$

has now been introduced.

The corner frequency of a bead can be described as the frequency where the transition from uncorrelated bead motion ('white noise') to correlated motion ('red noise') occurs. Extracting the corner frequency requires separating the spatial amplitude of a signal across frequency space, a textbook application of Fourier analysis. Discrete Fourier transforms were performed in MATLAB to obtain the power spectrum of the thermal motions of a free bead held in a trap and sampled with frequency f_{sample} over time series of length N using the formula

$$x(k) = \Delta t \sum_{j=1}^{N} x(j)\, \omega_N{}^{(j-1)(k-1)} \tag{5.10}$$

where $\omega_N = e^{(-2\pi i)/N}$, $\Delta t \equiv 1/f_{sample}$, and $k = -N/2, \ldots N/2$. The measured power spectrum is well-approximated by the Lorentzian function

$$P_k = \frac{D/(2\pi^2)}{f_c^2 + f_k^2} \tag{5.11}$$

describing the expected power spectral density P_k of a trapped bead with corner frequency f_c and diffusion coefficient D. Note that the power spectrum contains both white noise (flat portion) and red noise (noise power decreasing as $1/f^2$). There is also noise at lower frequencies that decreases as 1/f, or so-called 'pink noise' that is not shown in the figure. Pink noise does not have a well-defined origin and is typical in power spectrums. Many external/internal factors, such as electrical noise and atmospheric perturbations can introduce noise over long timescales that could possibly contribute to 1/f noise. For most biological systems, kinetic events of interest happen at much faster timescales, therefore the presence of pink noise would not have a significant effect.

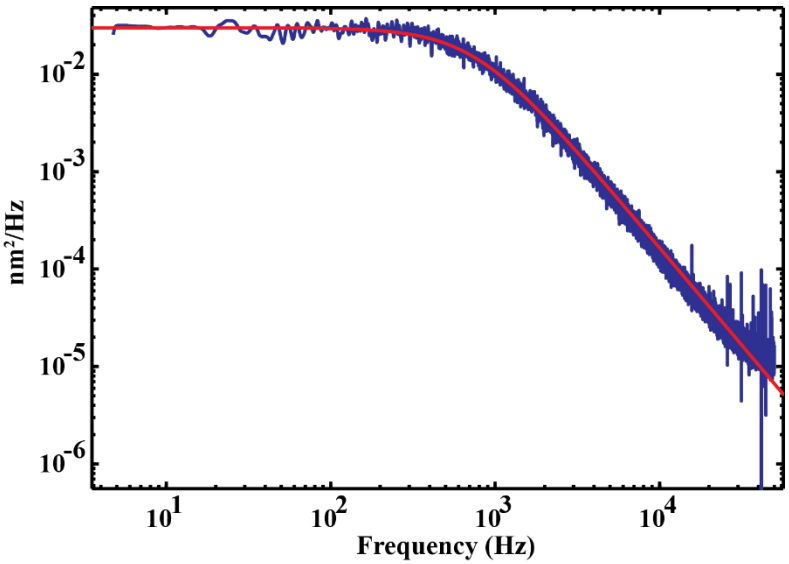

Figure 5.8 Power Spectrum of a Free Bead

Blue lines is the measured fluctuations of a free bead sampled at 100 kHz. Red line is a least squares Lorentzian fit yielding an f_c of ~750 Hz.

The drag coefficient γ is known for commercially available beads, using Eq. (5.9) the trap stiffness can be determined. With an accurate measurement of the trap stiffness, we can relate the voltage measurements towards position displacement using Eq. (5.2) and an accurate force readout via Hooke's law.

5.5.2 Internal distance standards

The optical trapping instrument used contains a single, counter-propagating trap, and a micropipette. The relative position of the trapped bead is known but the absolute distance between the trapped bead and the bead held in the micropipette must be measured. A straightforward method of determining the distance between the two beads is to manually move the trapped bead close to the pipette bead. A force readout will indicate when the two beads have touched. The total distance traveled by the trapped bead is the distance between the two beads. To test the accuracy of this technique, a dsDNA tether of known length was held between the two beads. Pulling the DNA tether to 30 pN of force will essentially fully extend the DNA. The distance between the two beads at 30 pN of force (taking into account the bead position) should be equal to the expected length of B-form dsDNA.

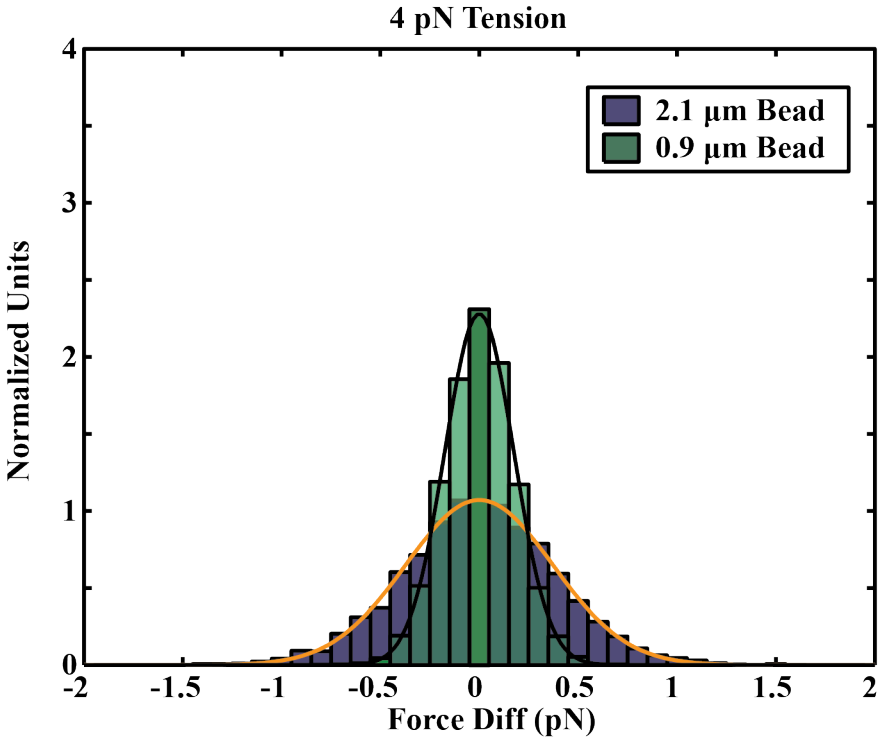

Figure 5.9 Noise Analysis of Beads Held Under Tension

A 2.1 micron bead (blue) or a 0.9 micron bead (green) was held under 4 pN of tension and noise in the force was measured. The 2.1 micron bead has a standard deviation of 0.37 pN and the 0.9 micron bead has a standard deviation of 0.17 pN of noise in the force calculated from a Gaussian fit to the histogram (orange and black lines). Both histograms are normalized. For technical reasons, a 0.9 micron bead cannot be stably trapped in a counter-propagating beam. Thus the 2.1 micron bead was used for all experiments.

Buffer Name	Composition
1x Reaction Buffer	50 mM Tris·HCl pH 7.5 10 mM $MgCl_2$ 0.25 – 5 mM ATP 5 µM P_i 5 µM ADP
1x Bead Blocking Buffer	50 mM Tris·HCl pH 7.5 10 mM $MgCl_2$ 4% BSA w/v 0.1% Tween-20
1x Lysis Buffer	50 mM HEPES pH 7.5 500 mM NaCl 5% Glycerol 0.5% Triton X-100 50 mM Imidazole
1x Wash Buffer	50 mM HEPES pH 7.5 500 mM NaCl 5% Glycerol 50 mM Imidazole
1x Elution Buffer	50 mM HEPES pH 7.5 500 mM NaCl 5% Glycerol 500 mM Imidazole
1x Dialysis Buffer	50 mM HEPES pH 7.5 30% Glycerol 100 mM NaCl 0.25 mM EDTA
1x TBS	50 mM Tris·HCl pH 7.5 150 mM NaCl
1x PBS	10 mM $NaPO_4$ pH 7.4 150 mM NaCl

Table 5-1 List of Buffers

Chapter 6 Conclusions and Future Directions

6.1 Conclusions

6.1.1 Mechanochemistry

The series of force-velocity curves produced for SpoIIIE have demonstrated that phosphate release acts as the primary force generating transition the motor's mechanochemical cycle. Furthermore, the force-velocity curves also display two force-sensitive regimes, giving rise to the possibility of a secondary loosely coupled force generating transition. Other models that could explain the force-velocity behavior would be a branched pathway kinetic model, in which SpoIIIE has two different mechanisms of generating force. This model seems unlikely given the structural gymnastics required for a protein to have two distinct mechanisms of force generation.

6.1.2 Intersubunit Coordination

The lack of high-resolution experiments and crystal structures of SpoIIIE translocation is a limiting factor in characterizing intersubunit coordination. Even so, experiments with MeP modified DNA has already produced an emerging picture of subunit coordination. I have determined that SpoIIIE makes critical contacts with the phosphates on DNA during translocation and that these contacts favor the 5'→3' strand in the direction of translocation. Strand tracking will essentially limit subunit coordination models to some variation of a sequential model of ATP hydrolysis around the ring. Experiments with non-hydrolysable ATP analogues demonstrate that the ring is not strictly sequential. Bulk activity assays of SpoIIIE have also been performed in the presence of mutant subunits, demonstrating that SpoIIIE can tolerate catalytically inactive subunits within a ring (personal communication: Carolina Caffaro). Finally, the related dsDNA translocase FtsK has also been demonstrated to tolerate catalytically inactive subunits (*90*). All of these pieces of information points to a model where SpoIIIE fires subunits sequentially, but is capable of skipping inactive subunits if necessary.

Mechanical flexibility within a motor's mechanochemical cycle is likely important for its role in fast DNA translocation. A strictly coordinated ring will pause indefinitely if a single subunit is 'broken'. The precise definition of strict coordination is also somewhat misleading as even ring NTPases, such as the φ29 packaging motor, that are traditionally considered 'strictly' coordinated have a small degree of flexibility built in (*33*). The question then becomes what is the degree of flexibility present in ring NTPases.

MeP stepping stone experiments have also revealed that SpoIIIE makes multiple contacts with the DNA substrate and yielded a physical step size of 2 bp. The step size serves as a critical starting point to build any model of translocation. A step size along with a sequential model of coordination also presents a symmetry mismatch between the periodicity of the hexamer and the phosphate backbone of DNA. This symmetry mismatch offers a prediction on SpoIIIE supercoiling that has been confirmed by previous members in the lab.

6.1.3 Motor-Substrate interactions

Processive motors must go through cycles of high affinity and low affinity towards their substrate. Pulling experiments with SpoIIIE and nucleotides have determined that SpoIIIE's

affinity towards its DNA substrate is coupled to its ATP hydrolysis cycle. The highest affinity towards DNA occurs when the motor is ATP bound, followed by decreasing affinity when ADP bound and empty. Since ATP hydrolysis is cyclical, coupling substrate affinity to ATP states is a straightforward mechanism of cyclical motor-substrate interactions.

6.1.4 SpoIIIE translocation model

The final model of SpoIIIE translocation which rationalizes all the results presented in this thesis is shown below. Two adjacent subunits that are ATP bound and ADP bound form a total of four contacts on the DNA backbone. Hydrolysis and release of phosphate then translocates the DNA by 2 bp. Hydrolysis proceeds in a sequential fashion around the ring. During translocation, all four contacts are still maintained in keeping with a coordinated escort model. After translocation, the next adjacent subunit that is ATP bound will reset the ring and form new contacts with the phosphate backbone. It must be noted that the timing of ADP release is not entirely clear from my data. Furthermore the model is not claiming that ATP must bind sequentially around the ring, only that hydrolysis must proceed sequentially (Figure 6.1 A). The translocation model presented below can be extended to include two force generating steps without any loss of generality.

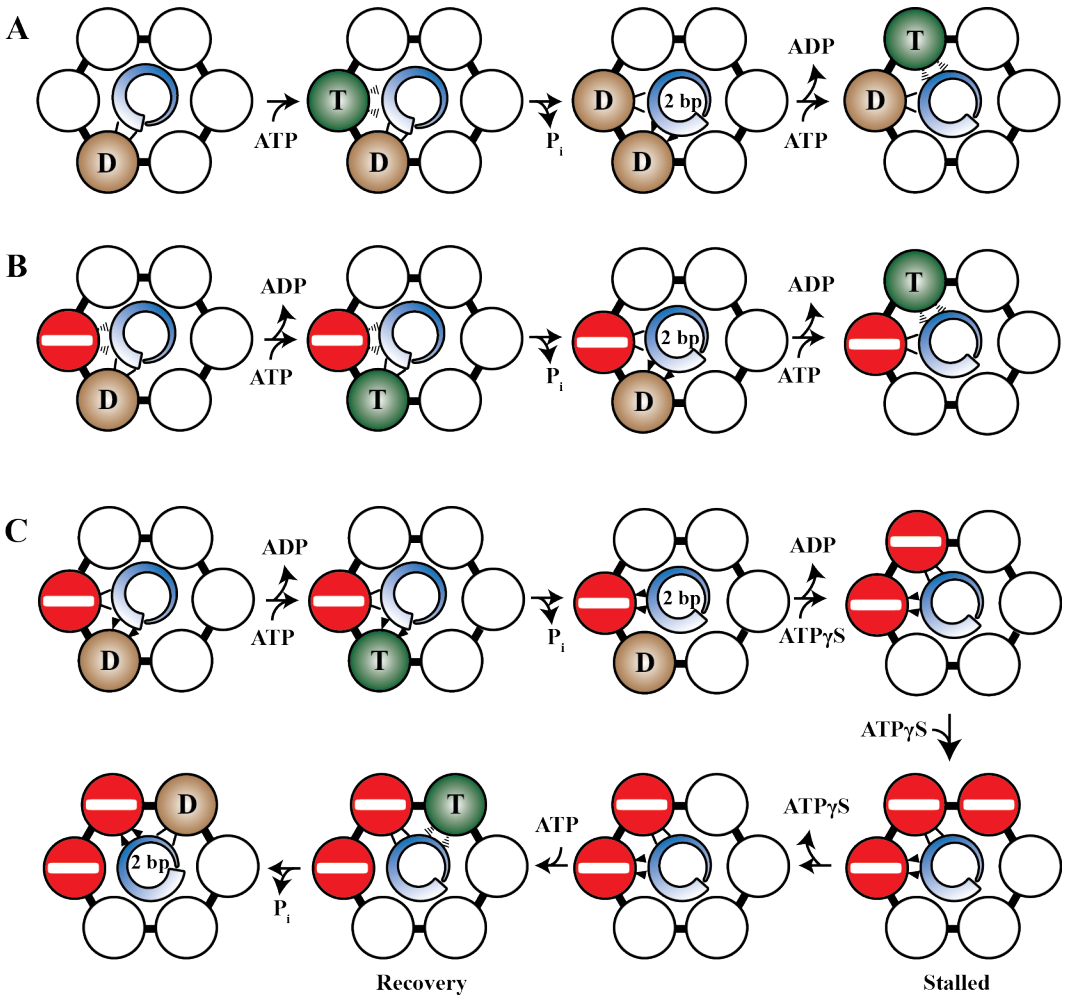

Figure 6.1 Model of SpoIIIE Translocation

(A) Model of SpoIIIE translocation. An ADP bound subunit (brown) forms two phosphate contacts in the same plane with the viewer (black lines) with the DNA (blue spiral), only one DNA strand is shown for clarity. Once ATP binds (green), two more contacts are formed in the plane away from the viewer (dashed projection). Hydrolysis and phosphate release translocates the DNA by 2 bp towards the viewer. The motor-DNA interactions are also moved towards the viewer (black line and wedged projection). The ring is reset by breaking the two contacts that are projected towards the viewer and making two contacts in the next adjacent subunit. The nucleotide state of the remaining subunits are not known and are intentionally left blank (white).
(B) Model of SpoIIIE navigating across an inactive ATPγS bound subunit, represented as a do-not-enter sign. The ADP bound subunit can bind an ATP molecule, hydrolyze it and then translocate the DNA by 2 bp. Normally at this point, both the inactive and the next adjacent subunit would be making contacts. However, the contacts made by the next active subunit are sufficient to rescue the motor.
(C) Model of ATPγS induced pause and recovery. The three subunits immediately ahead of the hydrolysis cycle must be bound to ATPγS in order to induce a pause. Recovery from a pause occurs when one ATPγS molecule is released, likely the third subunit as that subunit is next in line for translocation in a sequential model. ATP then binds, forms new phosphate contacts and then begins translocation.

The ATP analogue experiments have also shown that SpoIIIE translocation can tolerate inactive subunits bound to ATPγS, likely tolerating at least two inactive subunits. Two models describing possible scenarios in which the motor can skip over an inactive subunit are shown (Figure 6.1 B, C). In both cases, the motor forms phosphate contacts using the next available subunit. As is shown in Figure 3.13, the SpoIIIE ring encircles over 10 bp of DNA, a little over one full turn of the double helix. This means that every subunit in a hexameric ring can potentially make a new contact with the phosphate backbone and take over if one subunit is inactive. In a sequential model of translocation, the nucleotide state of the subunits immediately ahead of the translocation cycle would effect translocation. Thus a model of ATPγS induced pausing has the three subunits immediately ahead of a translocation cycle bound to γS. Pause recovery is independent of [ATPγS] and follows a single-exponential decay, thus recovery is modeled to occur only when a single, specific subunit releases its γS molecule.

6.2 Future Directions

6.2.1 Sequence recognition and directionality

It has previously been proposed that SpoIIIE passively diffuses on DNA and translocation is activated or stimulated upon encountering the SRS sequence (*10*, *124*). My single-molecule experiments have not demonstrated any sequence preference for SpoIIIE assembly and translocation on the lambda DNA tether (data not shown). Furthermore I see fast, ATP-dependent translocation even in the absence of SRS, suggesting instead that initiation of translocation is sequence-independent. However, the SRS motif does impart directionality to SpoIIIE translocation, the exact mechanism of how this happens is not entirely clear. To better understand whether SpoIIIE recognizes the SRS motif and how translocation is effected, a 3x tandem repeat of SRS was placed at the 4 kb mark on the DNA tether in the non-permissive orientation. Preliminary results show that SpoIIIE displays two different responses to SRS (Figure 6.2). The

first response shown is a complete detachment from the DNA tether. This is interpreted as ring disassembly when the motor encounters SRS in the non-permissive orientation, consistent with the model proposed previously (*12*). The second response shows SpoIIIE pausing at the SRS location and then translocating over it.

The domain responsible for recognizing the SRS sequence is the gamma domain of the motor. Figure 1.2 shows that the gamma domain is connected by a short flexible linker to the alpha, beta motor domain. The direction of translocation places the gamma domain 'ahead' of the motor, giving rise to the possibility that when SpoIIIE encounters SRS, the gamma domain will bind to SRS and act as a brake to DNA translocation. By immobilizing the SpoIIIE motor on a bead, there is no longer any ambiguity on the location of the motor on the DNA tether. Ultimately, this experimental set-up will allow a more thorough characterization of SpoIIIE directionality.

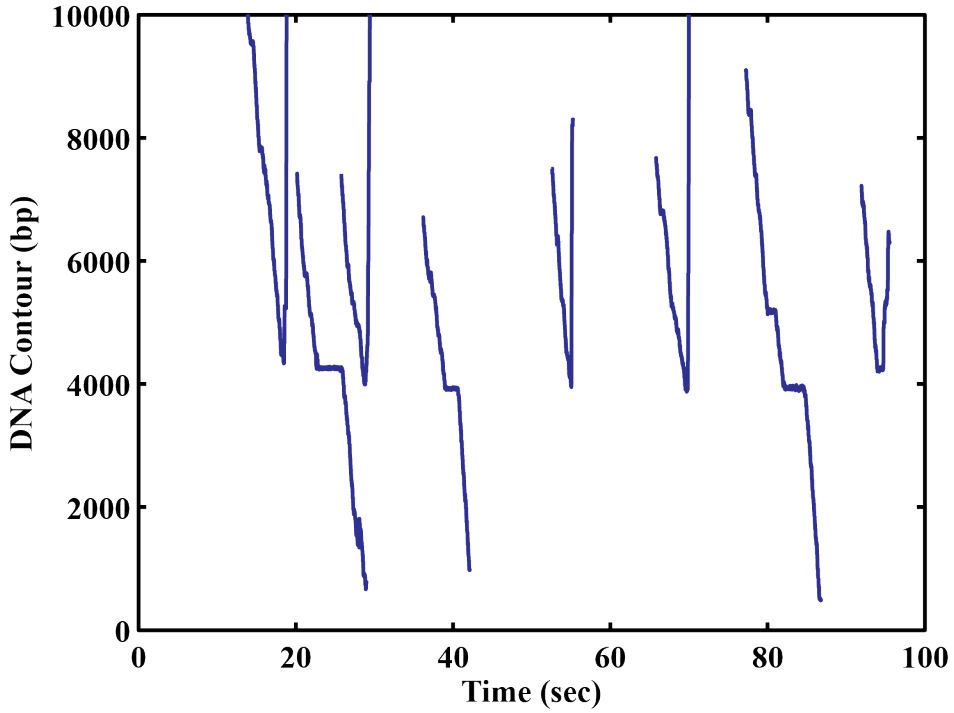

Figure 6.2 SpoIIIE Response to 3x SRS Non-Permissive

Representative SpoIIIE translocation traces when it encounters a 3x SRS in non-permissive orientation. The SRS sequence was placed at the 4 kb mark.

6.2.2 Measuring stepping periodicity

MeP stepping stone experiments have revealed that SpoIIIE takes a step size of 2 bp during translocation. It would be of great interest to determine whether the motor consistently maintains this step size. High-resolution experiments where the step size is directly measured could shed some light on the question. However, these experiments are immensely difficult for a fast motor such as SpoIIIE. Alternatively, the stepping stone experiments can be extended to a series of 2, 3, 4 or more stepping stones. With a long enough stepping stone DNA construct, we would be able to observe how far SpoIIIE can translocate before the stepping periodicity goes off register from the MeP construct periodicity.

6.3 Final Thoughts

The SpoIIIE project has been a long, difficult, and fulfilling journey into biophysics. There are many factors of SpoIIIE biology that I later realized I took for granted. Foremost of these is the sheer simplicity of the system. SpoIIIE can function at full capacity without the need for co-factors and with minimal buffer components. In a scientific landscape where signaling pathways and gene networks become increasingly labyrinthine, it is a refreshing break to focus on a biological function that is accomplished by a single, remarkable little motor. The minimalism of SpoIIIE gives it great potential to be a model system for ring NTPases. The hexameric symmetry of the ring and canonical RecA-like fold makes the SpoIIIE ring widely applicable to a diverse range of ring NTPases.

At the time of writing this thesis, almost nothing was known about the mechanical details of the FtsK/SpoIIIE rings. The work presented in this thesis has shed light on the core operating principles of SpoIIIE translocation, but it is only the first step in what will hopefully be a series of experiments describing the FtsK/SpoIIIE rings in greater detail.

References

1. N. R. Cozzarelli, G. J. Cost, M. Nöllmann, T. Viard, J. E. Stray, Giant proteins that move DNA: bullies of the genomic playground., *Nat. Rev. Mol. Cell Biol.* **7**, 580–8 (2006).

2. J. G. Yodh, M. Schlierf, T. Ha, Insight into helicase mechanism and function revealed through single-molecule approaches., *Q. Rev. Biophys.* **43**, 185–217 (2010).

3. K. M. Herbert, W. J. Greenleaf, S. M. Block, Single-molecule studies of RNA polymerase: motoring along., *Annu. Rev. Biochem.* **77**, 149–76 (2008).

4. J. Errington, J. Bath, L. J. Wu, DNA transport in bacteria., *Nat. Rev. Mol. Cell Biol.* **2**, 538–45 (2001).

5. R. a Maillard *et al.*, ClpX(P) generates mechanical force to unfold and translocate its protein substrates., *Cell* **145**, 459–69 (2011).

6. M. Sen *et al.*, The ClpXP Protease Unfolds Substrates Using a Constant Rate of Pulling but Different Gears, *Cell* **155**, 636–646 (2013).

7. D. Keller, C. Bustamante, The mechanochemistry of molecular motors., *Biophys. J.* **78**, 541–56 (2000).

8. J. Bath, L. J. Wu, J. Errington, J. C. Wang, Role of Bacillus subtilis SpoIIIE in DNA transport across the mother cell-prespore division septum., *Science* **290**, 995–7 (2000).

9. L. J. Wu, J. Errington, Bacillus subtilis SpoIIIE protein required for DNA segregation during asymmetric cell division., *Science* **264**, 572–5 (1994).

10. D. I. Cattoni *et al.*, SpoIIIE mechanism of directional translocation involves target search coupled to sequence-dependent motor stimulation., *EMBO Rep.* **14**, 473–9 (2013).

11. K. A. Marquis *et al.*, SpoIIIE strips proteins off the DNA during chromosome translocation., *Genes Dev.* **22**, 1786–95 (2008).

12. J. L. Ptacin *et al.*, Sequence-directed DNA export guides chromosome translocation during sporulation in Bacillus subtilis., *Nat. Struct. Mol. Biol.* **15**, 485–93 (2008).

13. B. M. Burton, K. a Marquis, N. L. Sullivan, T. a Rapoport, D. Z. Rudner, The ATPase SpoIIIE transports DNA across fused septal membranes during sporulation in Bacillus subtilis., *Cell* **131**, 1301–12 (2007).

14. L. J. Wu, J. Errington, Septal localization of the SpoIIIE chromosome partitioning protein in Bacillus subtilis., *EMBO J.* **16**, 2161–9 (1997).

15. J.-B. Fiche *et al.*, M. K. Waldor, Ed. Recruitment, Assembly, and Molecular Architecture of the SpoIIIE DNA Pump Revealed by Superresolution Microscopy, *PLoS Biol.* **11**, e1001557 (2013).

16. C. Kaimer, J. E. González-Pastor, P. L. Graumann, SpoIIIE and a novel type of DNA translocase, SftA, couple chromosome segregation with cell division in Bacillus subtilis., *Mol. Microbiol.* **74**, 810–25 (2009).

17. L. M. Iyer, K. S. Makarova, E. V Koonin, L. Aravind, Comparative genomics of the FtsK-HerA superfamily of pumping ATPases: implications for the origins of chromosome segregation, cell division and viral capsid packaging., *Nucleic Acids Res.* **32**, 5260–79 (2004).

18. N.-J. L. Liu, R. J. Dutton, K. Pogliano, Evidence that the SpoIIIE DNA translocase participates in membrane fusion during cytokinesis and engulfment., *Mol. Microbiol.* **59**, 1097–113 (2006).

19. M. Sharp, K. Pogliano, The membrane domain of SpoIIIE is required for membrane fusion during Bacillus subtilis sporulation, *J. Bacteriol.* **185**, 2005–2008 (2003).

20. F.-X. Barre, FtsK and SpoIIIE: the tale of the conserved tails., *Mol. Microbiol.* **66**, 1051–5 (2007).

21. T. H. Massey, C. P. Mercogliano, J. Yates, D. J. Sherratt, J. Löwe, Double-stranded DNA translocation: structure and mechanism of hexameric FtsK., *Mol. Cell* **23**, 457–69 (2006).

22. J. Löwe *et al.*, Molecular mechanism of sequence-directed DNA loading and translocation by FtsK., *Mol. Cell* **31**, 498–509 (2008).

23. S. Bigot *et al.*, KOPS: DNA motifs that control E. coli chromosome segregation by orienting the FtsK translocase., *EMBO J.* **24**, 3770–80 (2005).

24. P. J. Pease *et al.*, Sequence-directed DNA translocation by purified FtsK., *Science* **307**, 586–90 (2005).

25. J. L. Ptacin, M. Nöllmann, C. Bustamante, N. R. Cozzarelli, Identification of the FtsK sequence-recognition domain., *Nat. Struct. Mol. Biol.* **13**, 1023–5 (2006).

26. D. I. Cattoni *et al.*, Structure and DNA-binding properties of the Bacillus subtilis SpoIIIE DNA translocase revealed by single-molecule and electron microscopies., *Nucleic Acids Res.* , 1–13 (2013).

27. L. a Kelley, M. J. E. Sternberg, Protein structure prediction on the Web: a case study using the Phyre server., *Nat. Protoc.* **4**, 363–71 (2009).

28. O. a Saleh, C. Pérals, F.-X. Barre, J.-F. Allemand, Fast, DNA-sequence independent translocation by FtsK in a single-molecule experiment., *EMBO J.* **23**, 2430–9 (2004).

29. T. C. Fleming *et al.*, Dynamic SpoIIIE assembly mediates septal membrane fission during Bacillus subtilis sporulation., *Genes Dev.* **24**, 1160–72 (2010).

30. J. P. Erzberger, J. M. Berger, Evolutionary relationships and structural mechanisms of AAA+ proteins., *Annu. Rev. Biophys. Biomol. Struct.* **35**, 93–114 (2006).

31. A. Y. Lyubimov, M. Strycharska, J. M. Berger, The nuts and bolts of ring-translocase structure and mechanism., *Curr. Opin. Struct. Biol.* **21**, 240–8 (2011).

32. L. M. Iyer, D. D. Leipe, E. V Koonin, L. Aravind, Evolutionary history and higher order classification of AAA+ ATPases., *J. Struct. Biol.* **146**, 11–31 (2004).

33. G. Chistol *et al.*, High Degree of Coordination and Division of Labor among Subunits in a Homomeric Ring ATPase, *Cell* **151**, 1017–1028 (2012).

34. J. R. Moffitt *et al.*, Intersubunit coordination in a homomeric ring ATPase., *Nature* **457**, 446–50 (2009).

35. S. B. Smith, Y. Cui, C. Bustamante, Optical-trap force transducer that operates by direct measurement of light momentum., *Methods Enzymol.* **361**, 134–62 (2003).

36. A. Ashkin, Acceleration and Trapping of Particles by Radiation Pressure, *Phys. Rev. Lett.* **24**, 156–159 (1970).

37. M. J. Davey, M. O'Donnell, Replicative helicase loaders: ring breakers and ring makers, *Curr. Biol.* **13**, R594–R596 (2003).

38. M. Velten *et al.*, A two-protein strategy for the functional loading of a cellular replicative DNA helicase., *Mol. Cell* **11**, 1009–20 (2003).

39. E. Arias-Palomo, V. L. O'Shea, I. V. Hood, J. M. Berger, The Bacterial DnaC Helicase Loader Is a DnaB Ring Breaker, *Cell* **153**, 438–448 (2013).

40. D. Foulger, J. Errington, The role of the sporulation gene spoIIIE in the regulation of prespore-specific gene expression in Bacillus subtilis., *Mol. Microbiol.* **3**, 1247–55 (1989).

41. A. E. Wallin, H. Ojala, E. Hæggström, R. Tuma, Stiffer optical tweezers through real-time feedback control, *Appl. Phys. Lett.* **92**, 224104 (2008).

42. C. Bustamante, J. F. Marko, E. D. Siggia, S. Smith, Entropic elasticity of lambda-phage DNA., *Science* **265**, 1599–600 (1994).

43. C. G. Baumann, S. B. Smith, V. a Bloomfield, C. Bustamante, Ionic effects on the elasticity of single DNA molecules., *Proc. Natl. Acad. Sci. U. S. A.* **94**, 6185–90 (1997).

44. S. B. Smith, L. Finzi, C. Bustamante, Direct mechanical measurements of the elasticity of single DNA molecules by using magnetic beads., *Science* **258**, 1122–6 (1992).

45. C. Bustamante, S. B. Smith, J. Liphardt, D. Smith, Single-molecule studies of DNA mechanics., *Curr. Opin. Struct. Biol.* **10**, 279–85 (2000).

46. S. B. Smith, Y. Cui, C. Bustamante, Overstretching B-DNA: the elastic response of individual double-stranded and single-stranded DNA molecules., *Science* **271**, 795–9 (1996).

47. D. E. Smith *et al.*, The bacteriophage f29 portal motor can package DNA against a large internal force, (2001).

48. N. Ribeck, D. L. Kaplan, I. Bruck, O. a Saleh, DnaB helicase activity is modulated by DNA geometry and force., *Biophys. J.* **99**, 2170–9 (2010).

49. K. Svoboda, S. M. Block, Force and velocity measured for single kinesin molecules., *Cell* **77**, 773–84 (1994).

50. C. Bustamante, Y. R. Chemla, N. R. Forde, D. Izhaky, Mechanical processes in biochemistry., *Annu. Rev. Biochem.* **73**, 705–48 (2004).

51. Y. R. Chemla *et al.*, Mechanism of force generation of a viral DNA packaging motor., *Cell* **122**, 683–92 (2005).

52. M. C. Morais *et al.*, Cryoelectron-microscopy image reconstruction of symmetry mismatches in bacteriophage phi29., *J. Struct. Biol.* **135**, 38–46 (2001).

53. M. R. Singleton, M. R. Sawaya, T. Ellenberger, D. B. Wigley, Crystal structure of T7 gene 4 ring helicase indicates a mechanism for sequential hydrolysis of nucleotides., *Cell* **101**, 589–600 (2000).

54. N. D. Thomsen, J. M. Berger, Running in reverse: the structural basis for translocation polarity in hexameric helicases., *Cell* **139**, 523–34 (2009).

55. E. J. Enemark, L. Joshua-Tor, Mechanism of DNA translocation in a replicative hexameric helicase., *Nature* **442**, 270–5 (2006).

56. J. R. Moffitt *et al.*, Supp-Intersubunit coordination in a homomeric ring ATPase., *Nature* **457**, 446–50 (2009).

57. H. Noji, R. Yasuda, M. Yoshida, K. Kinosita, Direct observation of the rotation of F1-ATPase., *Nature* **386**, 299–302 (1997).

58. D. Gai, R. Zhao, D. Li, C. V Finkielstein, X. S. Chen, Mechanisms of conformational change for a replicative hexameric helicase of SV40 large tumor antigen., *Cell* **119**, 47–60 (2004).

59. A. Martin, T. a Baker, R. T. Sauer, Rebuilt AAA + motors reveal operating principles for ATP-fuelled machines., *Nature* **437**, 1115–20 (2005).

60. J.-C. Liao, Y.-J. Jeong, D.-E. Kim, S. S. Patel, G. Oster, Mechanochemistry of t7 DNA helicase., *J. Mol. Biol.* **350**, 452–75 (2005).

61. Q. Wang, J. J. Arnold, A. Uchida, K. D. Raney, C. E. Cameron, Phosphate release contributes to the rate-limiting step for unwinding by an RNA helicase., *Nucleic Acids Res.* **38**, 1312–24 (2010).

62. J. L. Adelman *et al.*, Mechanochemistry of transcription termination factor Rho., *Mol. Cell* **22**, 611–21 (2006).

63. K. Adachi *et al.*, Coupling of rotation and catalysis in F(1)-ATPase revealed by single-molecule imaging and manipulation., *Cell* **130**, 309–21 (2007).

64. H. Wang, G. Oster, Ratchets, power strokes, and molecular motors, *Appl. Phys. A Mater. Sci. Process.* **75**, 315–323 (2002).

65. G. Oster, H. Wang, How protein motors convert chemical energy into mechanical work, *Mol. Mot.* (2003) (available at http://onlinelibrary.wiley.com/doi/10.1002/3527601503.ch8/summary).

66. G. Oster, H. Wang, Reverse engineering a protein: the mechanochemistry of ATP synthase., *Biochim. Biophys. Acta* **1458**, 482–510 (2000).

67. B. Derrida, Velocity and diffusion constant of a periodic one-dimensional hopping model, *J. Stat. Phys.* **31**, 433–450 (1983).

68. M. J. Schnitzer, K. Visscher, S. M. Block, Force production by single kinesin motors., *Nat. Cell Biol.* **2**, 718–23 (2000).

69. H. Kramers, Brownian motion in a field of force and the diffusion model of chemical reactions, *Physica* , 284–304 (1940).

70. J. Howard, *Mechanics of Motor Proteins and the CytoSkeleton* (2001).

71. D. N. Fuller *et al.*, Measurements of single DNA molecule packaging dynamics in bacteriophage lambda reveal high forces, high motor processivity, and capsid transformations., *J. Mol. Biol.* **373**, 1113–22 (2007).

72. C. Bustamante, D. Keller, G. Oster, The Physics of Molecular Motors †, *Acc. Chem. Res.* **34**, 412–420 (2001).

73. R. D. Astumian, M. Bier, Mechanochemical coupling of the motion of molecular motors to ATP hydrolysis., *Biophys. J.* **70**, 637–53 (1996).

74. P. Bieling, I. a Telley, J. Piehler, T. Surrey, Processive kinesins require loose mechanical coupling for efficient collective motility., *EMBO Rep.* **9**, 1121–7 (2008).

75. Y. Harada, K. Sakurada, T. Aoki, D. D. Thomas, T. Yanagida, Mechanochemical coupling in actomyosin energy transduction studied by in vitro movement assay., *J. Mol. Biol.* **216**, 49–68 (1990).

76. M. J. Schnitzer, S. M. Block, Kinesin hydrolyses one ATP per 8-nm step., *Nature* **388**, 386–90 (1997).

77. M. D. Wang *et al.*, Force and velocity measured for single molecules of RNA polymerase., *Science* **282**, 902–7 (1998).

78. E. J. Enemark, A. Stenlund, L. Joshua-Tor, Crystal structures of two intermediates in the assembly of the papillomavirus replication initiation complex., *EMBO J.* **21**, 1487–96 (2002).

79. E. a Galburt *et al.*, Backtracking determines the force sensitivity of RNAP II in a factor-dependent manner., *Nature* **446**, 820–3 (2007).

80. M. Dangkulwanich *et al.*, Complete dissection of transcription elongation reveals slow translocation of RNA polymerase II in a linear ratchet mechanism, *Elife* **2**, e00971–e00971 (2013).

81. V. I. Kottadiel, V. B. Rao, Y. R. Chemla, The dynamic pause-unpackaging state, an off-translocation recovery state of a DNA packaging motor from bacteriophage T4., *Proc. Natl. Acad. Sci. U. S. A.* **109**, 20000–5 (2012).

82. K. Svoboda, P. P. Mitra, S. M. Block, Fluctuation analysis of motor protein movement and single enzyme kinetics., *Proc. Natl. Acad. Sci. U. S. A.* **91**, 11782–6 (1994).

83. M. J. Schnitzer, S. M. Block, Statistical kinetics of processive enzymes., *Cold Spring Harb. Symp. Quant. Biol.* **60**, 793–802 (1995).

84. Y. R. Chemla, J. R. Moffitt, C. Bustamante, Exact solutions for kinetic models of macromolecular dynamics., *J. Phys. Chem. B* **112**, 6025–44 (2008).

85. J. R. Moffitt, Y. R. Chemla, C. Bustamante, *Methods in statistical kinetics.* (Elsevier Inc., ed. 1, 2010; http://www.ncbi.nlm.nih.gov/pubmed/20627160), pp. 221–57.

86. J. R. Moffitt, Y. R. Chemla, C. Bustamante, Mechanistic constraints from the substrate concentration dependence of enzymatic fluctuations., *Proc. Natl. Acad. Sci. U. S. A.* **107**, 15739–44 (2010).

87. J. R. Moffitt, C. Bustamante, Extracting Signal from Noise: Kinetic Mechanisms from a Michaelis-Menten-Like Expression for Enzymatic Fluctuations, *FEBS J.* (2013), doi:10.1111/febs.12545.

88. S. C. Kou, B. J. Cherayil, W. Min, B. P. English, X. S. Xie, Single-molecule Michaelis-Menten equations., *J. Phys. Chem. B* **109**, 19068–81 (2005).

89. M. J. Moreau, A. T. McGeoch, A. R. Lowe, L. S. Itzhaki, S. D. Bell, ATPase site architecture and helicase mechanism of an archaeal MCM., *Mol. Cell* **28**, 304–14 (2007).

90. E. Crozat *et al.*, Separating speed and ability to displace roadblocks during DNA translocation by FtsK., *EMBO J.* **29**, 1423–33 (2010).

91. a. Rosa, M. Di Ventra, C. Micheletti, Topological jamming of spontaneously knotted polyelectrolyte chains driven through a nanopore., *Phys. Rev. Lett.* **109**, 118301 (2012).

92. A. Yildiz, M. Tomishige, A. Gennerich, R. D. Vale, Intramolecular strain coordinates kinesin stepping behavior along microtubules., *Cell* **134**, 1030–41 (2008).

93. B. E. Clancy, W. M. Behnke-Parks, J. O. L. Andreasson, S. S. Rosenfeld, S. M. Block, A universal pathway for kinesin stepping., *Nat. Struct. Mol. Biol.* **18**, 1020–7 (2011).

94. S. Nishikawa *et al.*, Switch between large hand-over-hand and small inchworm-like steps in myosin VI., *Cell* **142**, 879–88 (2010).

95. M. a DeWitt, A. Y. Chang, P. a Combs, A. Yildiz, Cytoplasmic dynein moves through uncoordinated stepping of the AAA+ ring domains., *Science* **335**, 221–5 (2012).

96. O. Itsathitphaisarn, R. a Wing, W. K. Eliason, J. Wang, T. a Steitz, The hexameric helicase DnaB adopts a nonplanar conformation during translocation., *Cell* **151**, 267–77 (2012).

97. E. Skordalakes, J. M. Berger, Structural insights into RNA-dependent ring closure and ATPase activation by the Rho termination factor., *Cell* **127**, 553–64 (2006).

98. M. J. Moreau, A. T. McGeoch, A. R. Lowe, L. S. Itzhaki, S. D. Bell, ATPase site architecture and helicase mechanism of an archaeal MCM., *Mol. Cell* **28**, 304–14 (2007).

99. M. L. Bochman, S. P. Bell, A. Schwacha, Subunit organization of Mcm2-7 and the unequal role of active sites in ATP hydrolysis and viability., *Mol. Cell. Biol.* **28**, 5865–73 (2008).

100. B. Sun *et al.*, ATP-induced helicase slippage reveals highly coordinated subunits., *Nature* **478**, 132–5 (2011).

101. I. Segel, *Enzyme Kinetics: Behavior and analysis of rapid equilibrium and steady state enzyme systems* (Wiley, 1975), p. 957.

102. B. Kalafut, K. Visscher, An objective, model-independent method for detection of non-uniform steps in noisy signals, *Comput. Phys. Commun.* **179**, 716–723 (2008).

103. A. E. Wallin, A. Salmi, R. Tuma, Step length measurement--theory and simulation for tethered bead constant-force single molecule assay., *Biophys. J.* **93**, 795–805 (2007).

104. J. R. Moffitt, Y. R. Chemla, S. B. Smith, C. Bustamante, Recent advances in optical tweezers., *Annu. Rev. Biochem.* **77**, 205–28 (2008).

105. G. Zoldák, J. Stigler, B. Pelz, H. Li, M. Rief, Ultrafast folding kinetics and cooperativity of villin headpiece in single-molecule force spectroscopy., *Proc. Natl. Acad. Sci. U. S. A.* , 1–6 (2013).

106. R. L. Eoff, T. L. Spurling, K. D. Raney, Chemically modified DNA substrates implicate the importance of electrostatic interactions for DNA unwinding by Dda helicase., *Biochemistry* **44**, 666–74 (2005).

107. M. S. Dillingham, P. Soultanas, D. B. Wigley, Site-directed mutagenesis of motif III in PcrA helicase reveals a role in coupling ATP hydrolysis to strand separation., *Nucleic Acids Res.* **27**, 3310–7 (1999).

108. J. Kawaoka, E. Jankowsky, A. M. Pyle, Backbone tracking by the SF2 helicase NPH-II., *Nat. Struct. Mol. Biol.* **11**, 526–30 (2004).

109. K. Aathavan *et al.*, Substrate interactions and promiscuity in a viral DNA packaging motor., *Nature* **461**, 669–73 (2009).

110. V. Thiviyanathan *et al.*, Structure of hybrid backbone methylphosphonate DNA heteroduplexes: effect of R and S stereochemistry., *Biochemistry* **41**, 827–38 (2002).

111. J. K. Strauss, L. J. Maher, DNA bending by asymmetric phosphate neutralization., *Science* **266**, 1829–34 (1994).

112. J. E. Graham, D. J. Sherratt, M. D. Szczelkun, Sequence-specific assembly of FtsK hexamers establishes directional translocation on DNA., *Proc. Natl. Acad. Sci. U. S. A.* **107**, 20263–8 (2010).

113. M. D. Sharp, K. Pogliano, Role of cell-specific SpoIIIE assembly in polarity of DNA transfer., *Science* **295**, 137–9 (2002).

114. O. a Saleh, S. Bigot, F.-X. Barre, J.-F. Allemand, Analysis of DNA supercoil induction by FtsK indicates translocation without groove-tracking., *Nat. Struct. Mol. Biol.* **12**, 436–40 (2005).

115. T. R. Strick, A. Quessada-Vial, FtsK: a groovy helicase., *Nat. Struct. Mol. Biol.* **13**, 948–50 (2006).

116. W. L. Nicholson, P. Setlow, Dramatic increase in negative superhelicity of plasmid DNA in the forespore compartment of sporulating cells of Bacillus subtilis., *J. Bacteriol.* **172**, 7–14 (1990).

117. W. D. Morgan, D. G. Bear, B. L. Litchman, P. H. von Hippel, RNA sequence and secondary structure requirements for rho-dependent transcription termination., *Nucleic Acids Res.* **13**, 3739–54 (1985).

118. E. Skordalakes, J. M. Berger, Structure of the Rho transcription terminator: mechanism of mRNA recognition and helicase loading., *Cell* **114**, 135–46 (2003).

119. A. Lehninger, M. Cox, D. Nelson, *Lehninger, Principles of Biochemistry* (W. H. Freeman; 5th edition, 2008).

120. E. Gajewski, D. K. Steckler, R. N. Goldberg, Thermodynamics of the hydrolysis of adenosine 5’-triphosphate to adenosine 5'-diphosphate., *J. Biol. Chem.* **261**, 12733–7 (1986).

121. K. Berg-Sørensen, H. Flyvbjerg, Power spectrum analysis for optical tweezers, *Rev. Sci. Instrum.* **75**, 594 (2004).

122. G. Uhlenbeck, L. Ornstein, On the Theory of the Brownian Motion, *Phys. Rev.* **36**, 823–841 (1930).

123. A. Einstein, Investigations on the Theory of the Brownian Movement, (1956).

124. M. Besprozvannaya, V. L. Pivorunas, Z. Feldman, B. M. Burton, SpoIIIE achieves directional DNA translocation through allosteric regulation of ATPase activity by an accessory domain., *J. Biol. Chem.* , 0–24 (2013).